WAVE FORCES
ON A
SUBMERGED HORIZONTAL CYLINDER

Frederick Conrad Schiller

United States
Naval Postgraduate School

THESIS

WAVE FORCES ON A SUBMERGED HORIZONTAL CYLINDER

by

Frederick Conrad Schiller

Thesis Advisor: C. J. Garrison

June 1971

Approved for public release; distribution unlimited.

Wave Forces on a Submerged Horizontal Cylinder

by

Frederick Conrad Schiller
Lieutenant Commander, United States Navy
B.S., Rensselaer Polytechnic Institute, 1962

Submitted in partial fulfillment of the
requirements for the degree of

MASTER OF SCIENCE IN MECHANICAL ENGINEERING

from the

NAVAL POSTGRADUATE SCHOOL
June 1971

ABSTRACT

The oscillatory forces generated by the interaction of a train of gravity waves with a rigid horizontal circular cylinder located near a simulated ocean floor were determined experimentally. A circular cylinder of six inch diameter was subjected to gravity waves of wave lengths varying from 2 to 18 feet in a two-dimensional wave channel. Both the horizontal and vertical components of the hydrodynamic force were measured.

Experimental results are plotted in dimensionless form. The horizontal and vertical dimensionless force coefficients are plotted as a function of the relative water depth, the relative wave length, and the relative wave height. It was found that the horizontal force coefficient varied quite linearly with the wave height, and the maximum value was approximately equal in either direction. The vertical force component, however, showed a much more complex variation. The upward and downward magnitudes were approximately equal for small amplitude waves, but as the wave height increased, the variations became quite nonlinear and the magnitudes in the two directions differed considerably.

TABLE OF CONTENTS

LIST OF TABLES

The above tables are presented in Appendix A.

LIST OF FIGURES

NOMENCLATURE

Symbol	Description
a	radius of circular cylinder
C_m	added-mass coefficient, dimensionless
d	depth of submergence of cylinder
F_x	maximum horizontal force per unit length
f_x	$F_x/[\rho g a^2 (H/2a)]$, horizontal force coefficient, dimensionless
F_y^+	maximum positive vertical force per unit length, (upward)
f_y^+	$F_y^+/[\rho g a^2 (H/2a)]$, positive vertical force coefficient, dimensionless
F_y^-	maximum negative vertical force per unit length, (downward)
f_y^-	$F_y^-/[\rho g a^2 (H/2a)]$, negative vertical force coefficient, dimensionless
g	acceleration due to gravity
H	height of the incident wave
h	water depth
k	wave number= $2\pi/L$
L	wave length of the incident wave
l	length of the cylinder
T	period of the incident wave
t	time
u	component of fluid velocity in the x-direction
$\dot{u}$	component of fluid acceleration in the x-direction
v	component of fluid velocity in the y-direction
$\dot{v}$	component of fluid acceleration in the y-direction

Symbol	Description
x	space coordinate
y	space coordinate
Φ	velocity potential
ρ	density of the fluid
σ	frequency of the incident wave= $2\pi/T$
μ	dynamic fluid viscosity

DIMENSIONLESS NOTATION

d/a	relative depth of submergence
$F_x/[\rho g a^2 (H/2a)]$	horizontal wave force coefficient
$F_y/[\rho g a^2 (H/2a)]$	vertical wave force coefficient
$H/2a$	relative wave height
h/a	relative water depth
$2\pi a/L$	relative wave length

ACKNOWLEDGEMENTS

The author wishes to acknowledge the following members of the Department of Mechanical Engineering Staff, Messrs. K. Mothersell, J. Beck, G. Baxter, G. Bixler, J. McKay, and T. Christian for their fine technical expertise as displayed in the construction of the apparatus.

The author gratefully acknowledges the participation of Dr. C. J. Garrison of the Naval Postgraduate School, his advisor, for the constructive supervision and continued encouragement contributed towards bringing the investigation to fruition.

The author's wife, Rena, has faithfully worked with him throughout the development of this work. She has been a constant source of encouragement and in so many ways deserves this special Thank-you.

I. INTRODUCTION

In recent years, there has been an accelerated interest in the exploration of the ocean bottom with special attention devoted to those depths encompassed by the Continental Shelf. This interest has been motivated in great part by the desire to exploit the mineral assets of the ocean bottom. Additionally, investigation of ocean bottom pipelines as specifically applied to sewage outfall lines, oil pipelines and large aqueducts are under consideration.

As a result, there has been considerable interest in the hydrodynamic interaction of gravity waves with large submarine structures resting on the ocean bottom. The design of large submarine offshore structures necessarily requires one to have an understanding of the forces induced by such environmental phenomena as surface waves. To this point, the theoretical work has yet to be a conclusive tool in assisting the design engineer to predict all expected conditions to which the anchored structure will be subjected as it lies on the ocean floor. Experimental observations of the forces induced by ocean waves are difficult to acquire, and it is therefore necessary to simulate as precisely as possible the conditions existing at the ocean bottom.

Extensive experimental work has been carried out since Stokes, who in one of the earliest papers on the subject [1], showed that, by experimentation with a pendulum-type

system, the expression for the force on a cylinder oscillating in an infinite fluid consists of two terms, one involving acceleration of the cylinder, and the other involving velocity.

Wave forces exerted on piles have been intensively investigated during the past two decades. It can be shown that when the relative size of the body, i.e., the cylinder diameter, is small compared to wave length, a condition which is generally satisfied in the case of piles, the familiar Morison equation [2] is a valid approach. This equation combines both a drag term and an inertia term, and the values of the experimental coefficients of drag and inertia are left to the ingenuity of the designer. At best, these two experimental coefficients are dependent upon the geometry of the objects under consideration and the amplitude of the fluid motion, and it would appear that 20 years of research has shed little light on understanding this interdependence. Moreover, the proximity of the free surface as well as the impermeable bottom surface affect these coefficients. In view of these difficulties, the Morison equation is not relied upon in the present approach to the problem, and the results are represented directly in dimensionless form rather than through the drag and inertia coefficient.

Keulegan and Carpenter [3] used periodic standing waves in their analysis of a cylinder subjected to a field of oscillatory motion. They were able to separate the total

resistance into drag and inertial components. They correlated values of inertia and drag coefficients under conditions of varying current intensity and cylinder sizes with a period parameter, U_mT/D, a dimensionless group combining the maximum fluid velocity U_m, the wave period T, and the cylinder diameter. This parameter is a form of the relative fluid displacement since U_mT is proportional to the amplitude of the fluid motion.

Sarpkaya and Garrison [4] studied both theoretically and experimentally unidirectional flow past a circular cylinder with constant acceleration. They also showed that the total resistance as well as the drag and inertia components of force may be represented as a function of relative fluid displacement. In the present analysis of the experimental data, this same general kind of dependence on fluid displacement is supposed, and, accordingly, the force coefficients are correlated with the ratio of the wave height to cylinder diameter.

Johnson [5] has investigated the horizontal forces resulting from the interaction of gravity waves with a circular cylinder placed relatively near the bottom. Since only long waves were studied, the resulting forces were supposed to be dependent on the water depth and wave height only. This study shed little light, however, on the basic problem.

Herbich and Shank, in a recent study [6], have conducted wave channel testing of vertical and horizontal loads

on submerged three-dimensional structures due to interaction with gravity waves. Several models were studied using a two-dimensional wave tank, and they concluded that the results of these experimental studies were sufficient to be applied to preliminary designs. Unfortunately, few actual experimental points were presented and therefore the degree of correlation is somewhat suspect.

Garrison, *et al.* [7], investigated the wave/structure interaction problem as applicable to larger objects where the Morison equation is no longer valid and a diffraction theory must be employed. In this situation, the incident wave is scattered upon encountering the large structure, and the assumption that the object does not affect the incident wave is no longer valid. The diffraction theory accounts for the relative size of the body and, neglecting viscous effects, assumes the existence of a velocity potential. When large structures, such as the recently deployed Chicago Bridge and Iron Persian Gulf oil storage tank, are designed, the analysis must include consideration for relative size and free surface effect, and this basic consideration is inherent in the diffraction theory.

It appears that there will continue to be heavy reliance on experimental model results in the design process until more reliable theoretical predictions of wave induced forces are assured. To this time, large structures have been placed on the ocean floor only after extensive model studies have been carried out.

The present study was undertaken to obtain an insight into the interaction of gravity waves with large submarine structures located at or near the ocean floor. The study includes direct measurement of horizontal and vertical forces on the submerged cylinder. The results are presented in dimensionless form as a function of the relative water depth, the relative wave length, and the relative wave height.

The interest in attempting this investigation was generated while participating in numerous discussions on the problem under the guidance of Dr. C. J. Garrison.

II. THEORETICAL CONSIDERATIONS

A schematic representation of the problem under consideration is shown in Figure (1). A rigid circular cylinder of radius a submerged with center at depth d in water of depth h is subjected to a train of regular waves of wave length L and height H progressing in the positive x-direction. The primary interest lies in the horizontal and vertical components of force induced by the waves on the circular cylinder.

The complete theoretical solution to the present problem is difficult, even assuming the flow to be unseparated; and, therefore, in order to proceed with an experimental approach, it is first necessary to apply dimensional analysis to the problem. It is known *a priori* that the maximum (horizontal or vertical) force per unit length of cylinder is dependent upon the following variables:

$$F_{xmax} \text{ or } F_{ymax} = f(h,d,a,L,H,\rho,g,\mu) \qquad (1)$$

where h denotes the water depth, d the depth of submergence, a the cylinder radius, L the wave length, H the wave height, ρ the fluid density, g the acceleration of gravity, and μ the fluid viscosity. The period of the incident wave is not required in the above relationship because a second relationship already exists between the wave period and the three variables h, H, and L. This is true not only in the case of

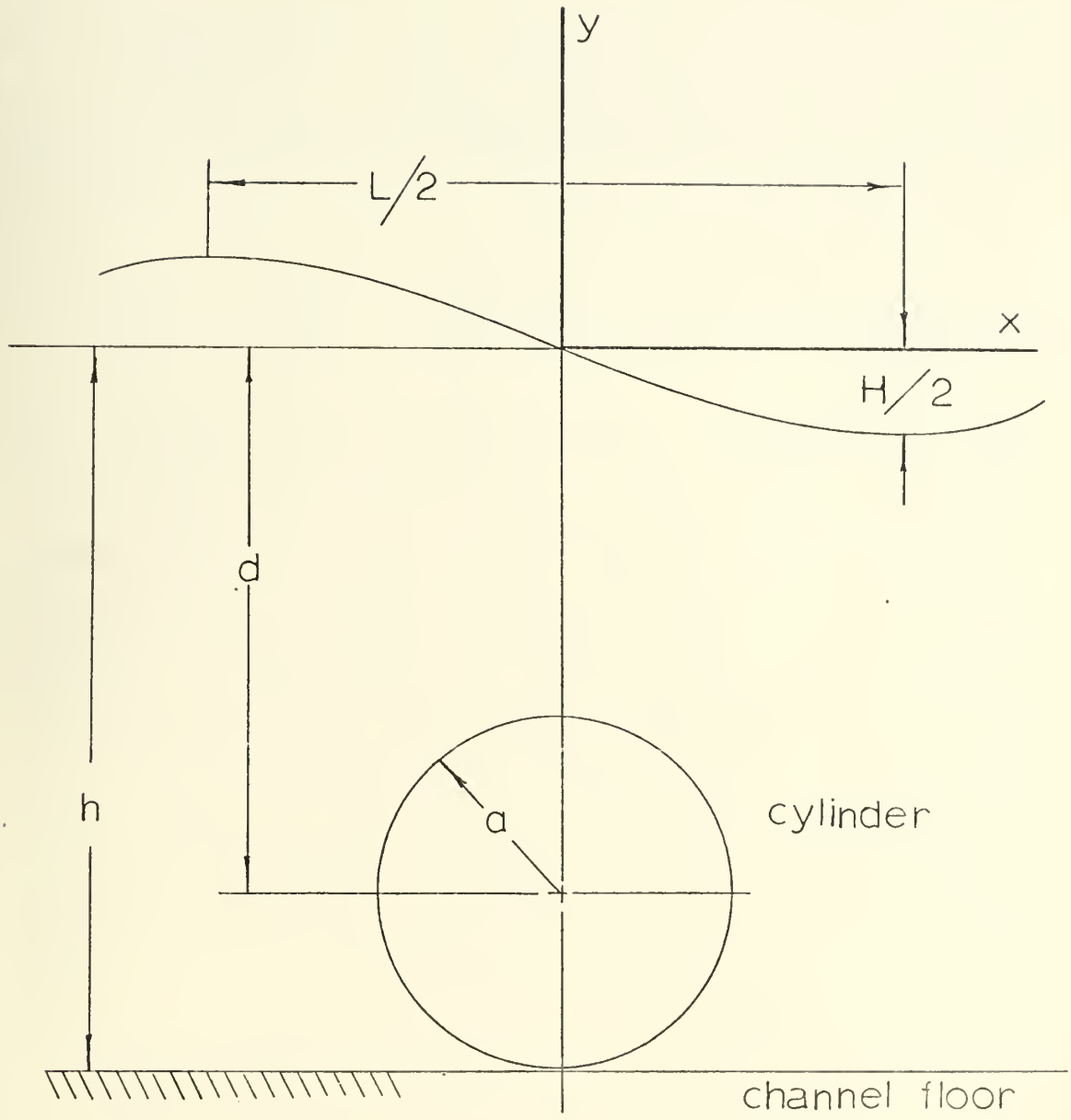

Figure 1. Definition Sketch.

linear waves, but in the case of large amplitude non-linear waves.

A dimensional analysis of the physical quantities indicated in Equation (1) yields the following dimensionless variables:

$$\frac{F_{xmax}}{\rho g a^2} \text{ or } \frac{F_{ymax}}{\rho g a^2} = f\left(\frac{2\pi a}{L}, h/a, d/a, H/2a, \frac{\mu}{\rho\sqrt{gha^2}}\right). \quad (2)$$

The last term on the right hand side of Equation (2) represents the ratio of the Froude number and the Reynolds number and, accordingly, is an indicator of the ratio of viscous forces to gravity induced forces. If this number is large, corresponding to a large scale flow and fluids of small viscosity, it may be suspected that the gravitational forces may dominate the flow, and the viscous effects may be considered unimportant. As a result, this parameter may be disregarded and Equation (2) may be written as:

$$\frac{F_{xmax}}{\rho g a^2} \text{ or } \frac{F_{ymax}}{\rho g a^2} = f\left(\frac{2\pi a}{L}, h/a, d/a, H/2a\right). \quad (3)$$

A second reason for the disregarding of this parameter may also be cited. In unidirectional motion starting from rest and moving with constant acceleration, it has been shown by Sarpkaya and Garrison [4] that the total force exerted on a circular cylinder can be expressed as a function of the relative displacement of the fluid only. Although the present problem involves oscillatory as opposed

to unidirectional motion, it is nevertheless suspected that the same general kind of dependence on relative displacement would result. In the present problem, the amplitude of the relative fluid motion is proportional to the wave height to cylinder diameter ratio and, therefore, H/2a represents an equivalent parameter. In the experimental program, an attempt is made to correlate the two force coefficients on the left hand side of Equation (3) with the dimensionless ratios on the right hand side.

Although the complete theoretical solution to the proposed problem is very complex, it is possible to obtain an approximate solution if certain simplifying assumptions are applied. The velocity potential associated with the regular progressive wave alone is given by:

$$\Phi = \frac{g\frac{H}{2}}{\sigma} \frac{\cosh k(y+h)}{\cosh kh} \cos (kx-\sigma t) \tag{4}$$

and from this expression, the velocity and acceleration of the fluid particles within a wave may be written, respectively, as:

$$u = -\frac{gk\frac{H}{2}}{\sigma} \frac{\cosh k(y+h)}{\cosh kh} \sin (kx-\sigma t) \tag{5}$$

$$v = \frac{gk\frac{H}{2}}{\sigma} \frac{\sinh k(y+h)}{\cosh kh} \cos (kx-\sigma t) \tag{6}$$

$$\dot{u} = \frac{gk\frac{H}{2}}{\sigma} \frac{\cosh k(y+h)}{\cosh kh} \cos (kx-\sigma t) \tag{7}$$

$$\dot{v} = \frac{gk\frac{H}{2}}{\sigma} \frac{\sinh k(y+h)}{\cosh kh} \sin (kx-\sigma t) \; . \tag{8}$$

In wave force problems involving objects whose dimensions are small in comparison to the wave length of the incident wave, it is common to assume that the object does not affect the incident wave. It is then assumed that the object is subjected to a uniform oscillatory flow having acceleration equal to that induced by the wave at the center of the object if the object were not there. Following this line of reasoning, the horizontal force per unit length of cylinder may be written as the product of the virtual mass and fluid acceleration as

$$F_x = \rho\pi a^2 (1+C_m) \dot{u}_{max} \tag{9}$$

if it can be assumed that flow separation does not occur. Substituting for $\dot{u}$ from Equation (7) and evaluating at y=d gives the dimensionless horizontal force coefficient as

$$\frac{F_x}{\rho g a^2} = \pi(1+C_m) \left(\frac{2\pi a}{L}\right) \frac{\cosh \frac{2\pi}{L} (h-d)}{\cosh \frac{2\pi}{L} h} \left(\frac{H}{2a}\right). \tag{10}$$

Since the dimensionless force coefficient is linear in the wave height, this expression may be written more conveniently as

$$\frac{F_x}{\rho g a^2 (H/2a)} = \pi(1+C_m) \left(\frac{2\pi a}{L}\right) \frac{\cosh \frac{2\pi a}{L} (h/a - d/a)}{\cosh \frac{2\pi a}{L} h/a}. \tag{11}$$

The parameter C_m occurring in Equation (11) denotes the added mass coefficient and depends on the shape of the object

in question as well as the proximity of the bottom and free surface. Values for the configuration in question which corresponds to a circular cylinder between a rigid boundary and free surface are not available to this writer's knowledge. The attempt in this thesis, therefore, is to determine by trial and error the value of C_m which gives the best fit to the experimental data.

III. EXPERIMENTAL INVESTIGATION

A. APPARATUS

The wave channel as depicted in Figure (2) was designed with a rectangular cross section two feet deep with a width of 15 inches. The channel was fabricated in sections. Each section was composed of two vertical walls and one horizontal floor member. The vertical walls were stiffened by use of three 4 foot long 2 x 4's attached to 3/4 inch x 8 foot x 3 foot sheets of plywood at the ends and middle of its longest dimension. The channel floor member was composed of two 15 inch x 8 foot long plywood sheets separated by a 1 inch x 4 inch strip around the edge. The bottom and side members were mated together with long 3/8 inch threaded rods and formed the basic channel cross section. Six of these 8 foot sections were then bolted together to form the basic channel. Squareness of the channel cross section was maintained by use of spacers placed between the stiffening members near the floor. Every butt joint was given a heavy application of silicone sealant to prevent leakage.

At a location 30 feet from the wave generator end of the channel, a 3 foot wide plexiglass observation window extending the full height of the channel was installed in both walls of the channel as shown in Figure (3). The test cylinder was then mounted in the center of this window.

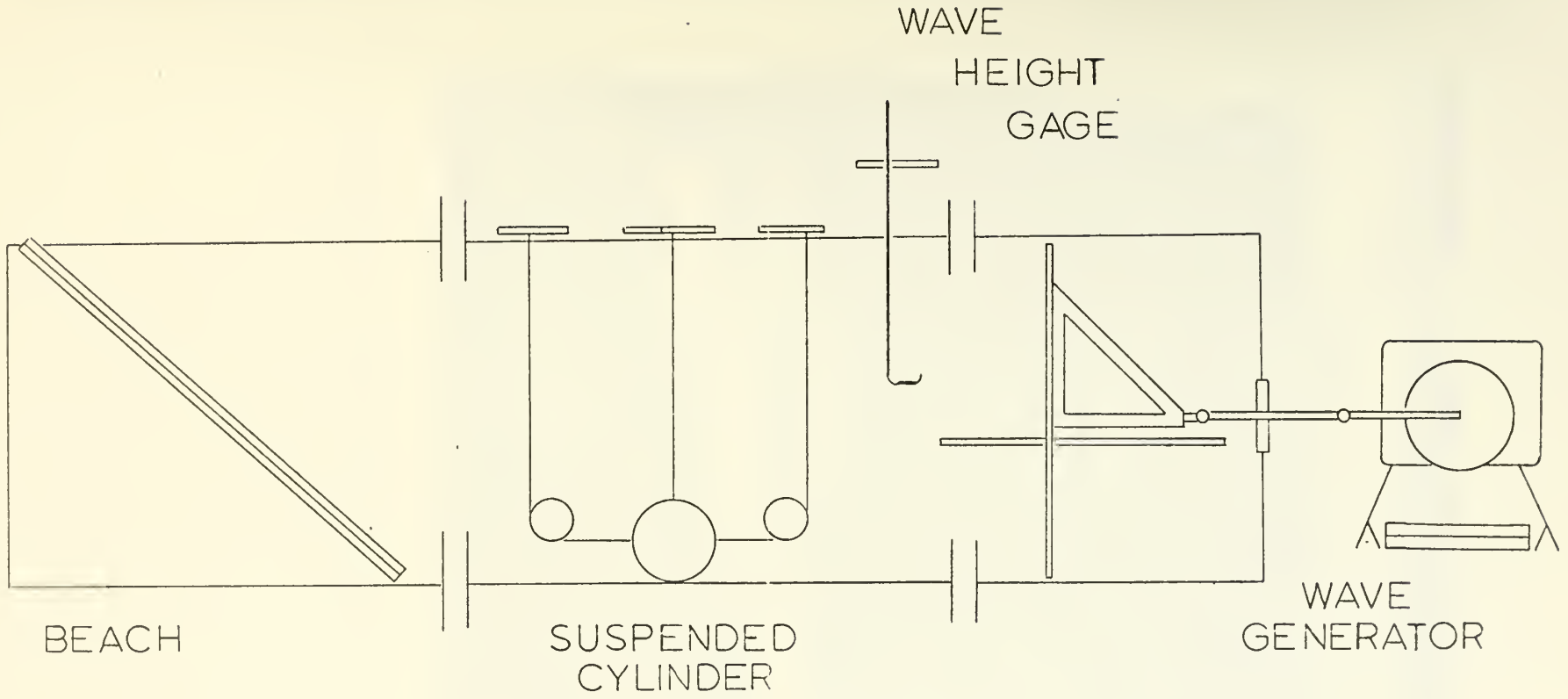

Figure 2. Wave Channel.

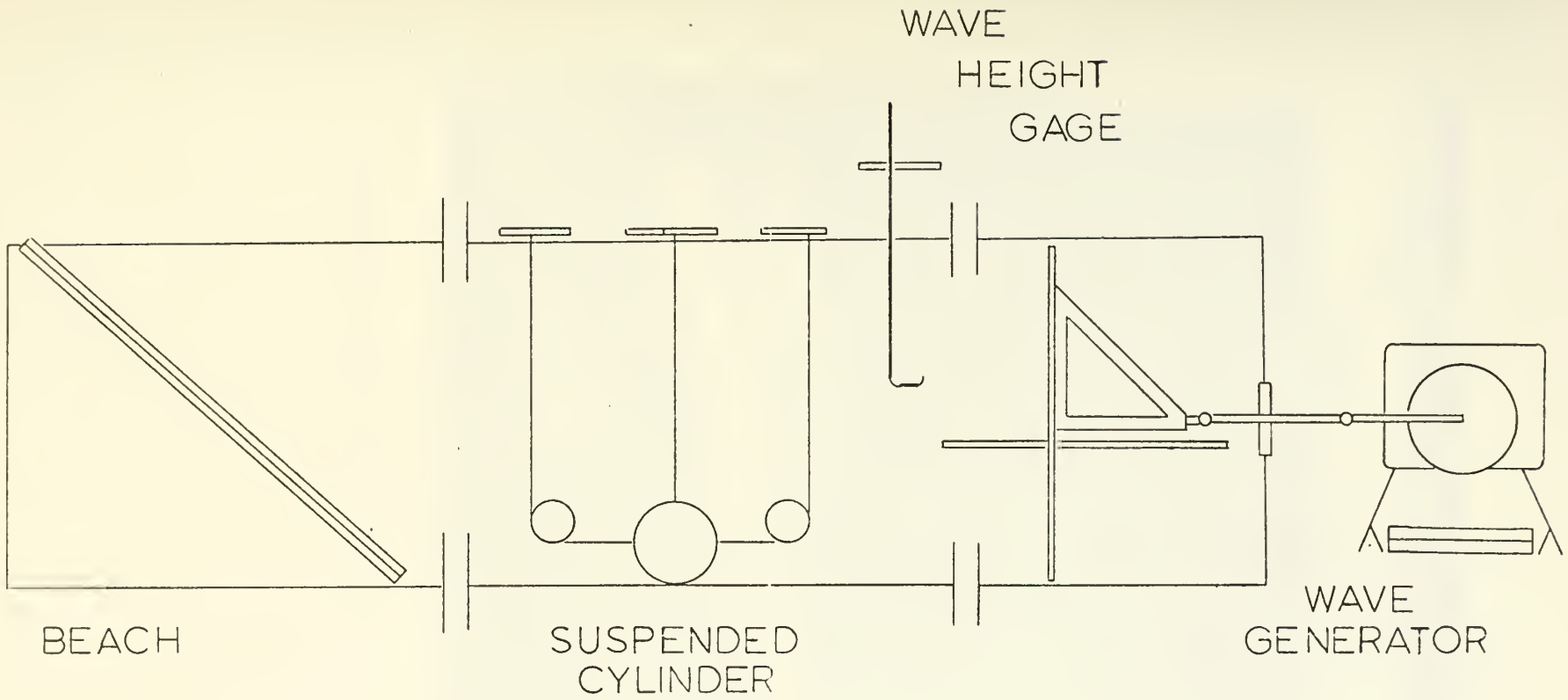

Figure 2. Wave Channel.

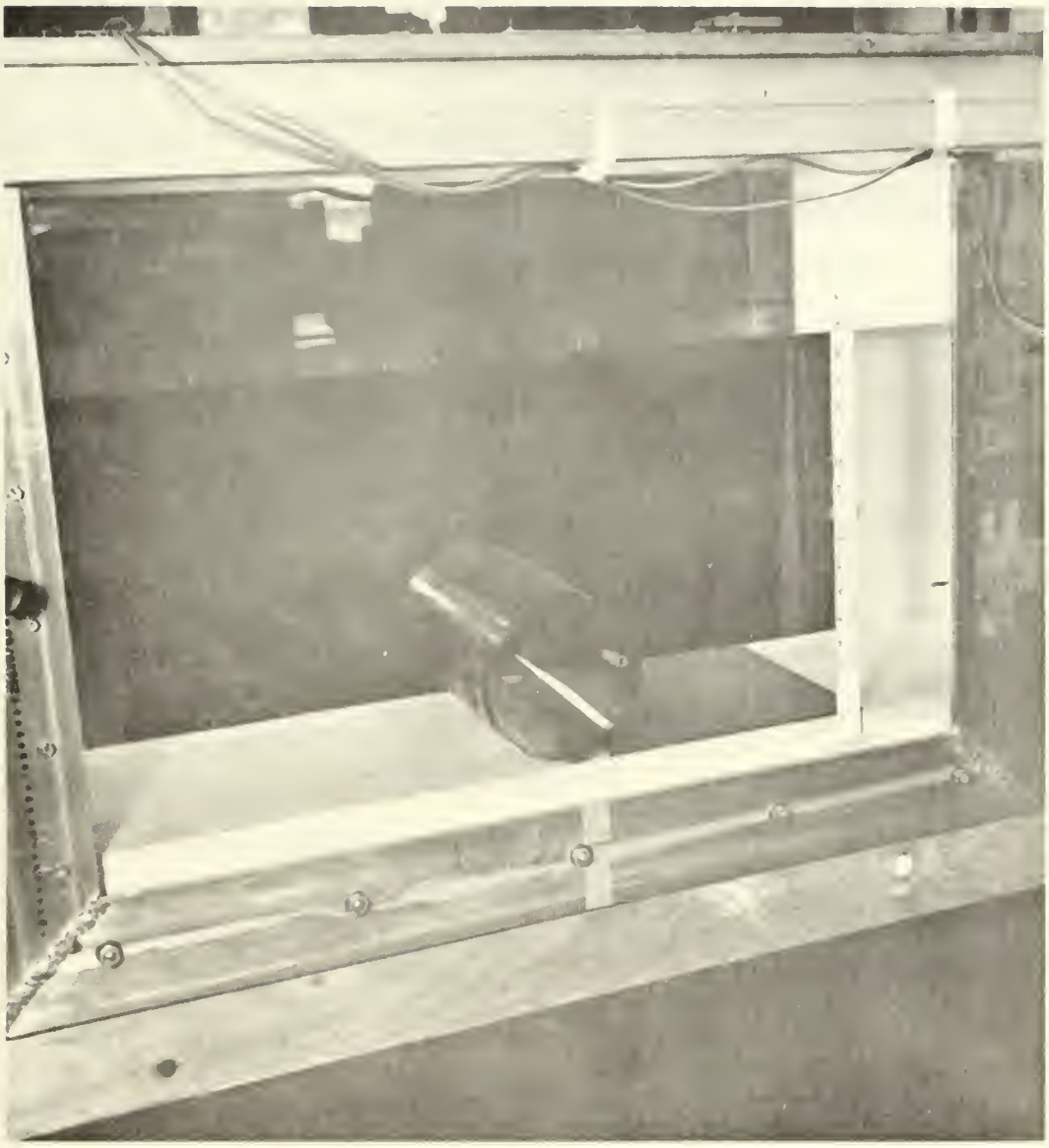

Figure 3. Wave Channel Observation Window.

Dissipation of the generated waves was provided by the beach structure located in the last section of the channel. The beach as shown in Figure (4) consisted of three layers of perforated stainless steel sheeting. Layer separation and structural framing were provided by 2 x 4 runners with their largest cross section dimension perpendicular to the sheeting. The slope of the channel beach was maintained at 6:1.

The wave generating component of the channel as shown in the photograph of Figure (5) had two basic elements, the piston-type plate and the driving motor. The plate was an aluminum sheet 1/8 inch thick with adjustable edges on the vertical sides giving it the capability of adjusting to conform to the sides of the channel. The plate was mounted on a framework attached to 4 slider bearings, and the slider bearings rode on two 1.0 inch brass rods attached to the channel walls. A driving rod was attached to the plate structural members and connected to a flywheel attached to the output shaft of a Vari-Drive motor. The drive rod was attached to the flywheel by means of a bolt and slot in such a manner that the eccentricity could be varied between zero and 6 inches. In this way, waves of various amplitudes could be generated. The variable speed transmission was driven by a 2 hp inductance motor and provided a speed range extending from 22 to 180 rpm giving wave lengths ranging from 18 feet to 1.5 feet at a water depth of 18 inches.

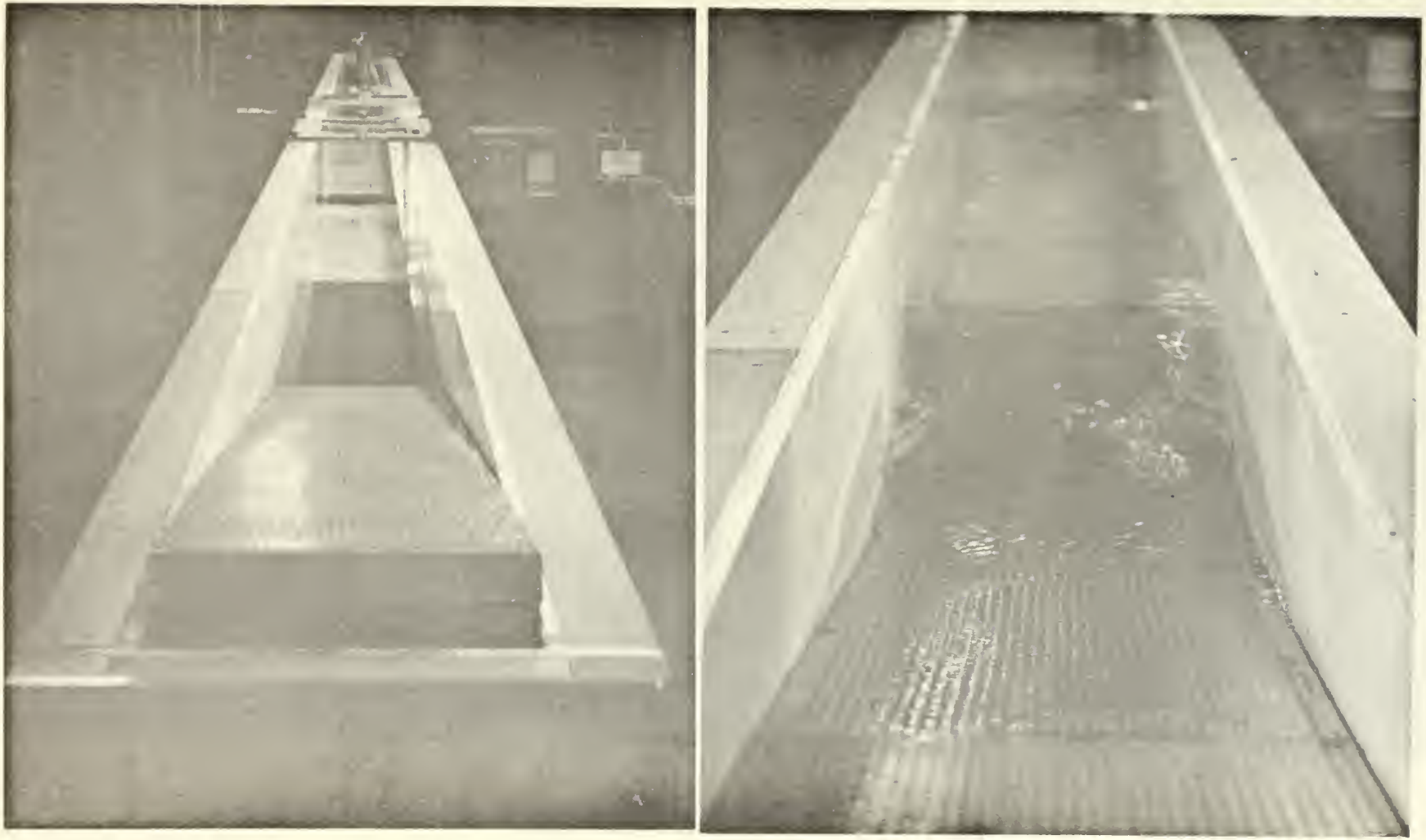

(a) (b)

Figure 4. Views of Channel Beach.

Figure 5. Wave Generator.

A plexiglass circular cylinder of 6 inch diameter with an end clearance of approximately 1/16 inch was used in the test reported herein. As depicted in Figure (6), the cylinder was hung by two fine wires at the appropriate distance off the wave channel floor. Weights were added inside the cylinder to pretension the wires and to prevent slack in the wires during testing.

The upper ends of the wires were attached to small aluminum cantilever beams equipped with strain gages on both the compression and tension side of the beams. These vertical force strain gages were then connected into a Wheatstone bridge and read-out on one channel of a two-channel Sanborn Model 296 amplifier/recorder. The cylinder was restrained in the horizontal direction by similar fine wires connected into a harness and around a 4 inch diameter ball bearing pulley mounted on the wave channel floor as shown in Figure (7). These wires were then attached to a pair of cantilever beams equipped with strain gages, and the strain gages were connected into a Wheatstone bridge and read-out on the second channel of the two-channel amplifier/recorder.

The four beams, two for the vertical force and two for the horizontal force, were attached to a plywood mounting board positioned over the channel as shown in Figure (8). The beams were all exactly alike, and the section of the beams where the strain gages were mounted was reduced to a cross section of 1/4 x 1/4 inches from a nominal beam cross

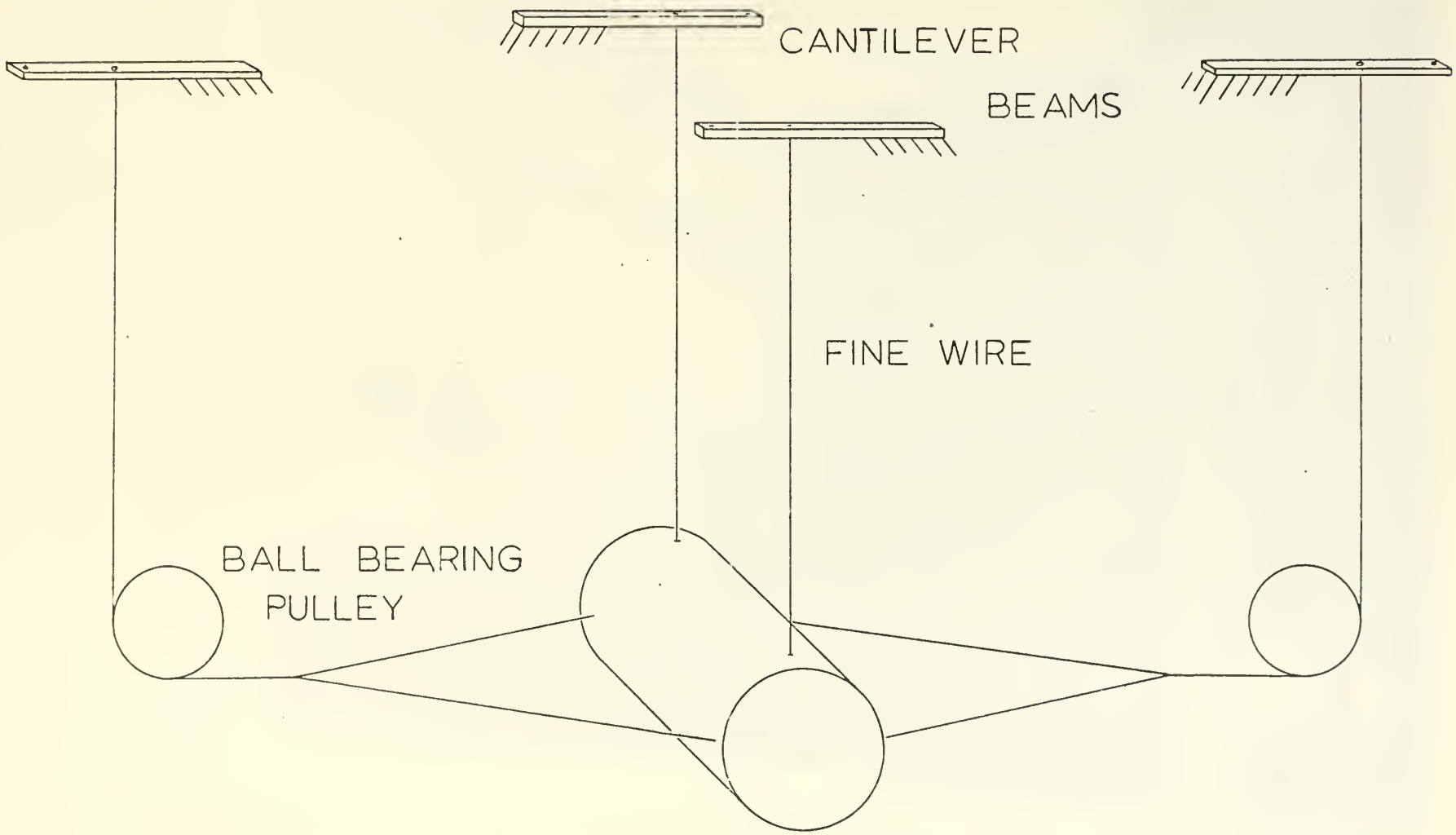

Figure 6. Cylinder Suspension System.

Figure 7. Horizontal Wire Harness and Pulley Assembly.

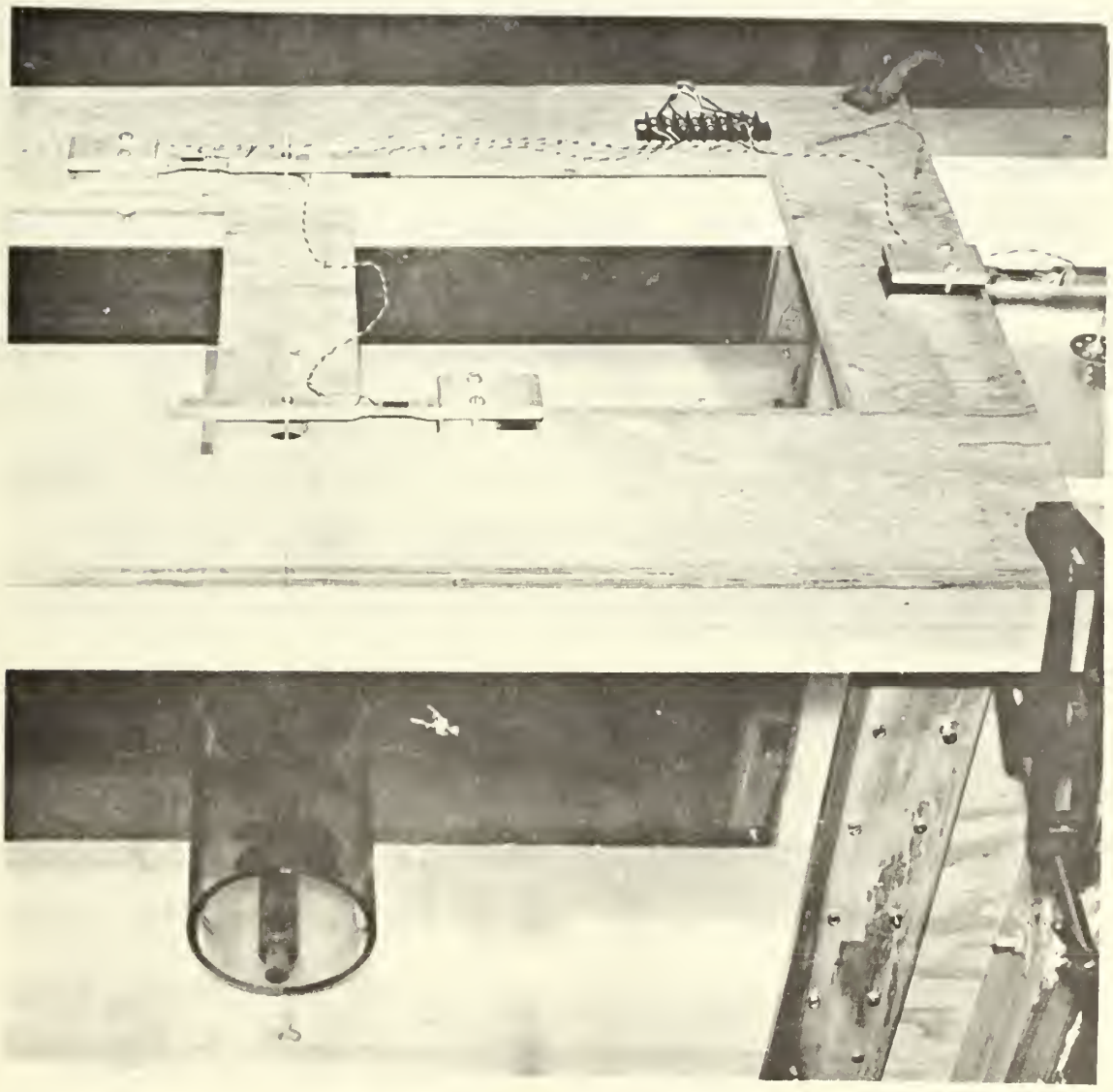

Figure 8. Beam Mounting Board.

section of 1/2 x 3/8 inches. The machining provided a smooth transition into the area of stress concentration. SR-4 FAE-25-12S13 strain gages were applied to the top and bottom surfaces of the beams. Each beam was 9 inches long and had mounting holes for two moment arm positions, one at 6 inches and one at 3 inches from the strain gage location. This variable load attachment point gave each beam a sensitive force measurement capability under a large range of values. The beams were designed to withstand a six-pound load at the largest moment arm.

The wave height gage, as shown in Figure (9), consisted of a small diameter aluminum rod acting as the basic frame to which a plexiglass mounting table was attached. The elements of the Wheatstone bridge were mounted on this table, and two 30-gage copper wires spaced 1/2 inch apart were extended from the table and attached to an insulator mounted at the end of the aluminum rod. An 18-inch separation between the levels of the table and insulator provides a large measurement range capability. The other end of the rod was mated to a traverse block stand which allowed the gage to travel ± 6 inches, and provided a convenient, yet accurate, means for calibration by adjusting the submergence of the wires. The complete unit was positioned over the channel and centered at approximately 5 feet in front of the cylinder.

The wave height probe was of the parallel wire resistance type. This type of gage operates on the principle

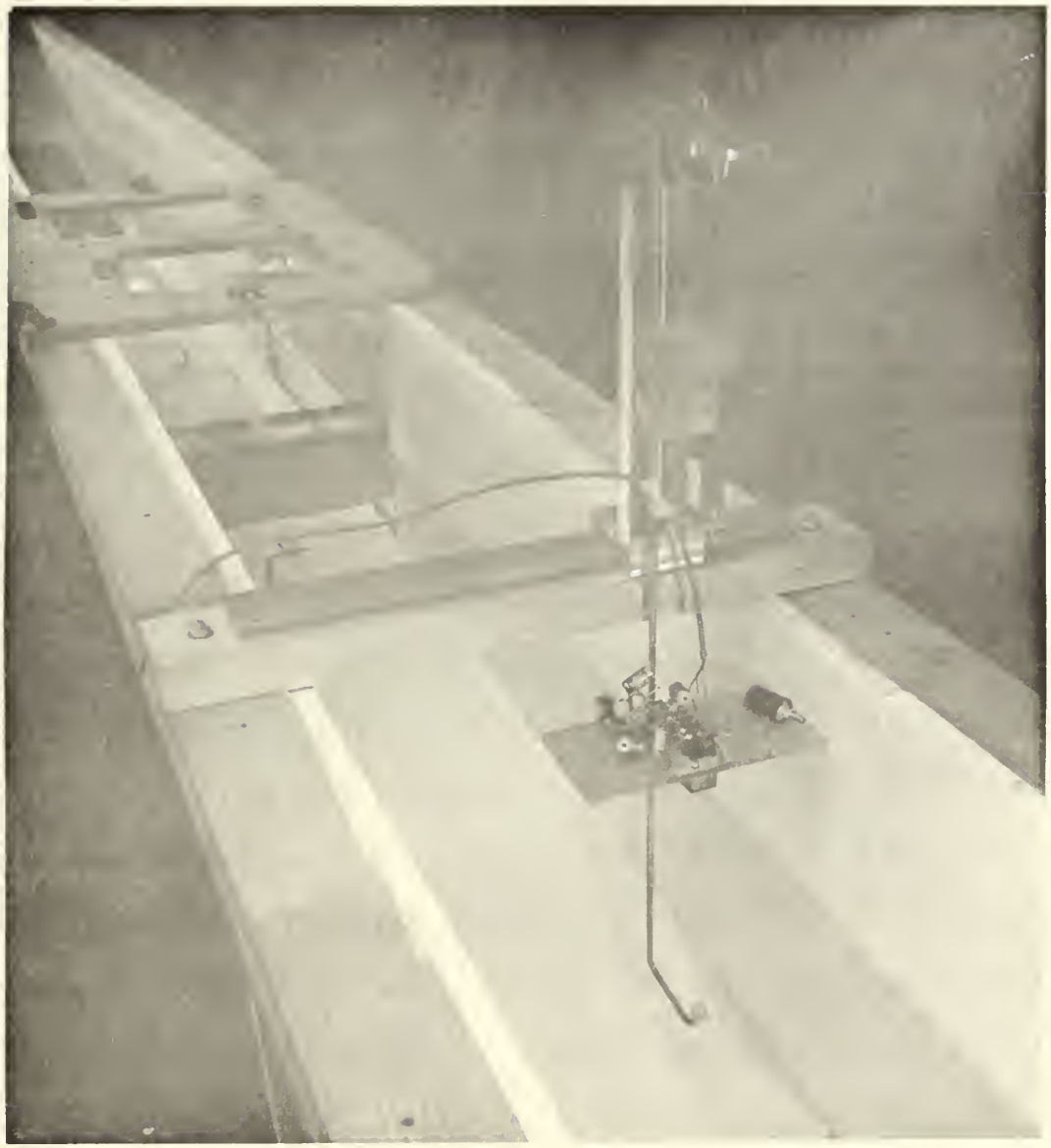

Figure 9. Wave Height Gage.

that the conductance between the two parallel submerged wires varies approximately proportionately to the length of wire submerged. The wave gage was connected in parallel to one leg of a Wheatstone bridge as depicted in Figure (10). To compensate for the inability of the carrier amplifier to offset the resistance of the immersed parallel wires, an external variable 10K ohm potentiometer was connected across an opposite leg of the bridge. This resistor was used for coarse balancing of the bridge. The Wheatstone bridge was connected via signal and excitation leads to a portable carrier preamplifier and read out on a one-channel H/P Sanborn 301 amplifier/recorder.

During preliminary operation while attempting to clear the problems from the system, it was found that installation of an impermeable wall between cylinder and channel floor was a necessity. The experiment was designed to simulate the placement of the circular cylinder on the bottom, but it was necessary to maintain a small but finite gap between cylinder and the bed of the channel to insure that the pair of wires connected to the cantilever beams provided the sole vertical support. However, it was found that the vertical forces as well as, to a lesser extent, the horizontal forces were strongly dependent on the gap width. Flow visualization studies showed that a high velocity jet occurred in the small gap under the cylinder. Thus, in order to eliminate the flow under the cylinder and yet not influence the force measurement system, a flexible plastic sheet was installed across the gap between the

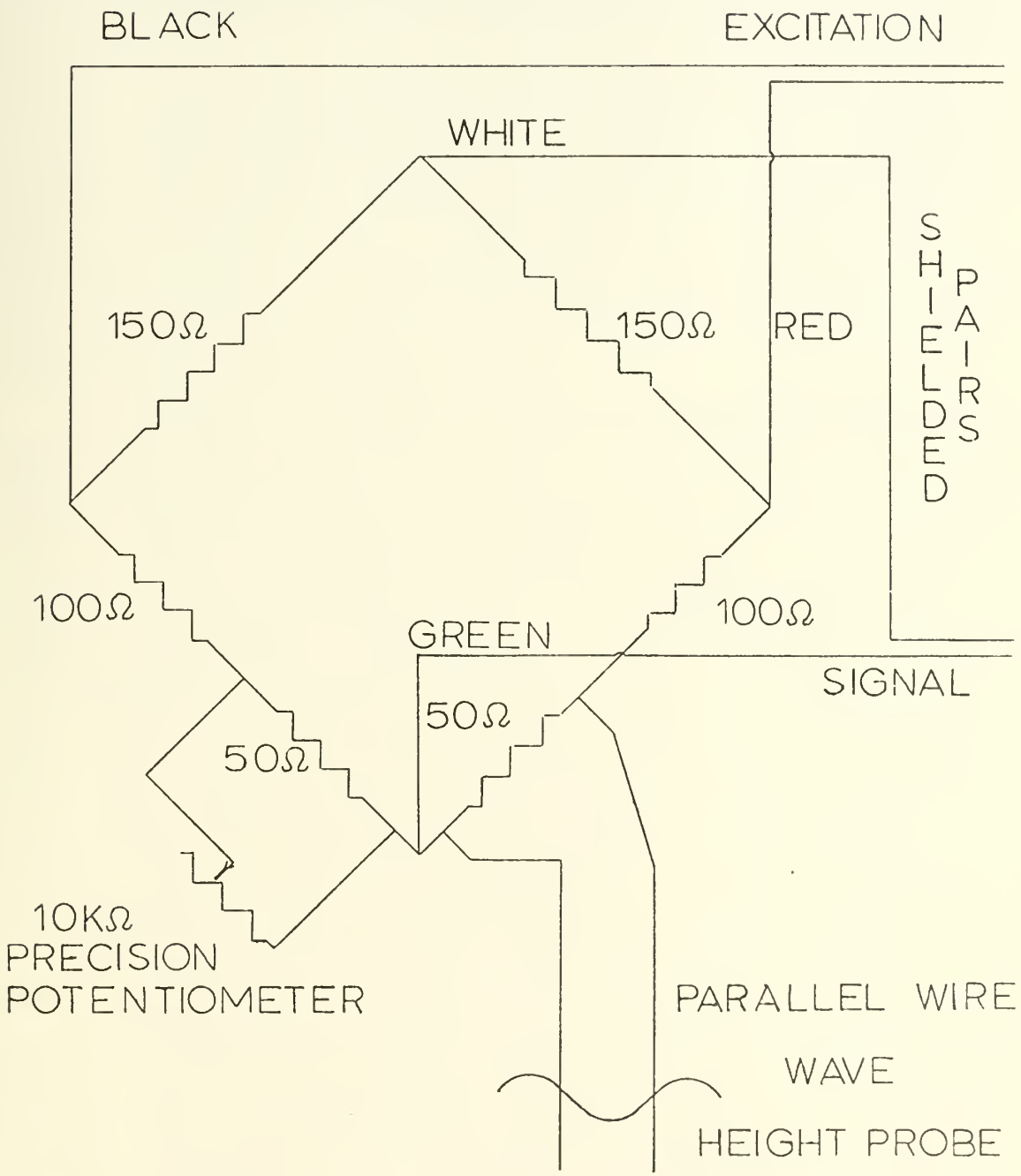

Figure 10. Wave Height Gage Bridge Schematic.

cylinder and floor. The sheet was joined to the cylinder by pressing the plastic into a machined slot in the cylinder wall, and then anchoring it with a length of "O"-ring. The other end of the plastic was laid under a metal sheet 12 inches x 14 1/2 inches and 1/16 inch thick and placed at the channel bottom as shown in Figure (11). The gap between the cylinder and floor was adjusted to approximately 1/8 inch. This gap was found to be large enough to insure that the cylinder never touched the bottom when subjected to the largest wave.

In order to demonstrate the rather large influence of this small gap under the cylinder, Figure (12) was prepared showing both the maximum horizontal and vertical force as a function of wave amplitude. It is apparent from this figure that removal of the plastic barrier had the effect of reducing the maximum horizontal force a slight amount. With the barrier in place, the upward force was generally quite large while the downward force was rather small. However, upon removal of the barrier, a rather high velocity flow through the gap was observed by injection of dye near the wave channel floor, and this local region of high velocity apparently resulted in low pressures on the underside of the cylinder causing the downward force to be increased considerably. The rather extreme effect of the gap is clearly demonstrated by comparison of the various curves indicated on Figure (12).

Figure 11. Barrier Assembly and Wave Profile.

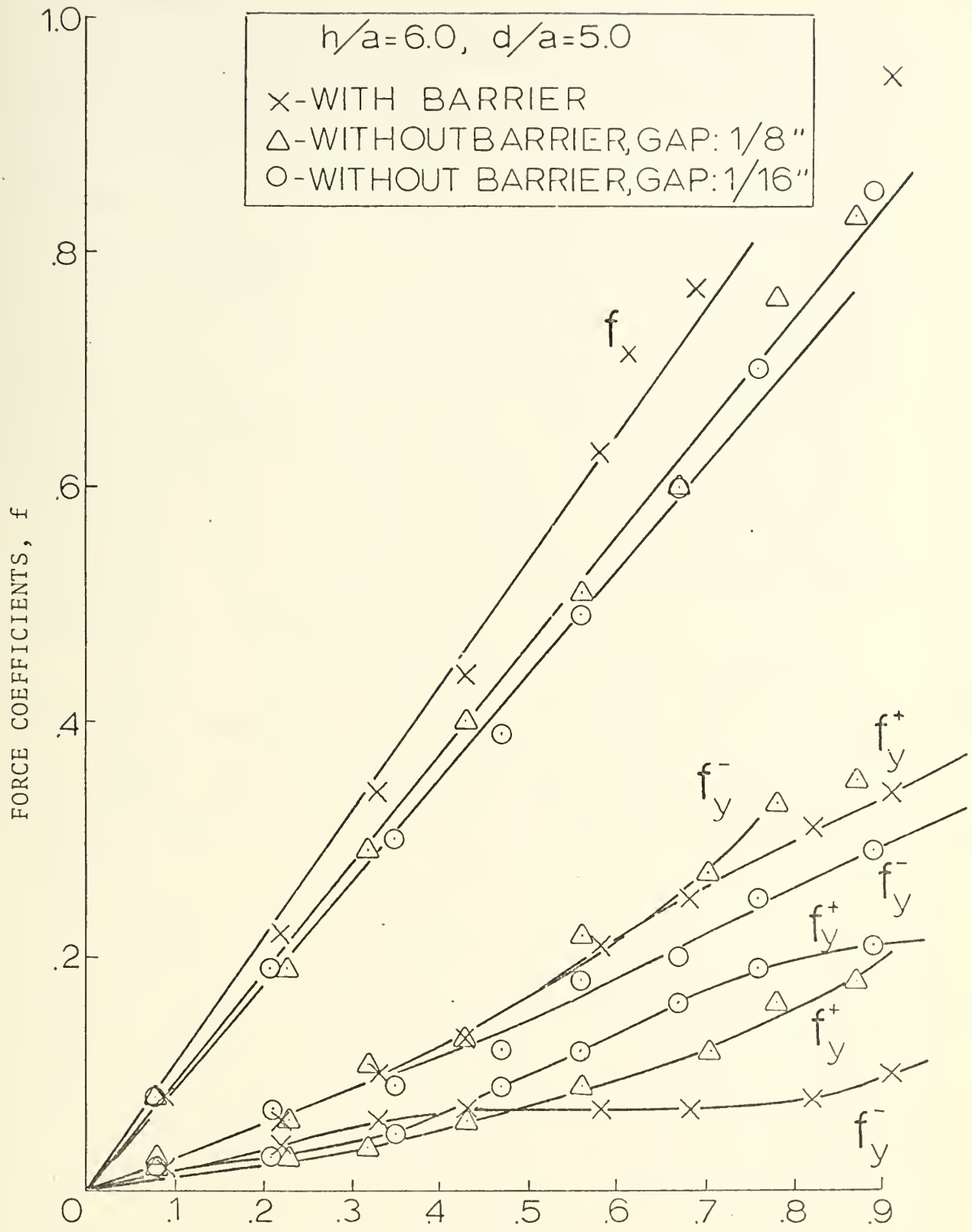

Figure 12. Comparison of Wave Force Coefficients Showing the Effect of the Barrier.

Inasmuch as the intent of the present study was to determine wave forces on a cylinder lying on the bottom wherein the gap would not be present, the plastic barrier was maintained in place throughout the test program for all cases where the cylinder was placed near the bottom.

B. TEST PROCEDURE

The first step in the test procedure was to fill the wave channel with water to obtain the desired water depth to cylinder diameter ratio, h/a. Experiments were conducted at the three depths, 12, 15, and 18 inches. After the desired water level was attained, a careful inspection was carried out to insure that all equipments were properly prepared for operation.

The vertical wire position screws were adjusted to obtain the desired elevation of the cylinder off the channel bottom. The horizontal wires were pretensioned to prevent slacking and the attendant errors in force measurements.

A typical run may be described as follows. With water adjusted to the proper depth, a given wave length, or equivalently, wave period was established by setting the speed of the Vari-Drive unit. Subsequent to a sufficient warm-up period, the amplifier/recorders shown in Figure (13) were balanced and readied for calibration. Calibration of the three recording channels, horizontal force, vertical force, and wave height was carried out at the attenuation expected

Figure 13. Experimental Equipment.

to be in use during the run. After calibration, the wave height was set by adjusting the eccentricity of the wave generator to the appropriate amplitude. The wave generator was then turned on, and after a steady state wave was established in the channel, the recorders were turned on and data was taken. The wave generator was then switched off, and the next wave height was set on the flywheel eccentric while maintaining the same speed setting. Wave heights at the fixed wave length were varied within the capability of the system to produce representative readings usually ranging from approximately 1/4 inch to 5 inches. At the conclusion of each series of runs at a given wave length, a check calibration on the three channels was quickly carried out. Then, a new wave length was selected and set on the Vari-Drive, and the cycle of balancing, calibration, wave height selection, and wave production was repeated.

Calibration was performed on the load cells as follows. The recording chart was set at 1^{mm}/sec. speed, and loads in one-pound steps were placed on the saddles located beneath and hung from the horizontal sensing wires as shown in Figure (14). Calibration loads were placed initially on the after beam, then on the forward beam. The vertical load cell was calibrated by use of a platform of known weight centered on the cylinder as shown in Figure (15). Weights were then placed on this platform.

Wave height gage calibration was performed by adjusting the vertical position of the gage through the use of a slider bearing and screw. The procedure was carried out as follows.

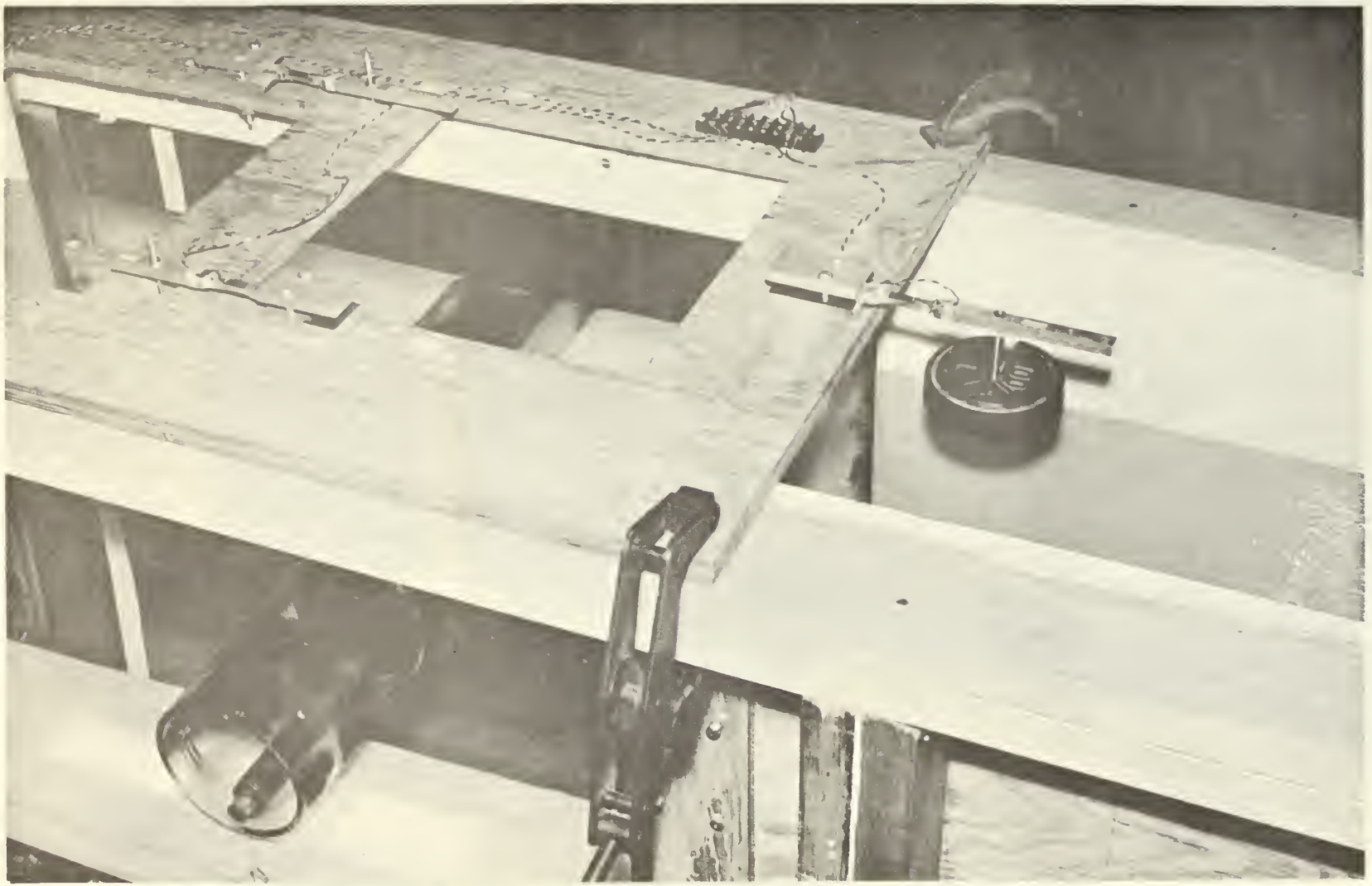

Figure 14. Horizontal Force Calibration Operation.

Figure 15. Vertical Force Calibration Operation.

The gage was raised 1/2 inch, simulating a decrease in water level, then lowered 1/2 inch below the null, simulating an increase in water level. Then, the gage was raised +1 inch and lowered -1 inch, etc. This procedure closely simulated the actual passage of a wave profile with crests and troughs. The generated wave crest passing through the test location is shown in Figure (11).

IV. EXPERIMENTAL RESULTS

As indicated in Equation (3) in the THEORETICAL CONSIDERATIONS, the wave force coefficients can be represented as functions of relative water depth, relative depth of submergence, relative wave length, and relative wave height parameters. Accordingly, a test program was devised to measure the wave force coefficients for practical ranges of the independent parameters. Four series of tests were conducted at different water depths and depths of submergence. Three of these corresponding to depth to cylinder radius ratios of 4.0, 5.0, and 6.0, were carried out with the cylinder near the bottom, i.e., at d/a= 3.0, 4.0, and 5.0, respectively. A fourth series of tests was conducted with the cylinder raised one radii off the bottom corresponding to d/a= 4.0 at a water depth ratio of 6.0.

A. TYPICAL WAVE FORCE TRACES

Inasmuch as it is difficult to completely characterize the force variations with a single number, typical strip chart read-outs for the various series of tests are presented in Figures (16-28). Figures (16-19) show the horizontal and vertical force variations with the cylinder on the bottom corresponding to a relative depth of submergence of d/a = 5.0 and a relative water depth ratio of h/a= 6.0. The figures are arranged according to increasing values of the wave length parameter ranging from $2\pi a/L$= 0.09 to 0.97.

On each figure, data corresponding to four values of relative wave height are presented in ascending order.

Figure (16) representing the largest wave length and having a depth to wave length ratio of h/L= 0.08 corresponds to waves which are somewhat outside the sinusoidal range. These long waves are characterized by long, smooth troughs and sharp crests. Accordingly, the horizontal force traces are characterized by positive and negative peaks which result from the maximum acceleration occurring on either side of the crest. These two peaks are followed by a relatively flat portion of the force trace corresponding to the long, smooth trough portion of the wave. As can be seen from the figure, this kind of variation appears to predominate even as the wave height is increased for this long wave case.

The vertical force, however, shows a much more inconsistent variation. If the system natural frequency is disregarded, definite upward peaks are observed at points on the trace corresponding to the wave crests. These peaks are apparently related to the reduced pressure over the upper portion of the cylinder which is associated with the velocity squared term in the Bernoulli equation since the maximum velocity occurs at the crests. In sinusoidal waves, an equal and opposite velocity occurs at the troughs which would naturally give rise to a second upward peak in the force trace. However, in shallow water waves, the velocity associated with a trough is much reduced and, therefore peaks corresponding to the crests only are observed.

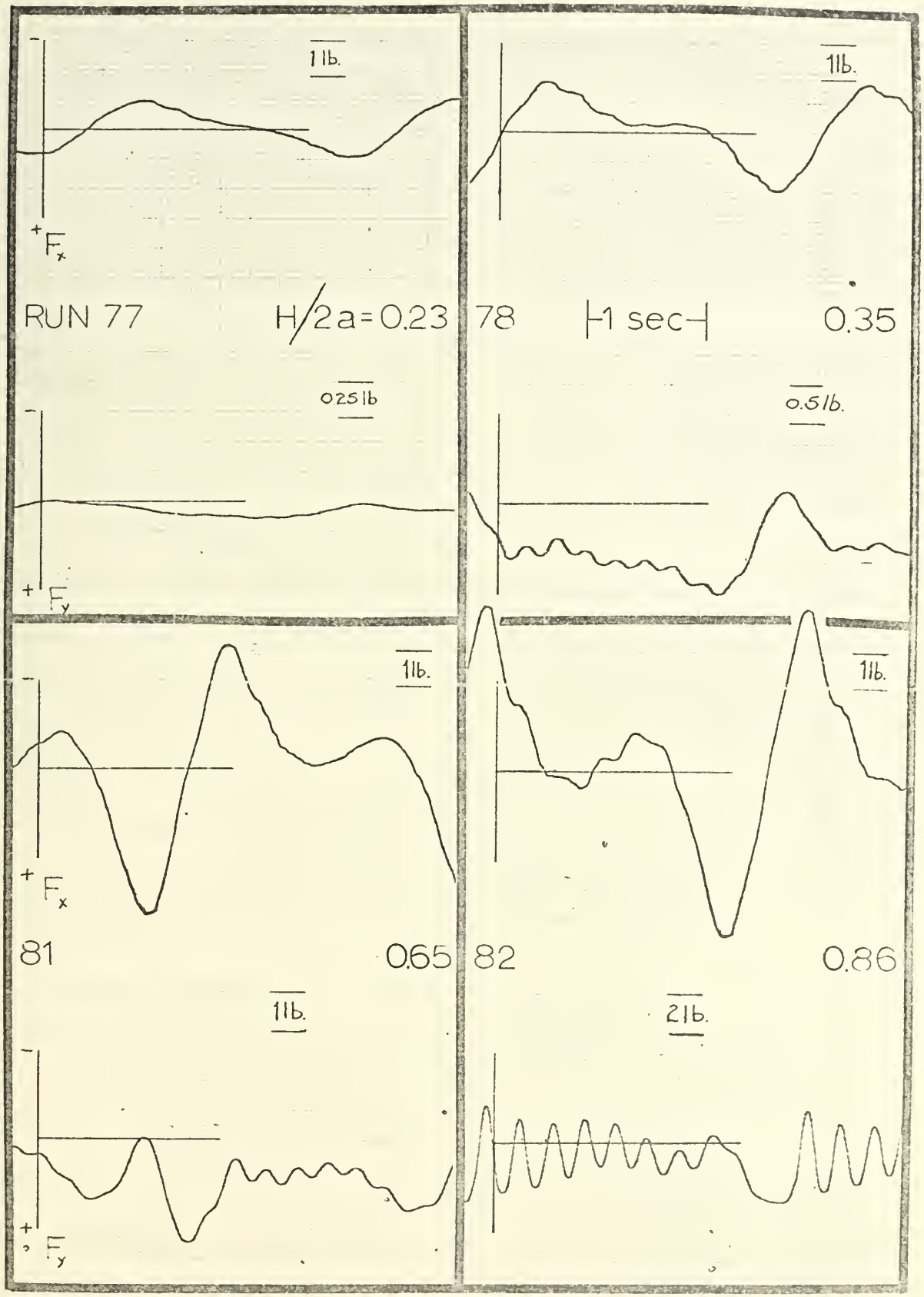

Figure 16. Wave Force Trace, h/a= 6.0, d/a= 5.0, $2\pi a/L$= 0.09.

Figure (17) corresponds to a shorter wave length having a relative wave length value of $2\pi a/L = 0.16$. It is apparent from the figure that both the horizontal and vertical forces vary sinusoidally for the smallest amplitude wave corresponding to $H/2a = 0.5$. As the wave height is increased, it is apparent that the horizontal force continues to vary sinusoidally for the full range of amplitudes. The vertical force, however, shows a sinusoidal variation for the smallest amplitude waves and becomes increasingly less sinusoidal as the wave height is increased. Moreover, two separate peaks appear to develop on the vertical force trace as wave height increases, one associated with the maximum velocity occurring at the crest and the other associated with the trough. The maximum velocity at both the crest and the trough results in reduced pressures on the upper portion of the cylinder and, consequently, corresponds to upward vertical forces.

Figures (18) and (19) correspond to still smaller wave lengths of $2\pi a/L = 0.24$ and 0.77, respectively. It may be noted that again the horizontal force shows a sinusoidal variation throughout the range of wave amplitudes while the vertical force shows the sinusoidal variation at small amplitudes becoming non-sinusoidal as the amplitude is increased. Figure (19), however, which corresponds to the shortest wave lengths shows sinusoidal variations throughout the range of wave amplitudes for the horizontal as well as vertical force.

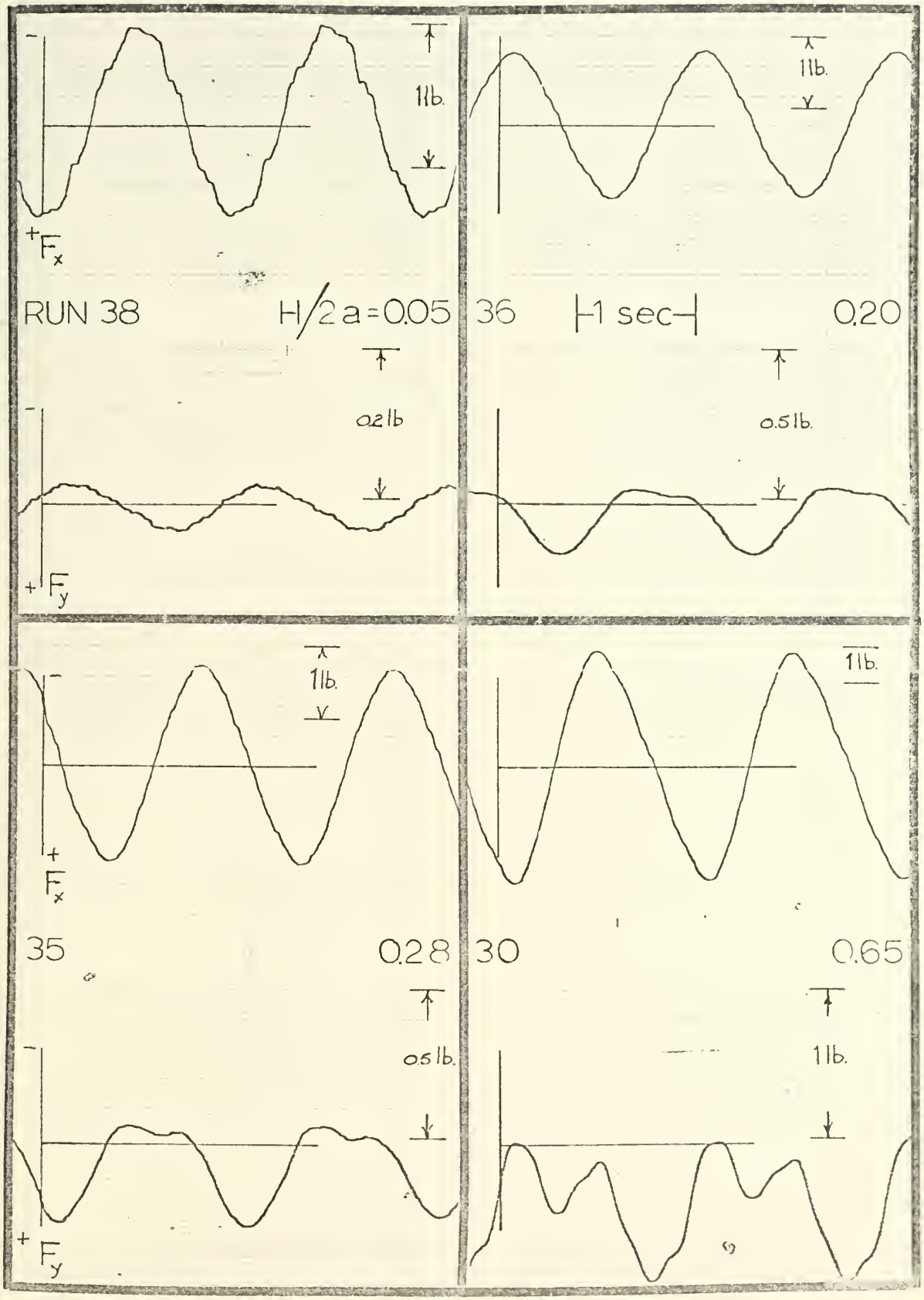

Figure 17. Wave Force Trace, h/a= 6.0, d/a= 5.0, $2\pi a/L$= 0.16.

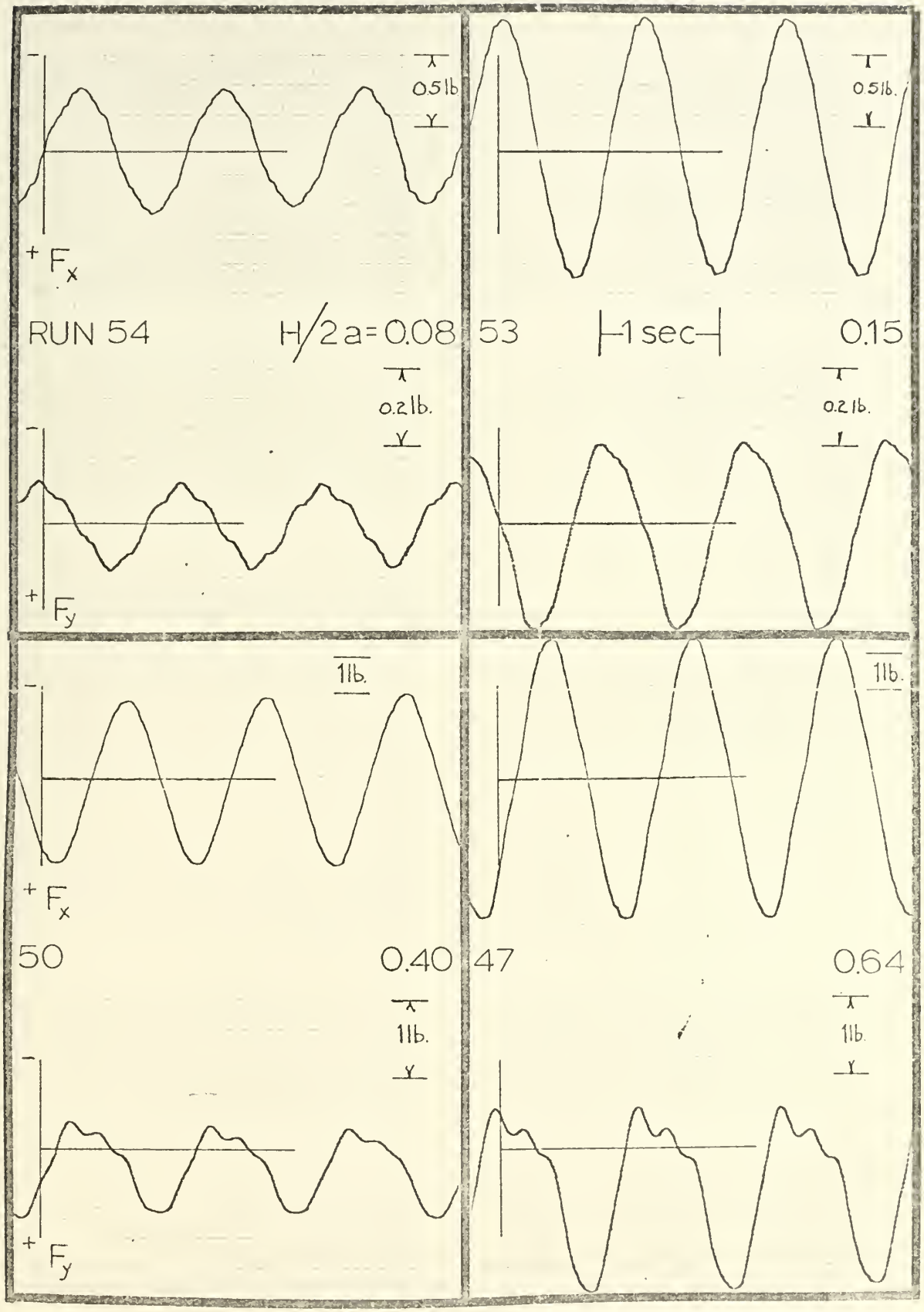

Figure 18. Wave Force Trace, h/a= 6.0, d/a= 5.0, $2\pi a/L$= 0.24.

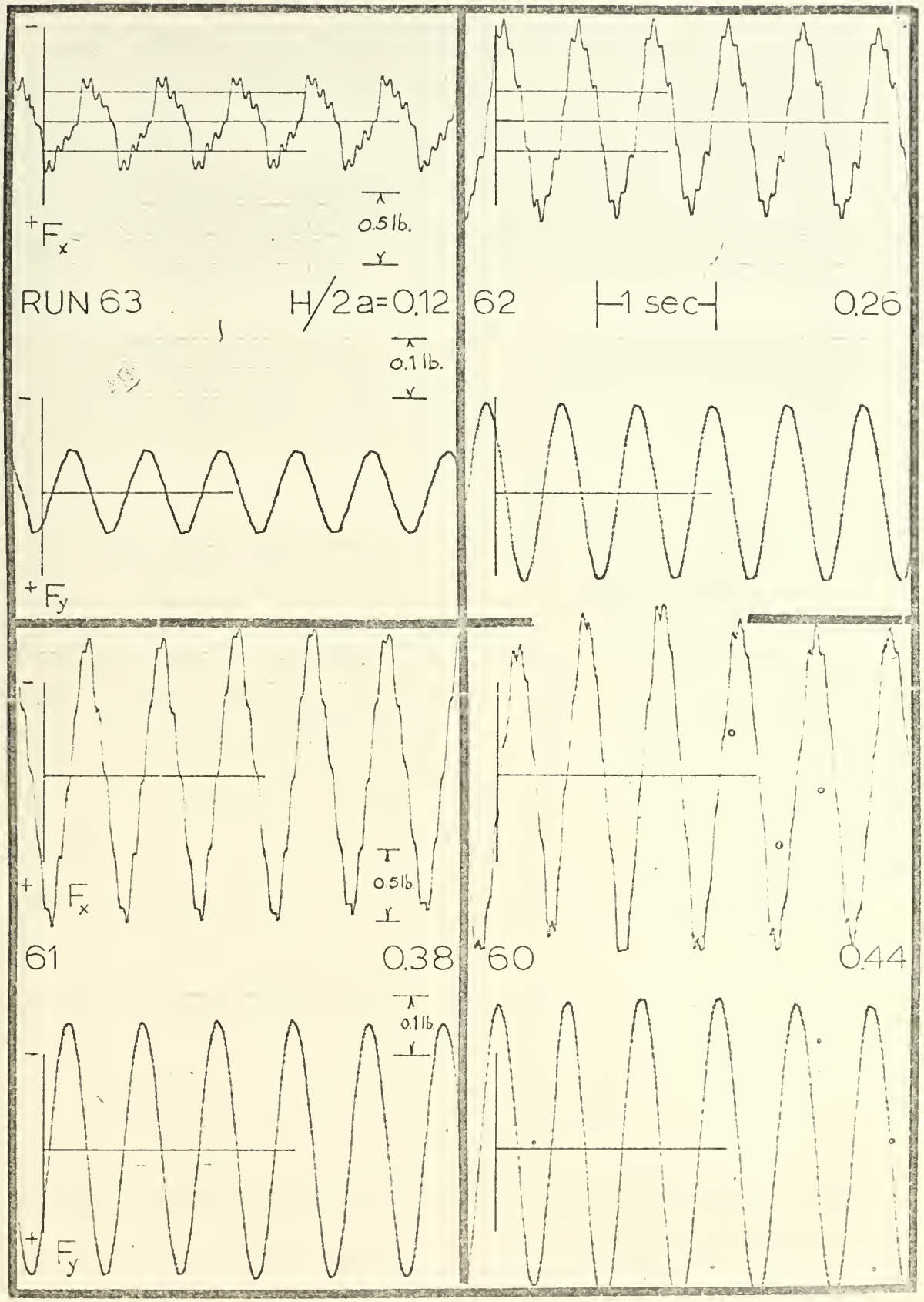

Figure 19. Wave Force Trace, h/a= 6.0, d/a= 5.0 $2\pi a/L$= 0.77.

Horizontal and vertical force coefficients corresponding to relative water depth of h/a= 5.0 with the cylinder on the bottom, i.e., d/a= 4.0 are shown in Figures (20-22). These three figures represent three different values of relative wave length extending from $2\pi a/L$= 0.10 to 0.67. The general trends tend to be similar to those corresponding to the larger depth of h/a as shown in Figures (16-19) and previously discussed. Data corresponding to the smallest value of $2\pi a/L$ as presented in Figure (20) shows trends typical of nonlinear shallow water waves. The horizontal force shows the null period associated with the long, smooth troughs, while the vertical force is characterized by the upward force peak corresponding to the wave crests. As the wave length is decreased, the horizontal force again displays sinusoidal variation as indicated in Figures (21) and (22). For the shorter wave lengths, the vertical force shows a sinusoidal variation at small amplitudes with superimposed upward peaks occurring near the maximum velocity location at the crests and troughs. Figure (22) corresponding to the shortest wave length shows a sinusoidal variation for both force components throughout the range of wave heights.

Typical force variation records for the series of tests conducted at h/a= 4.0 are presented in Figures (23-25). Three representative values of relative wave length, $2\pi a/L$= 0.11, 0.21, and .45 are presented. Figure (23) shows variations similar to those of equal values of $2\pi a/L$ at the two larger depths already discussed. Figures (24) and (25) are

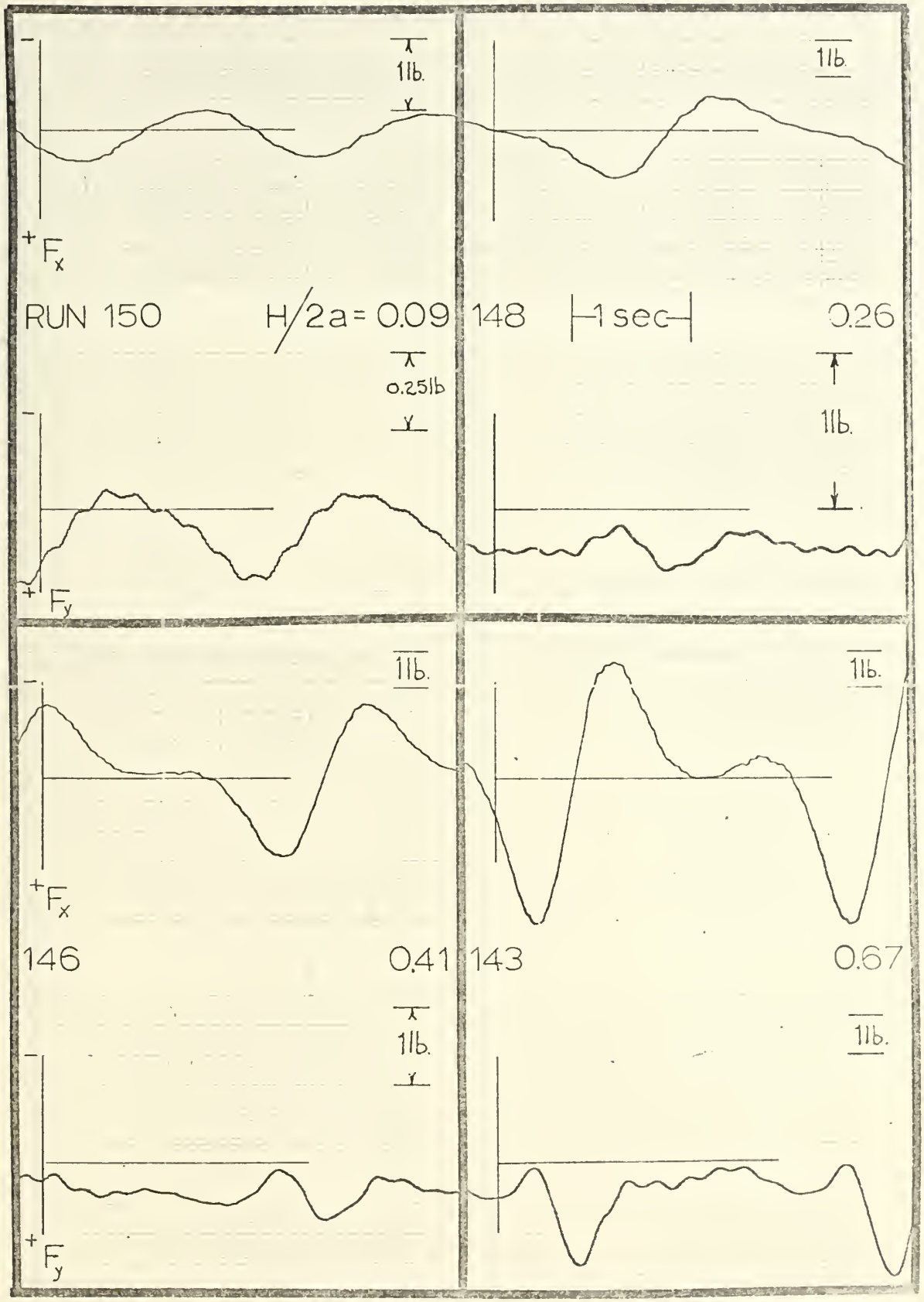

Figure 20. Wave Force Trace, h/a= 5.0, d/a= 4.0, 2πa/L= 0.10.

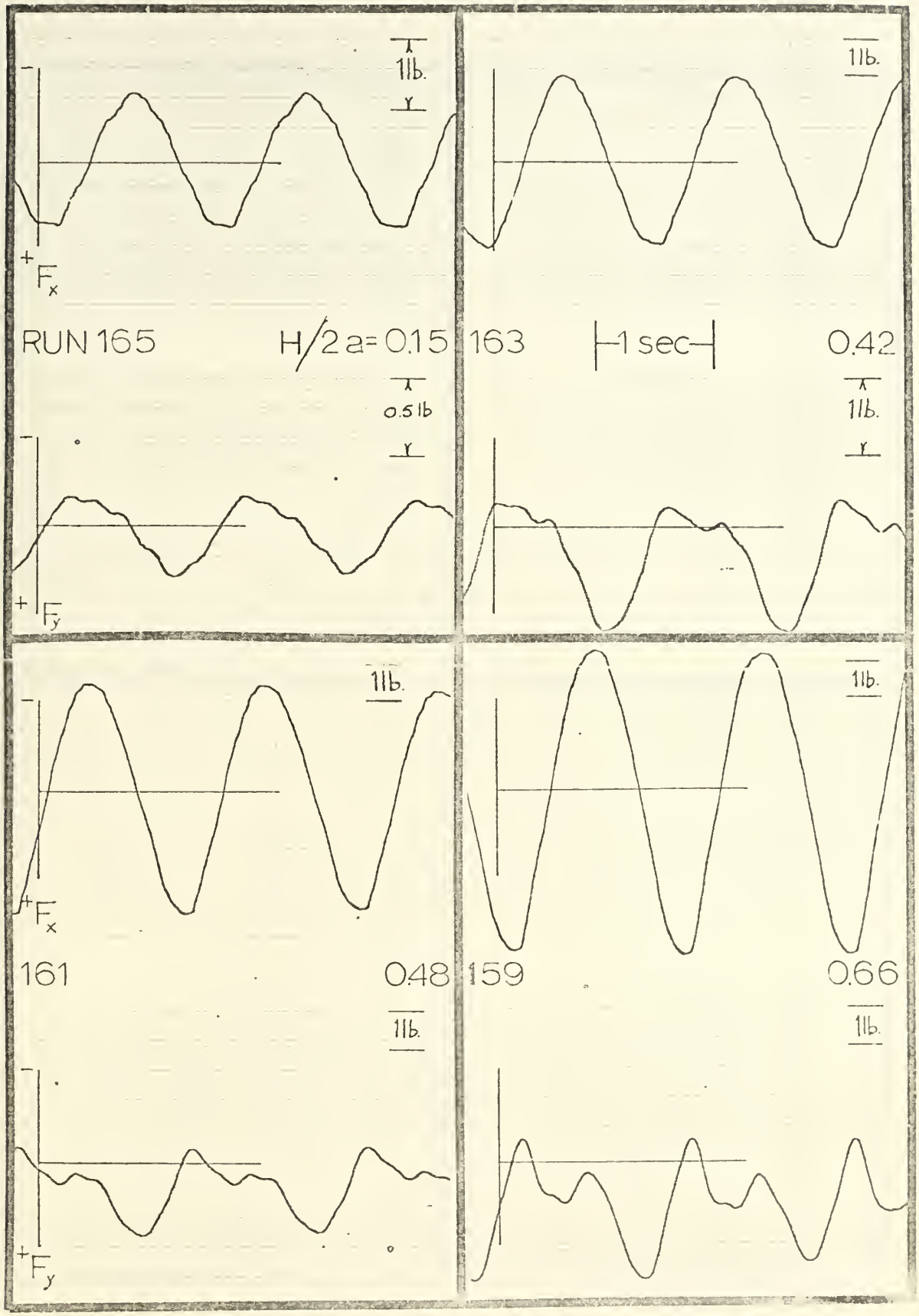

Figure 21. Wave Force Trace, h/a= 5.0, d/a= 4.0, $2\pi a/L$= 0.19.

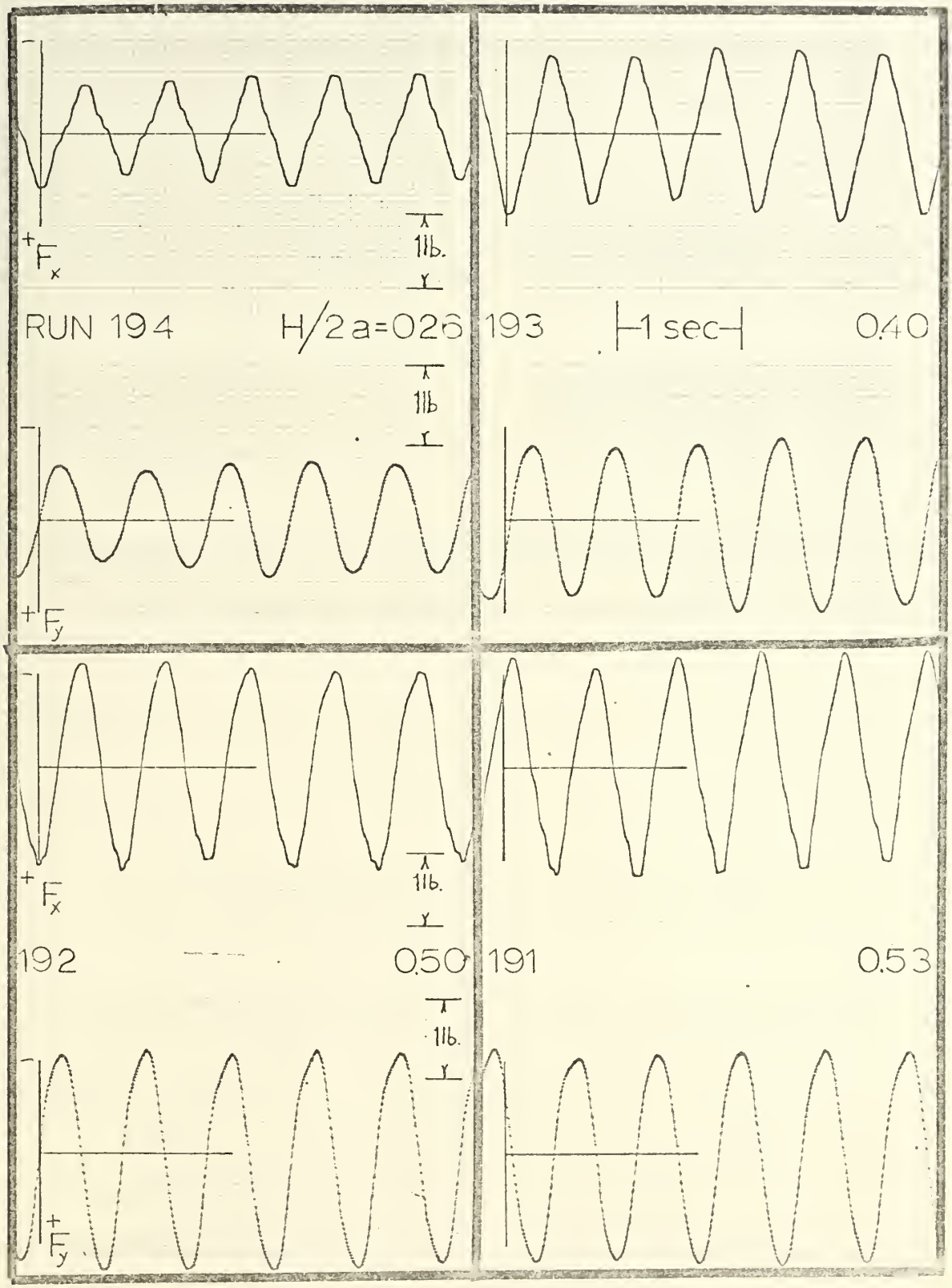

Figure 22. Wave Force Trace, h/a= 5.0, d/a= 4.0, 2πa/L=0.87.

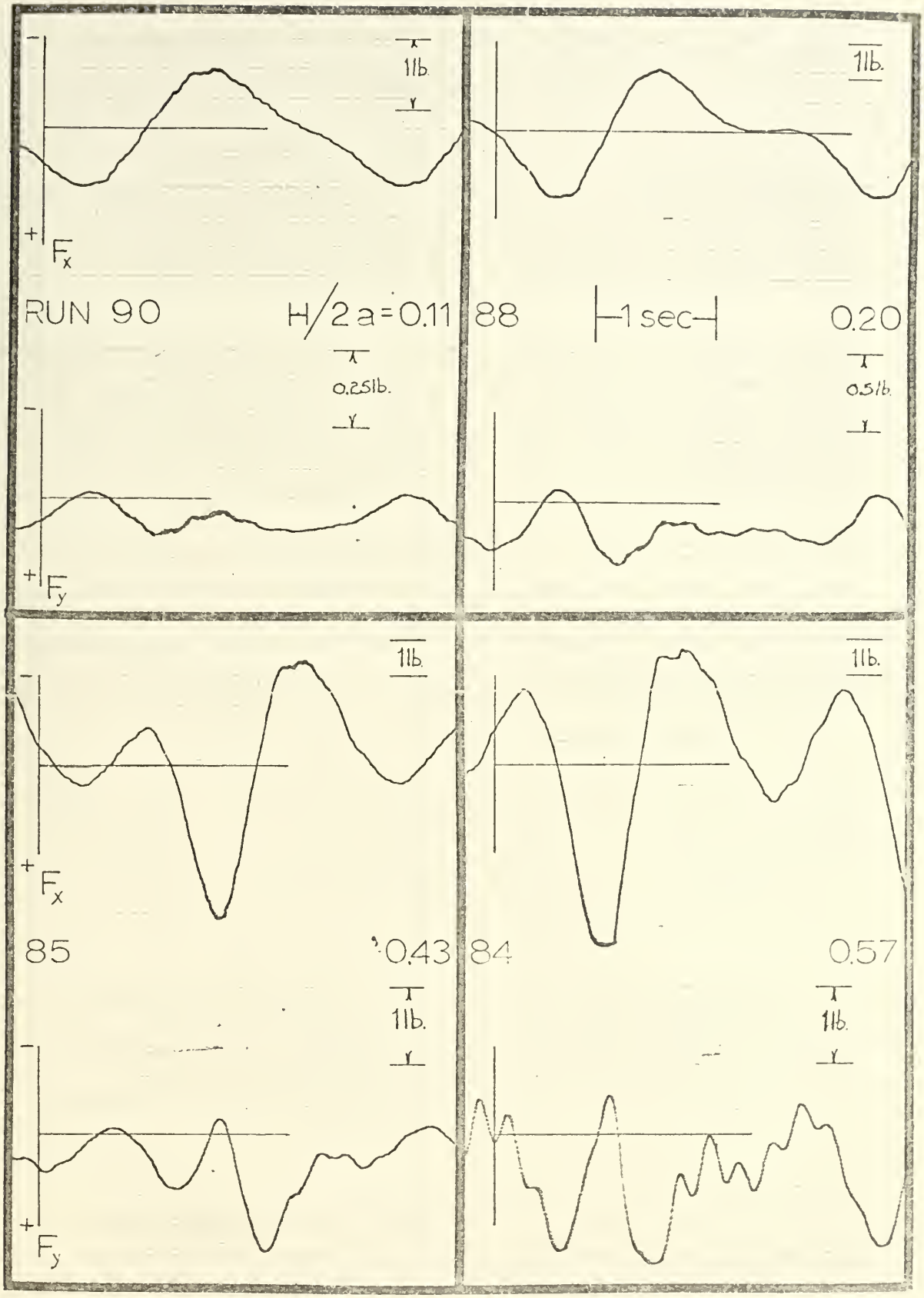

Figure 23. Wave Force Trace, h/a= 4.0, d/a= 3.0, $2\pi a/L$= 0.11.

also similar to previous runs, the primary difference being the increased magnitude occurring at the smaller depths.

The final series of runs was carried out at a relative water depth ratio of h/a= 6.0 with the cylinder suspended one radii off the bottom, i.e., d/a= 4.0. Typical force traces at three different values of relative wave length, $2\pi a/L$= 0.10, 0.16, and 0.6, are presented in Figures (26), (27), and (28), respectively. The horizontal force trace as shown on the figures reflects the same general trends as the previously described series. The vertical component of force also shows trends similar to those previously discussed with the cylinder on the bottom, but the peaks associated with maximum velocity in the wave occurring at the crests and troughs are seen to be in the opposite direction. That is, the velocity of the fluid through the one radii gap between the cylinder and the floor is apparently considerably larger than the velocity through the space above the cylinder and beneath the free surface and, therefore, a sucking-down action as opposed to a lifting action results. As in previous runs, it may be noted that Figure (28), corresponding to the largest value of $2\pi a/L$, shows a sinusoidal variation for both force components throughout the range of wave heights.

B. WAVE FORCE COEFFICIENTS

In order to represent the results of the experiments in a simpler, albeit less descriptive form, the maximum values

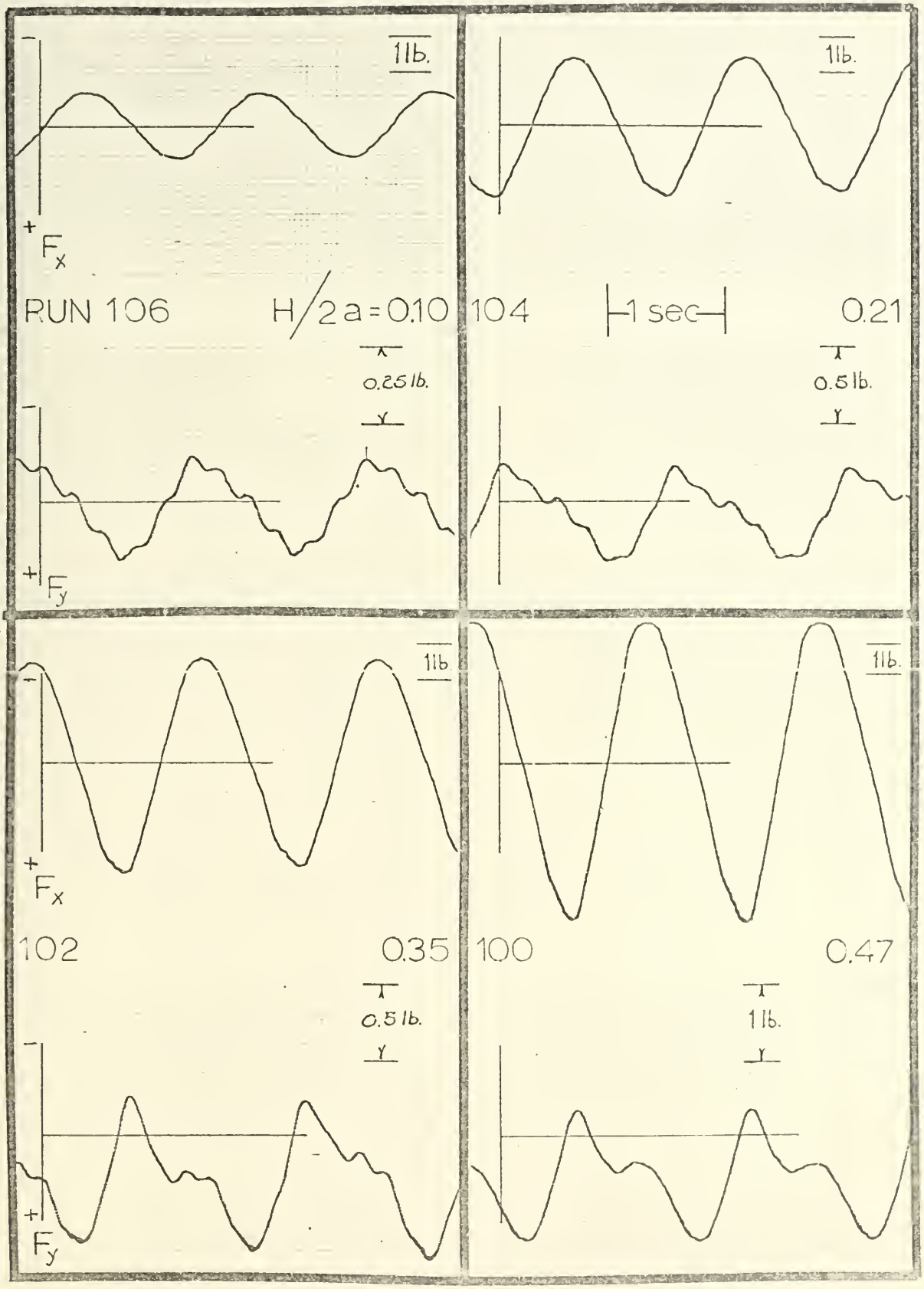

Figure 24. Wave Force Trace, h/a= 4.0, d/a= 3.0, $2\pi a/L$= 0.21.

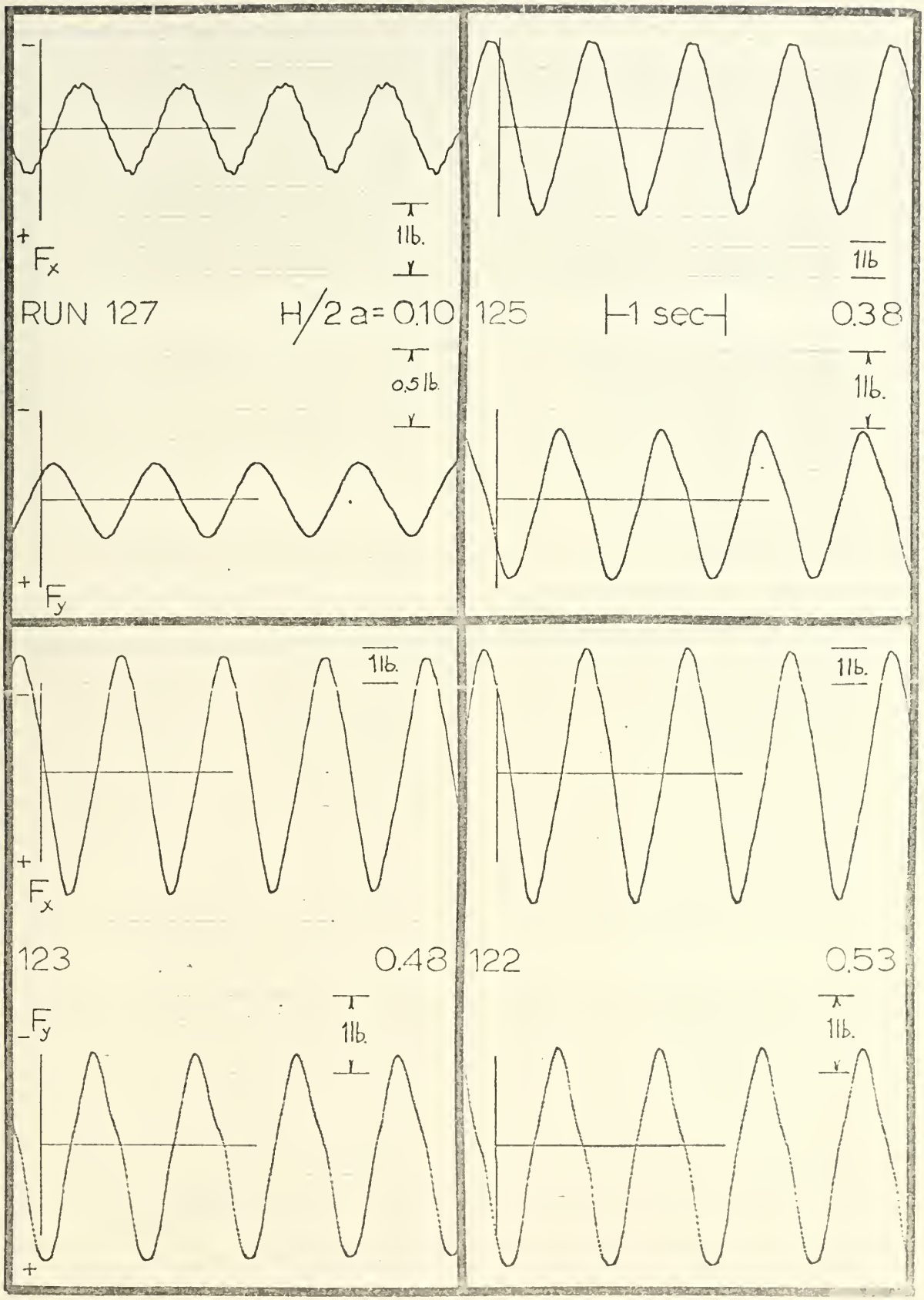

Figure 25. Wave Force Trace, h/a= 4.0, d/a= 3.0, $2\pi a/L$= 0.15.

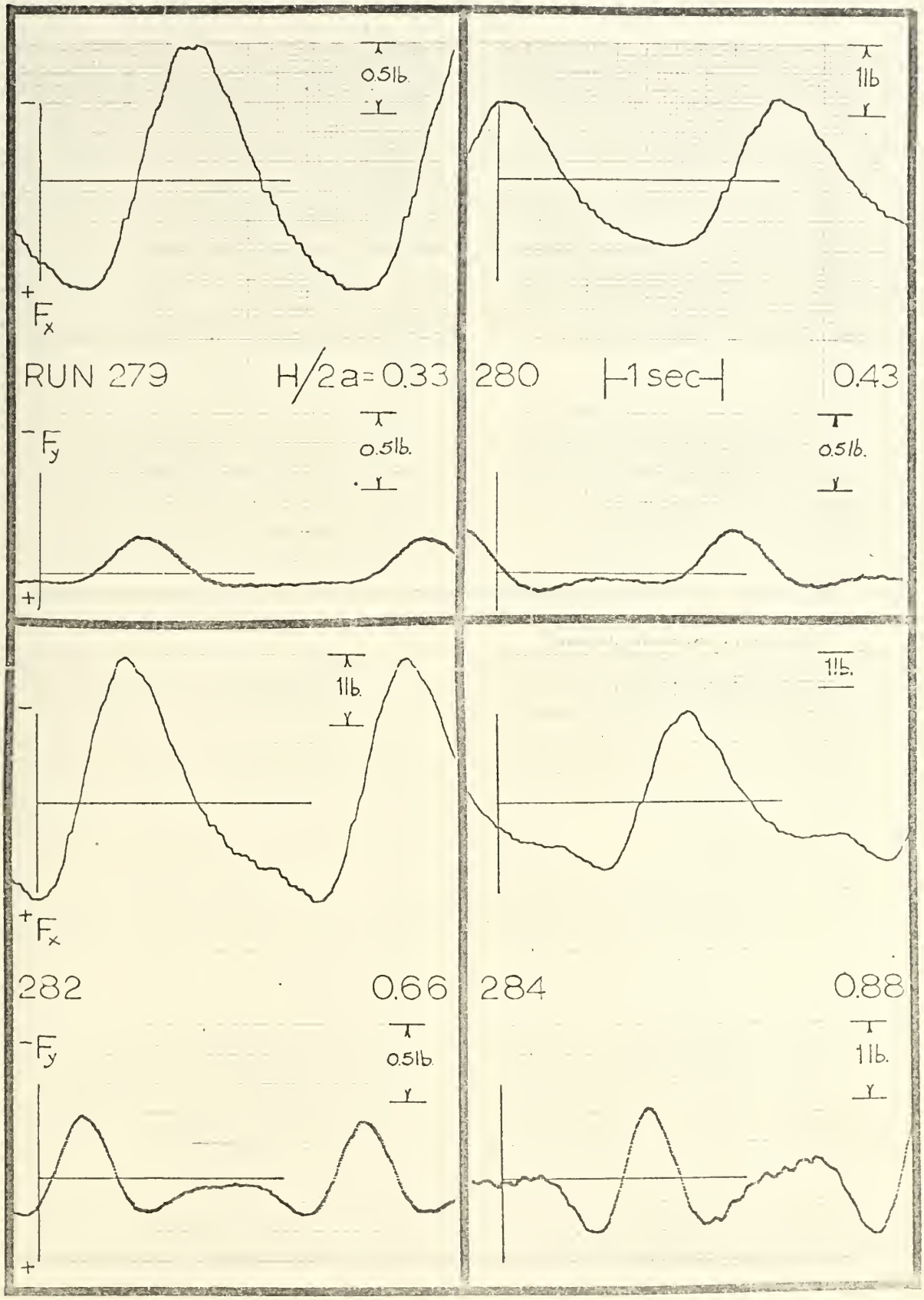

Figure 26. Wave Force Trace, h/a= 6.0, d/a= 4.0, $2\pi a/L$= 0.30.

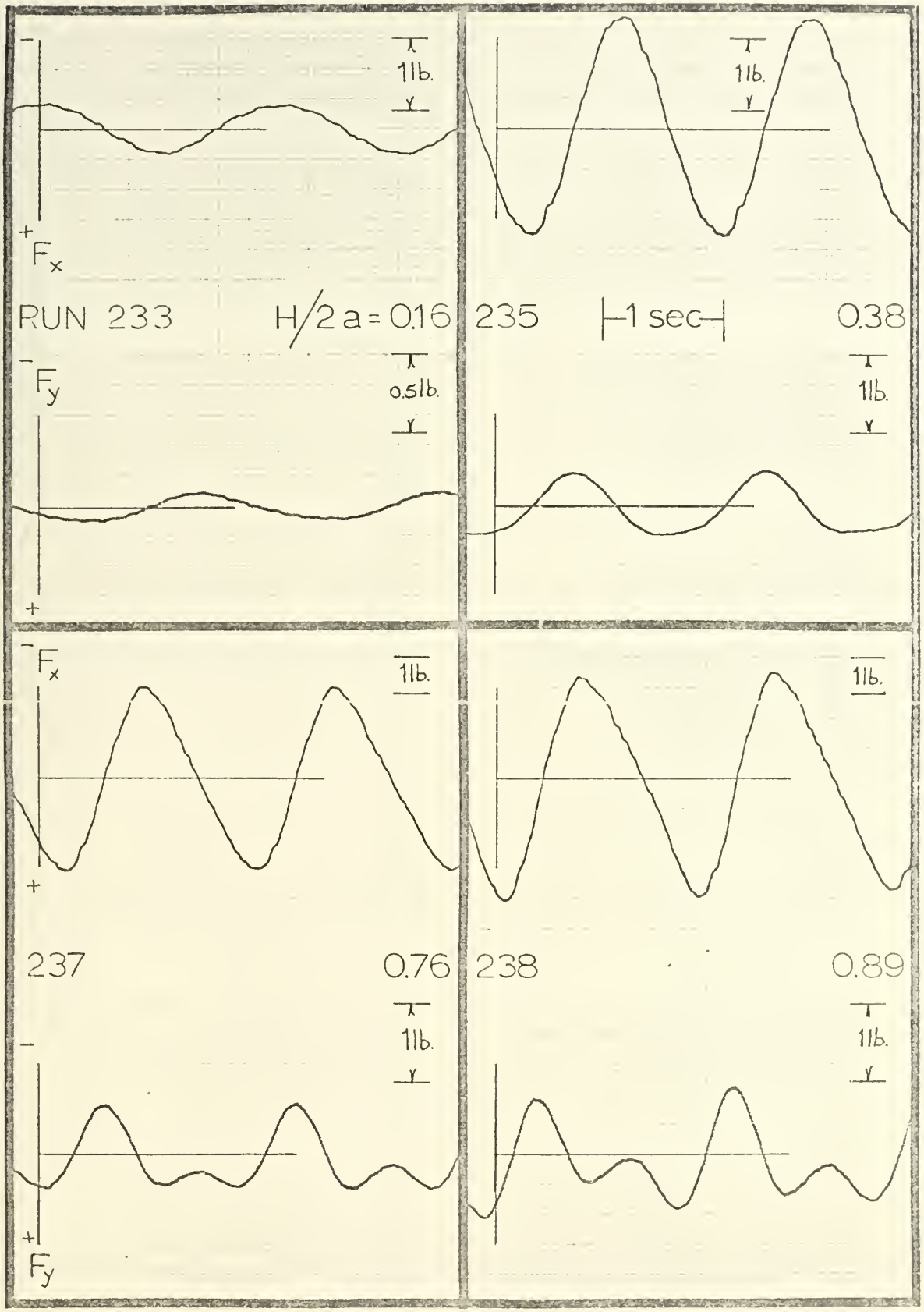

Figure 27. Wave Force Trace, h/a= 6.0, d/a= 4.0, $2\pi a/L$= 0.16.

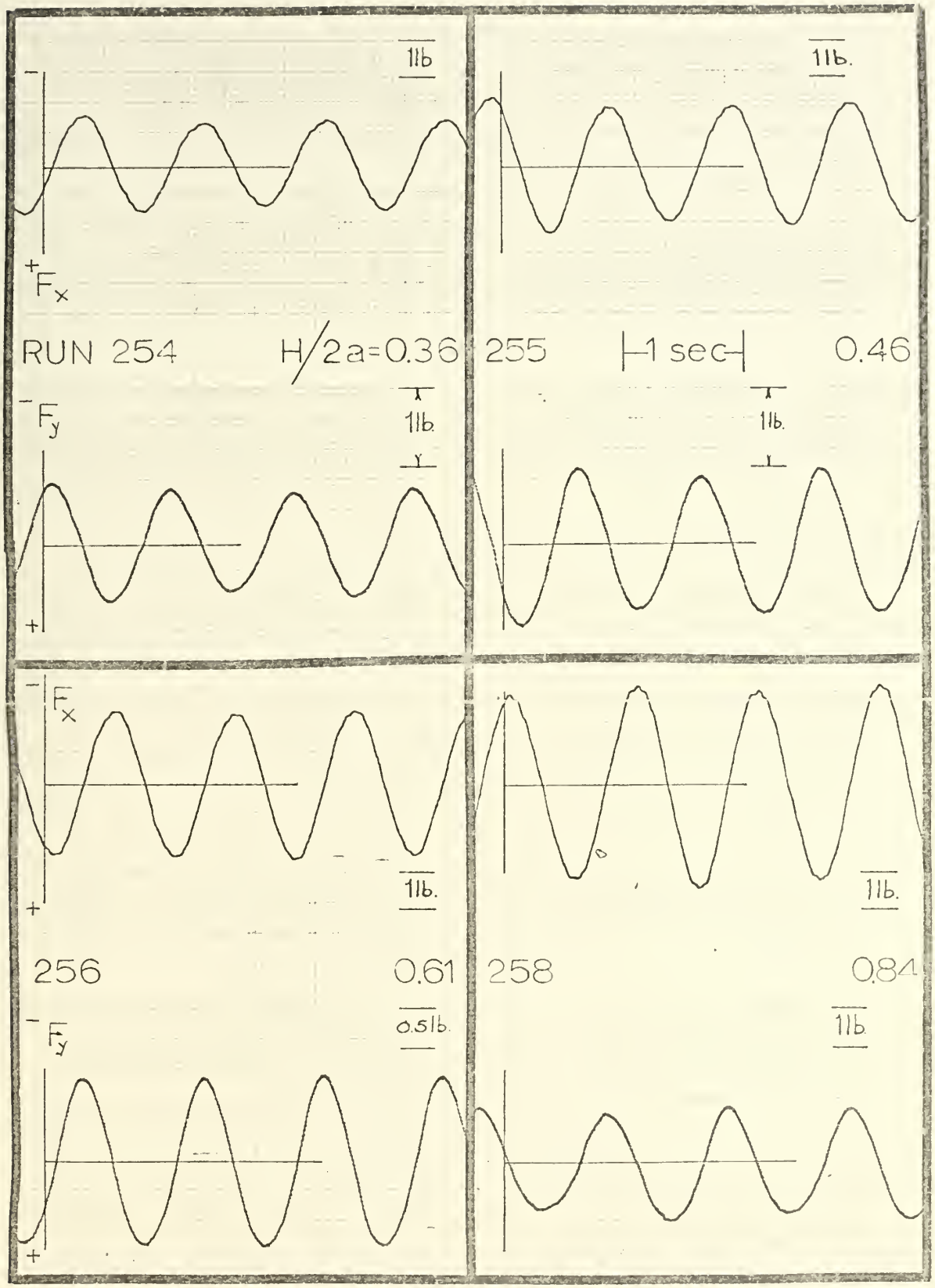

Figure 28. Wave Force Trace, h/a= 6.0, d/a= 4.0, $2\pi a/L$= 0.32.

of the dimensionless force coefficients obtained from the force traces were plotted as a function of relative wave height, H/2a. Results corresponding to the relative water depth of h/a= 6.0 with the cylinder on the bottom, i.e., d/a= 5.0, are presented in Figures (29-32). Results corresponding to the other two relative water depths of h/a= 5.0 and 4.0 also with the cylinder on the bottom are presented in Figures (33-36) and (37-40), respectively. These results correspond to values of $2\pi a/L$ ranging from approximately $2\pi a/L$= 0.08 to 0.97.

As was apparent from the force traces, the horizontal force showed sinusoidal variations with equal magnitude in both directions and, therefore, only one curve was required to represent the amplitude of this variation with relative wave height. The dimensionless force coefficients are defined as $f=F/\rho ga^2$, and three curves are noted on each figure, one for the horizontal and one each for the upward and downward vertical force. As is evident from the figures, the horizontal force coefficient shows a linear variation with the wave height in all cases.

However, as the vertical force showed, in general, larger upward than downward magnitudes, the two curves labeled f_y^+ and f_y^- are presented showing the maximum upward and downward values of the vertical force coefficient, respectively. Throughout the range of the data, the vertical force coefficient for the cylinder located on the bottom showed a quite consistent variation, the upward force being always larger

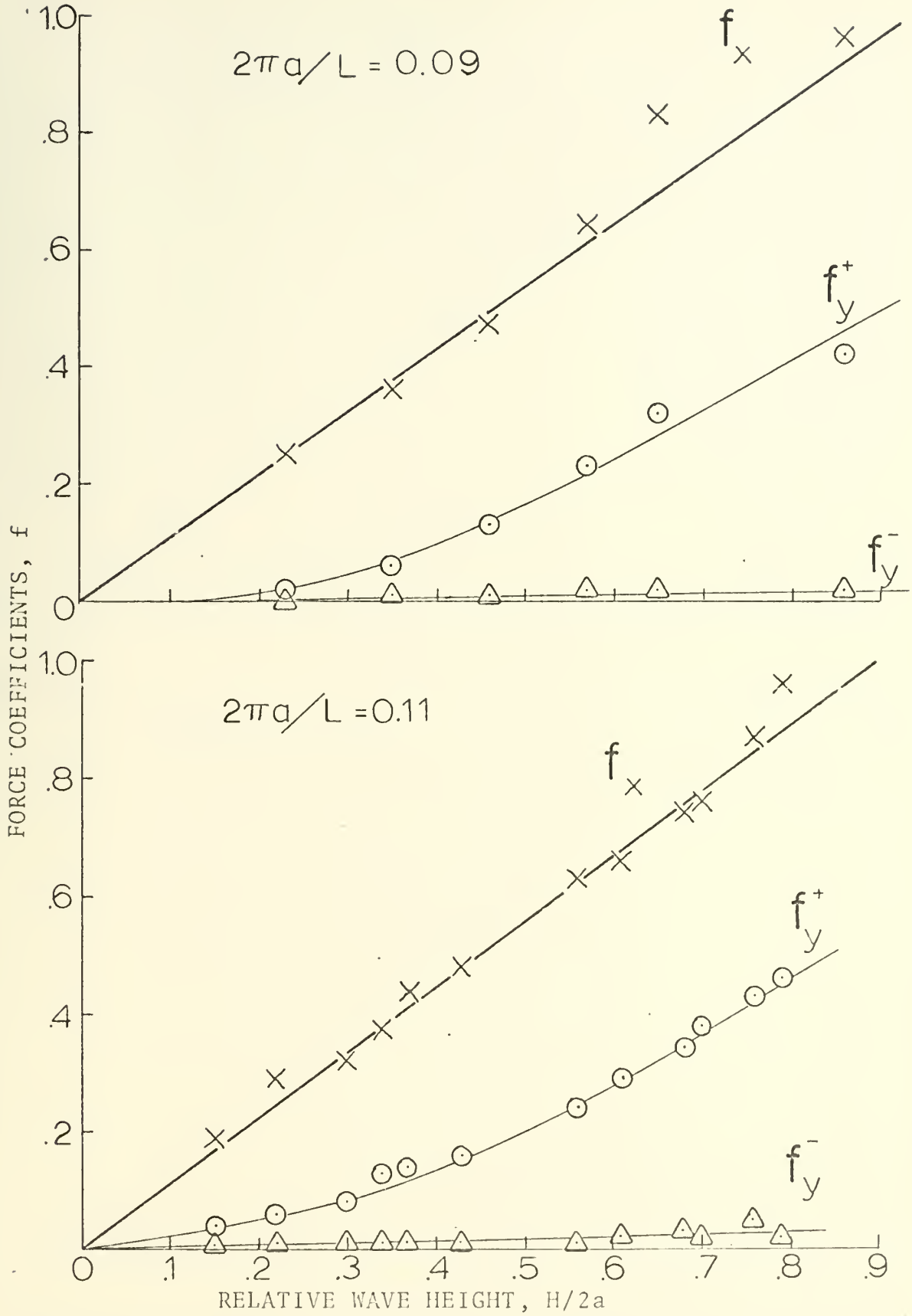

Figure 29. Wave Force Coefficients for h/a= 6.0, d/a= 5.0.

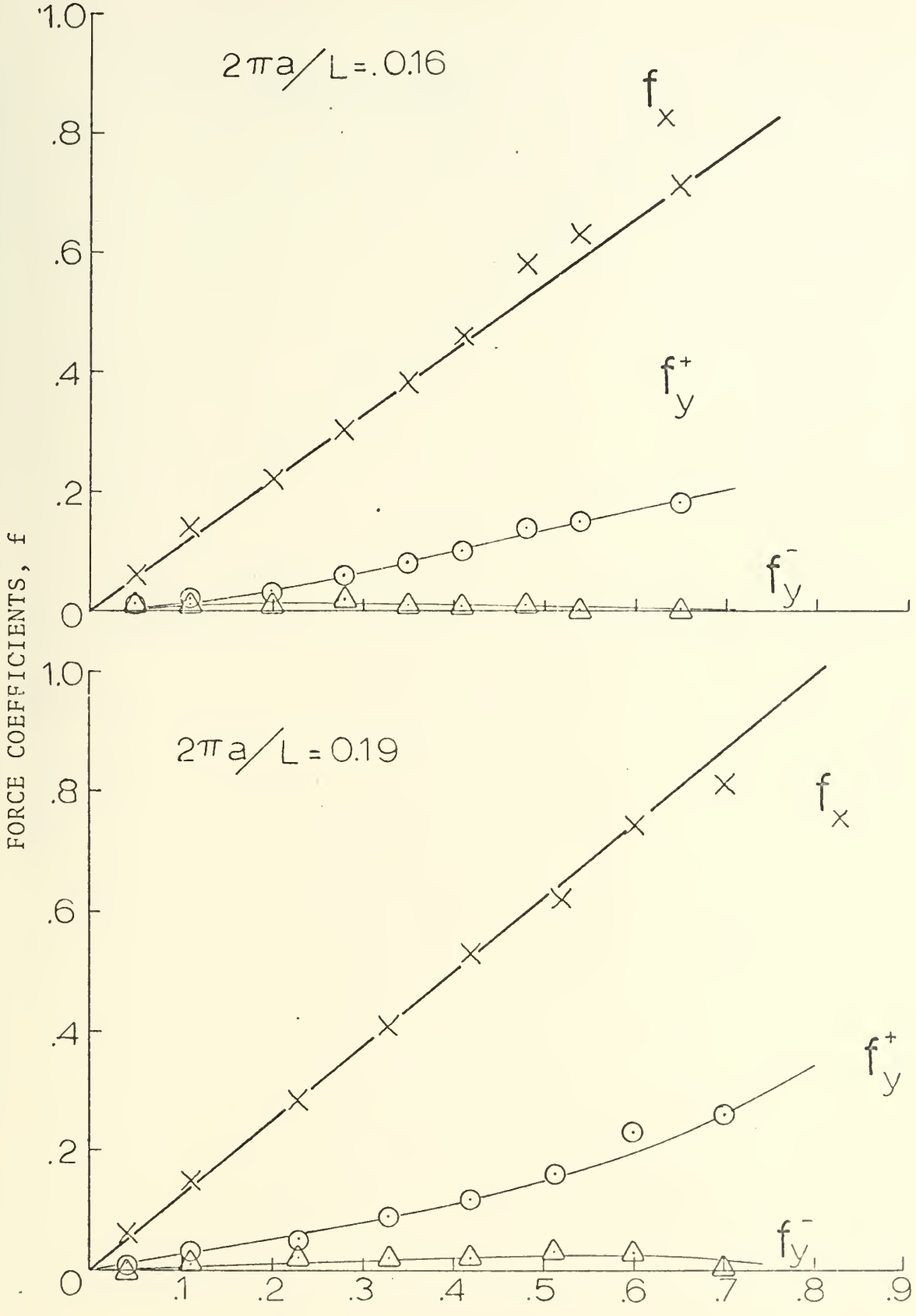

Figure 30. Wave Force Coefficients for h/a= 6.0, d/a= 5.0.

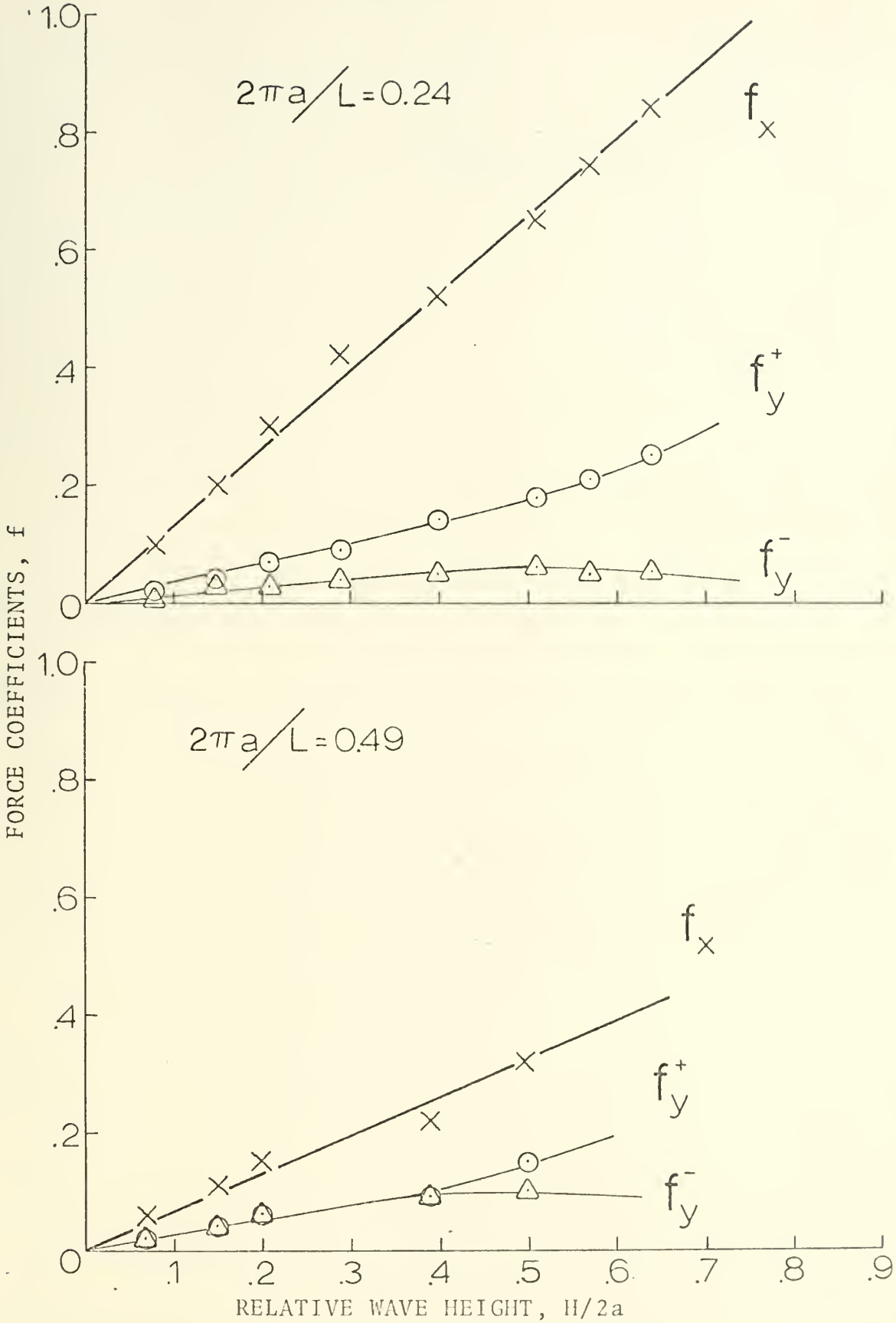

Figure 31. Wave Force Coefficients for h/a= 6.0, d/a= 5.0.

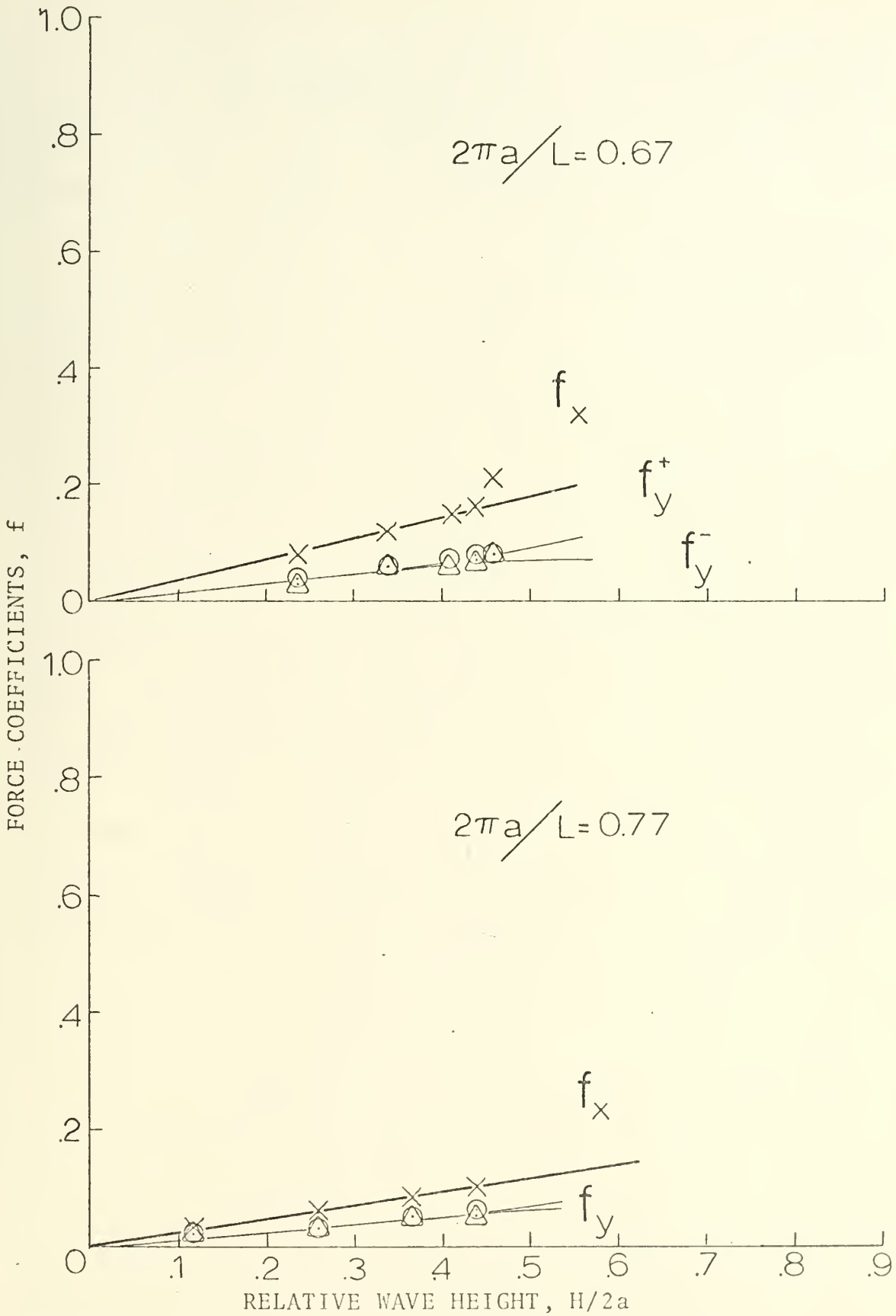

Figure 32. Wave Force Coefficients for h/a= 6.0, d/a= 5.0.

than the downward force and having a generally concave upward trend. The downward force was always quite small showing a nearly linearly increasing variation followed by a breaking off at higher wave amplitudes.

The variations of the force coefficients as observed in Figures (29-40) can be justified if one considers the components which make up the dynamic pressure acting on the surface of the cylinder. Two components of pressure are generally recognized, the one component being associated with the unsteady term in the Bernoulli equation, and the second being associated with the velocity squared term occurring therein. The unsteady term involves the velocity potential to the first power and, therefore, is linear in $H/2a$. The second term involves the spatial derivative of the velocity potential squared and is, therefore, proportional to $(H/2a)^2$. Thus, linear variation of the horizontal force with $H/2a$ apparently results from contributions from the unsteady component of pressure only. The velocity squared term which would contribute a nonlinear component of force can contribute nothing to the horizontal force if the flow pattern is symmetrical about the y-axis. This, of course, is expected provided separation does not occur and accounts for the linear variation in the horizontal force with the parameter $H/2a$.

The vertical force variation with $H/2a$, however, shows markedly different trends. Both the upward and downward components seem to vary linearly with relative wave height

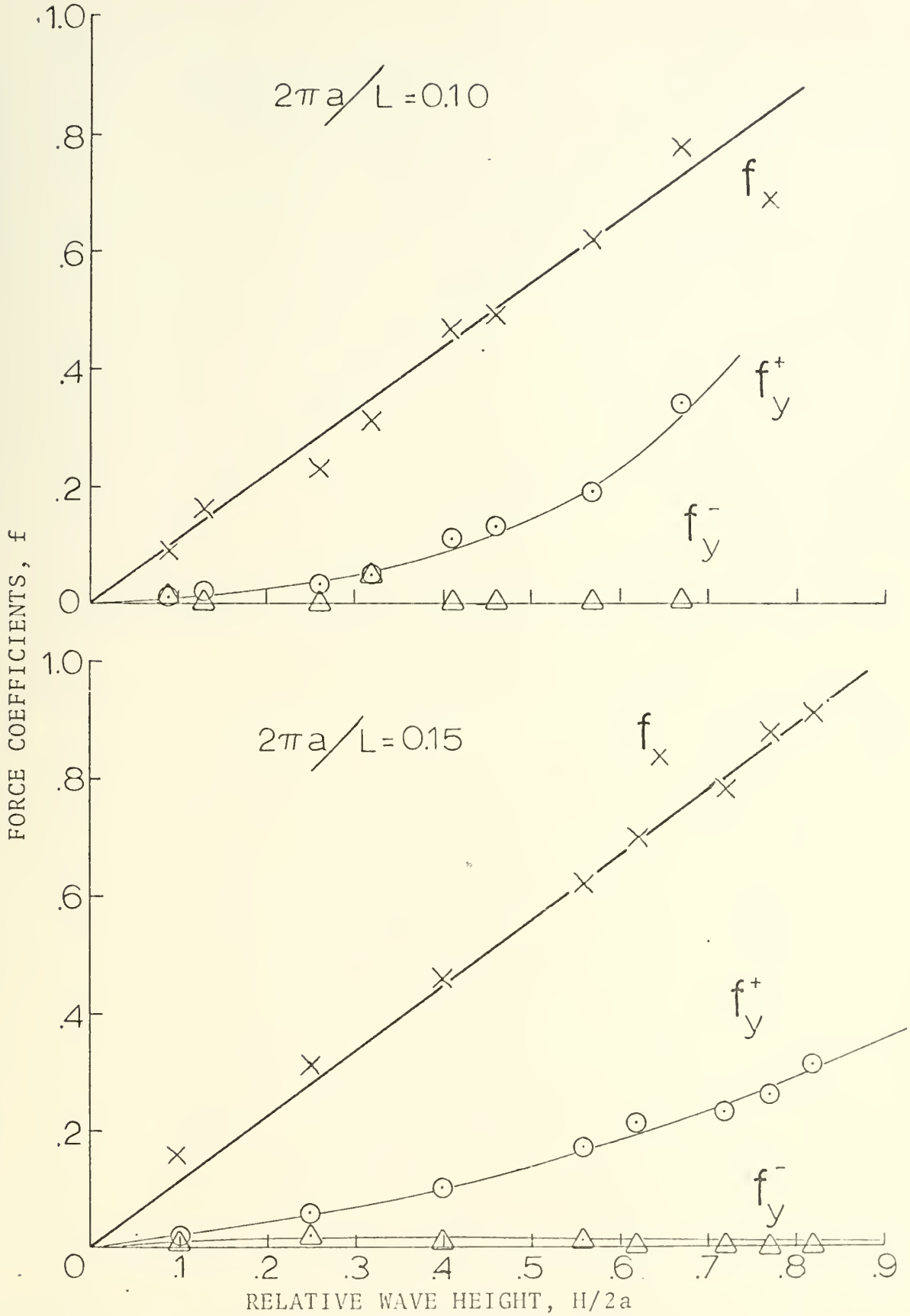

Figure 33. Wave Force Coefficients for h/a= 5.0, d/a= 4.0.

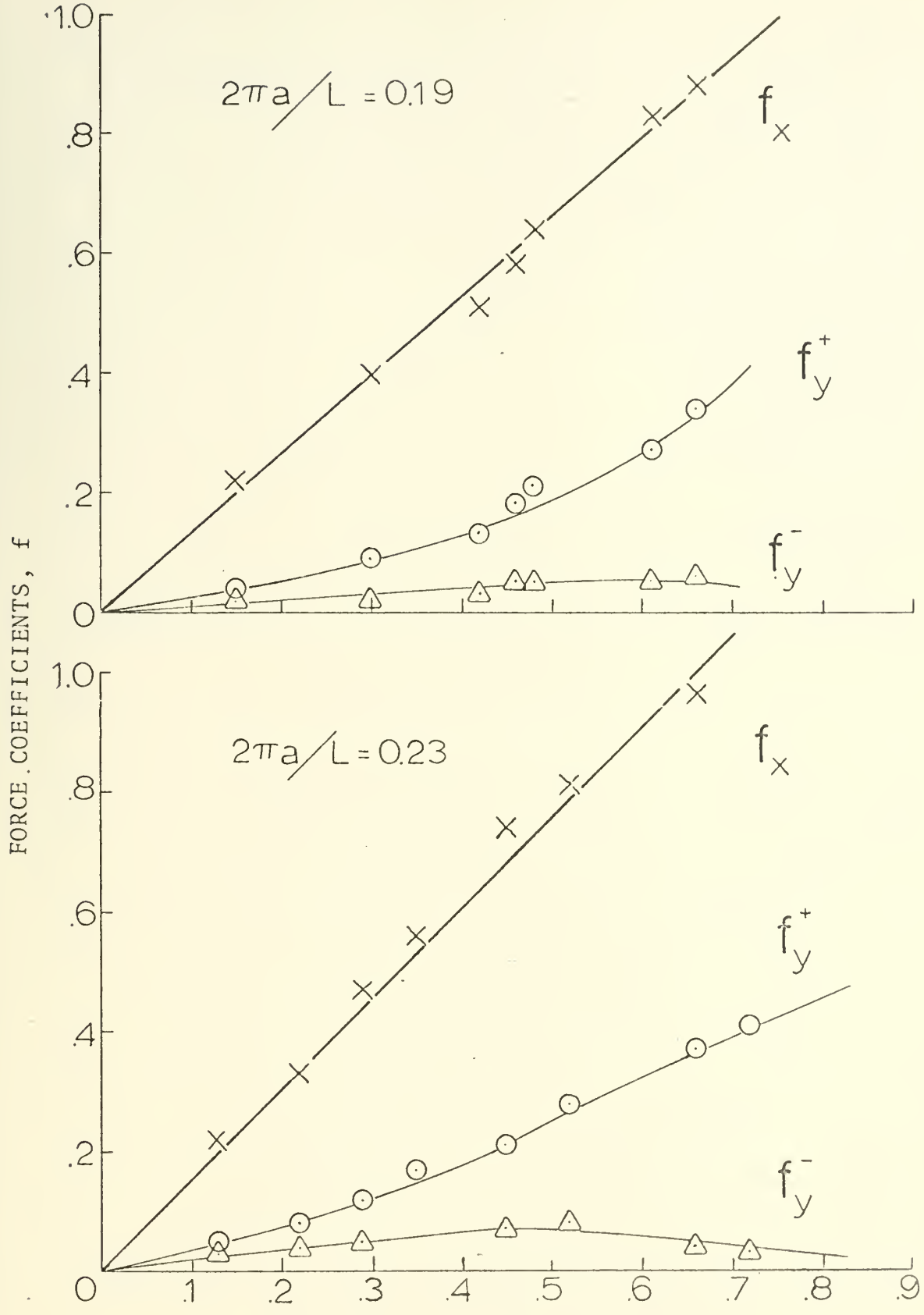

Figure 34. Wave Force Coefficients for h/a= 5.0, d/a= 4.0

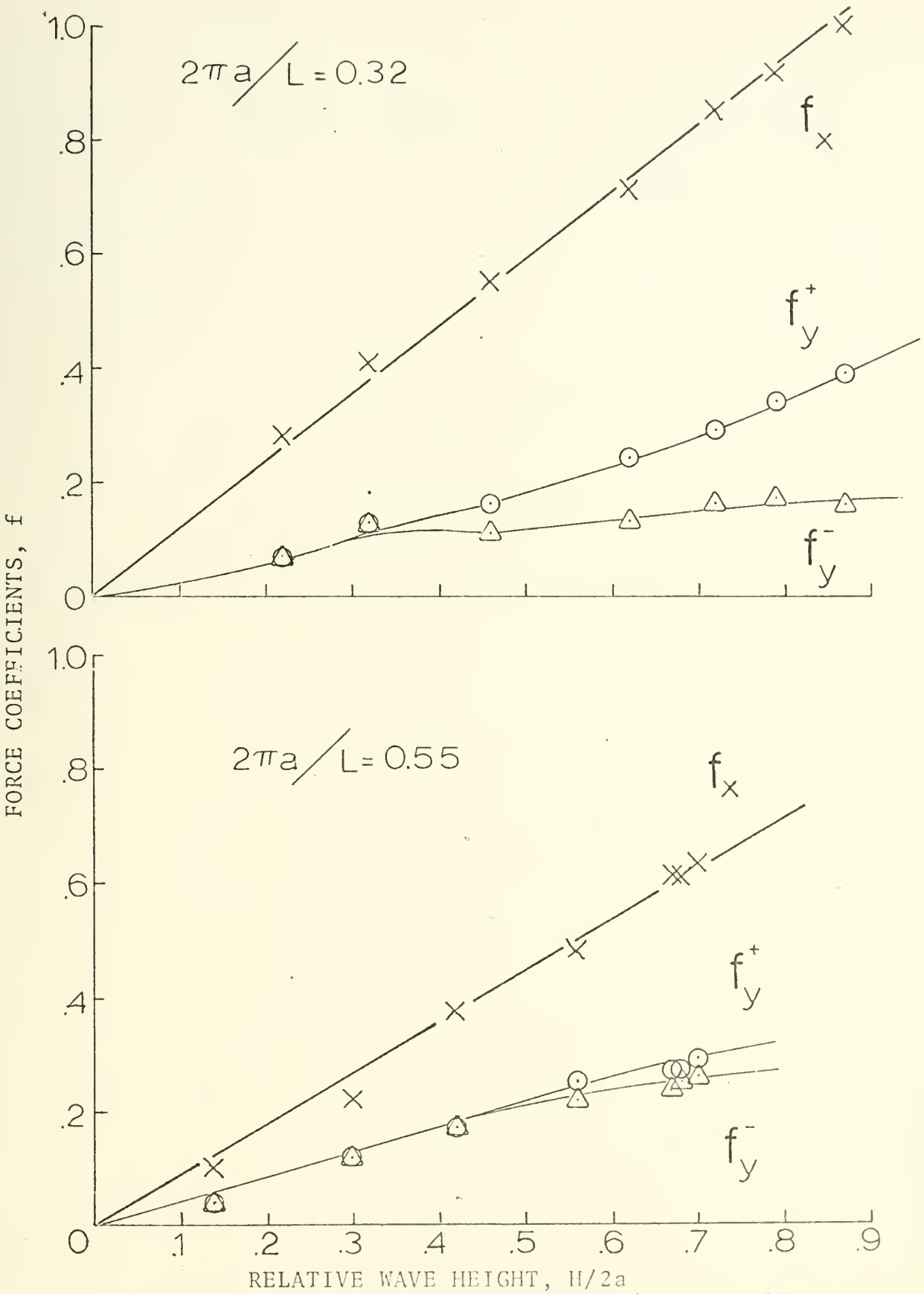

Figure 35. Wave Force Coefficients for h/a= 5.0, d/a= 4.0.

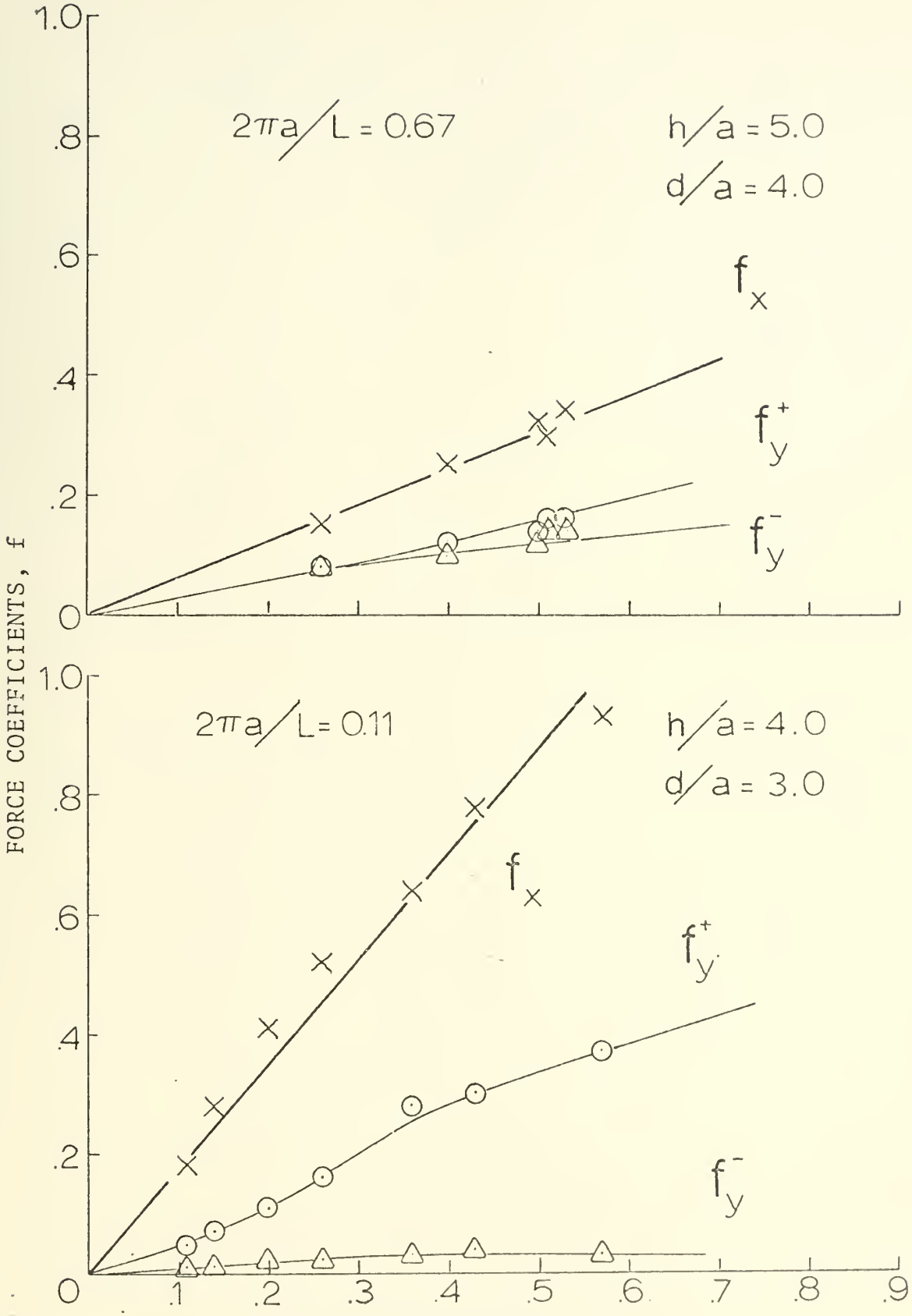

Figure 36. Wave Force Coefficients.

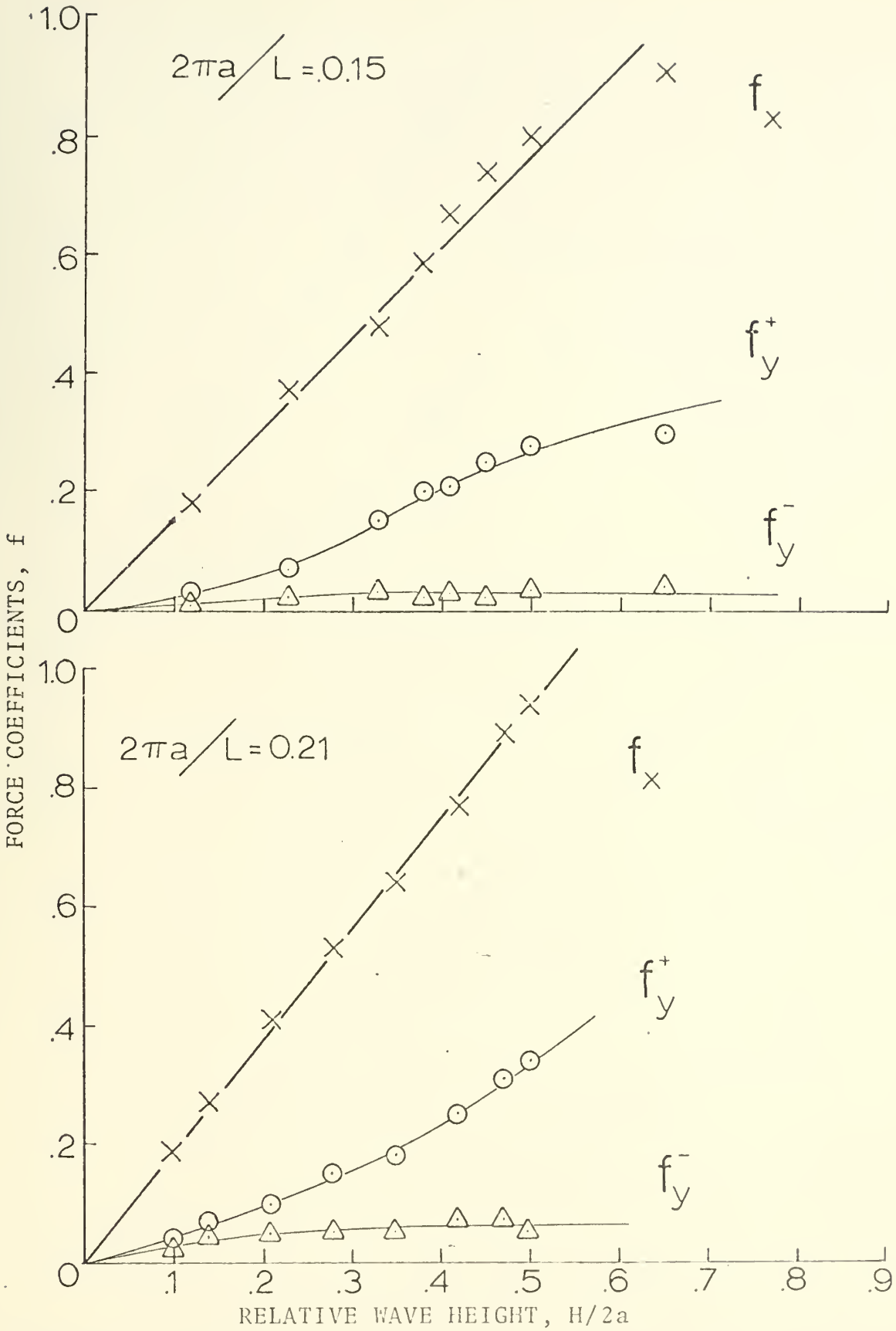

Figure 37. Wave Force Coefficients for h/a= 4.0, d/a= 3.0.

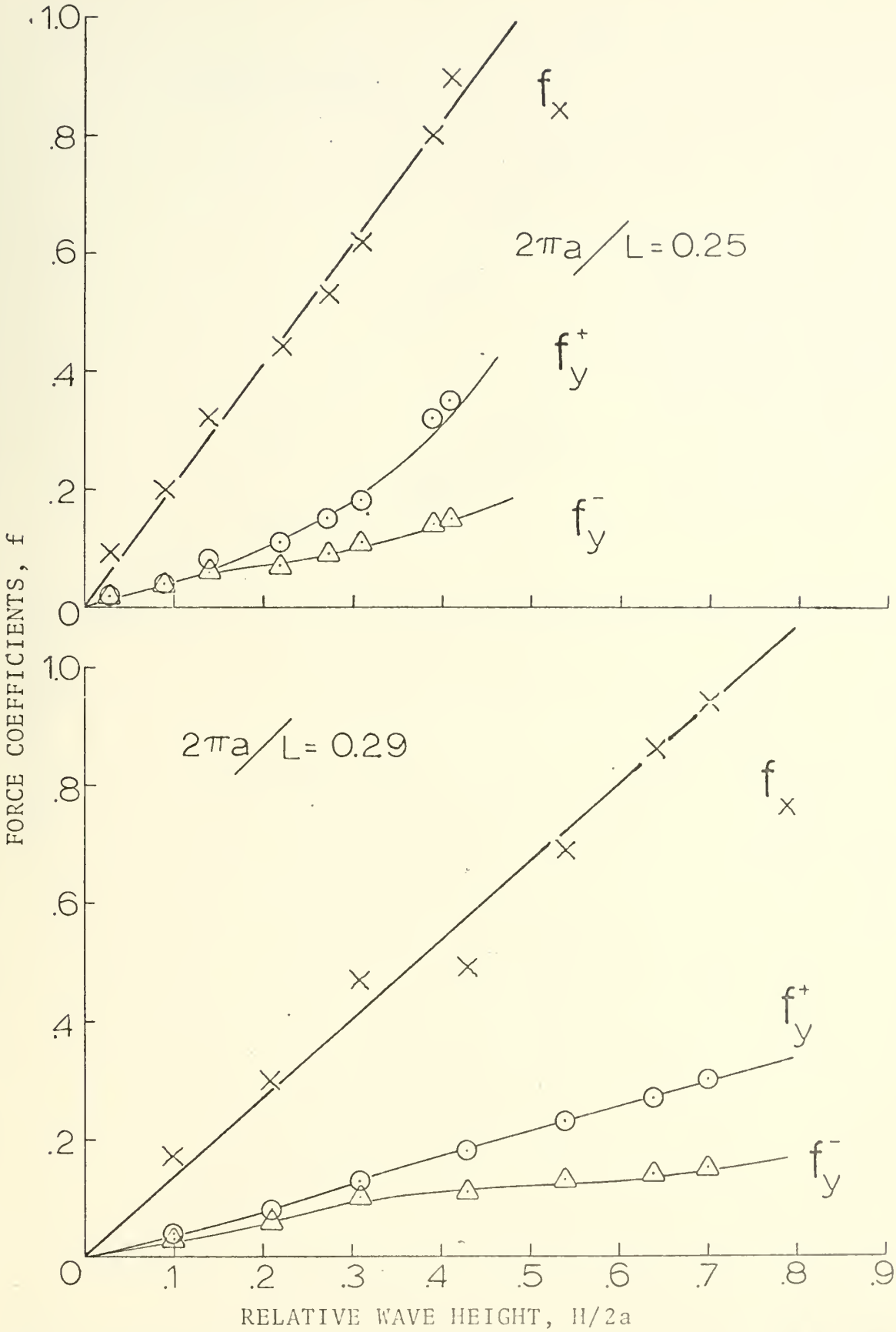

Figure 38. Wave Force Coefficients for h/a= 4.0, d/a= 5.0.

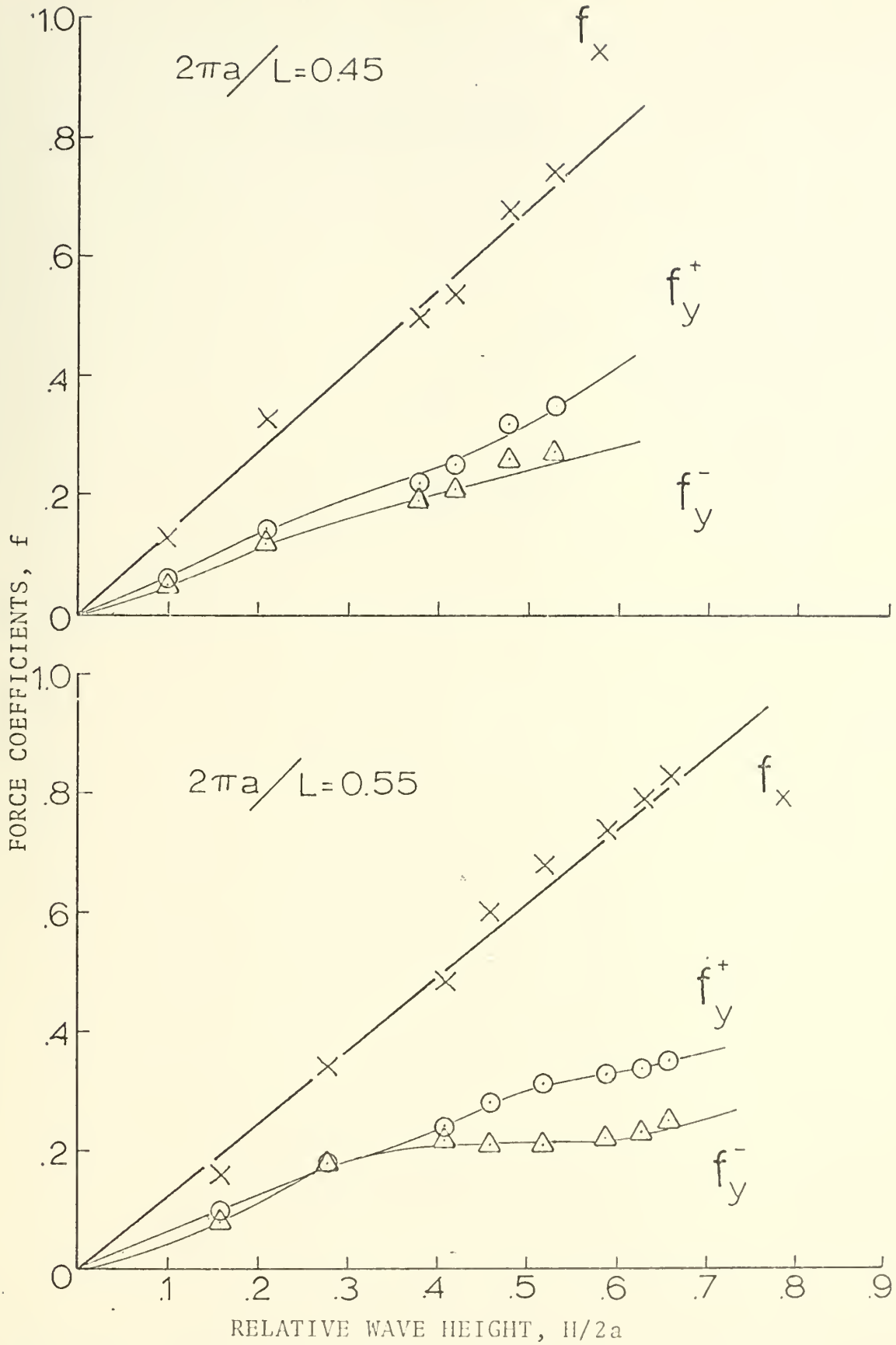

Figure 39. Wave Force Coefficients for h/a= 4.0, d/a= 3.0.

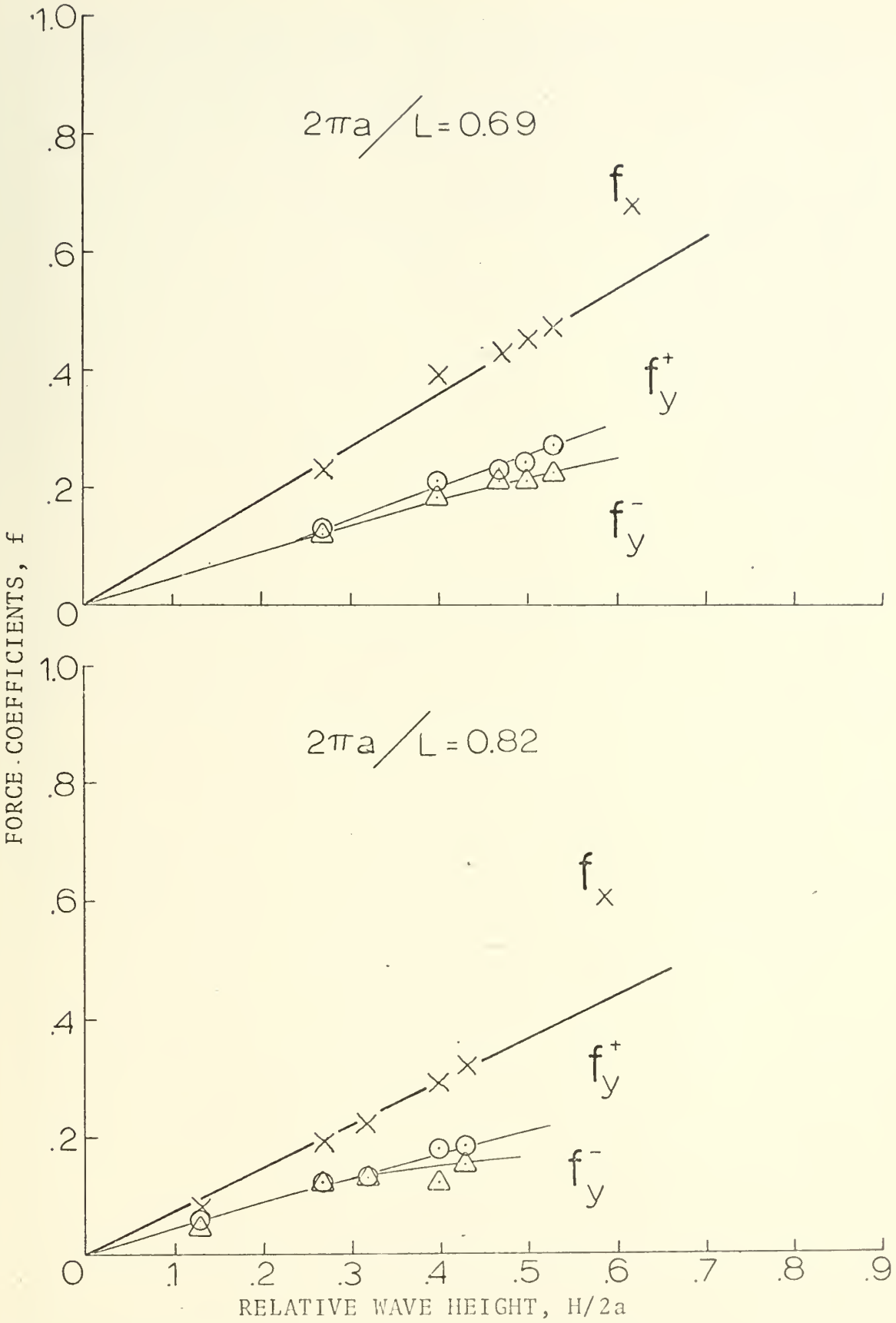

Figure 40. Wave Force Coefficients for h/a= 4.0, d/a= 3.0.

for small amplitude waves, and the upward force tends to bend upwards while the downward force tends to decrease at larger values of H/2a. These variations, however, are consistent with the previous discussion regarding the pressure on the surface of the cylinder. In the case of the vertical force, the flow pattern is not symmetrical about a horizontal axis passing through the center of the cylinder, and, therefore, the contribution from the velocity squared term in the Bernoulli equation does not cancel. As a crest or trough passes the cylinder, the wave induced velocity is a maximum giving rise to a component of pressure (or force) proportional to $(H/2a)^2$. The vertical force coefficient variation with H/2a, therefore, is composed of two terms, one proportional to H/2a and one proportional to $(H/2a)^2$. Thus, its somewhat parabolic shape is not unexpected.

The maximum values of the horizontal and vertical force coefficients for the final series of runs conducted at a water depth ratio of h/a= 6.0 with the cylinder suspended off the bottom, i.e., d/a= 4.0, are presented in Figures (41) through (44). As in the previously described tests, the horizontal force coefficients showed a linear variation with wave amplitude whereas the vertical force coefficients showed an initial linear portion followed by a nonlinear portion. However, in this series of runs, the high velocity in the gap beneath the cylinder caused a net nonlinear contribution to the force in the downward direction making the magnitude of f_y^- larger than f_y^+, a trend opposite to those associated with the cylinder near the bottom.

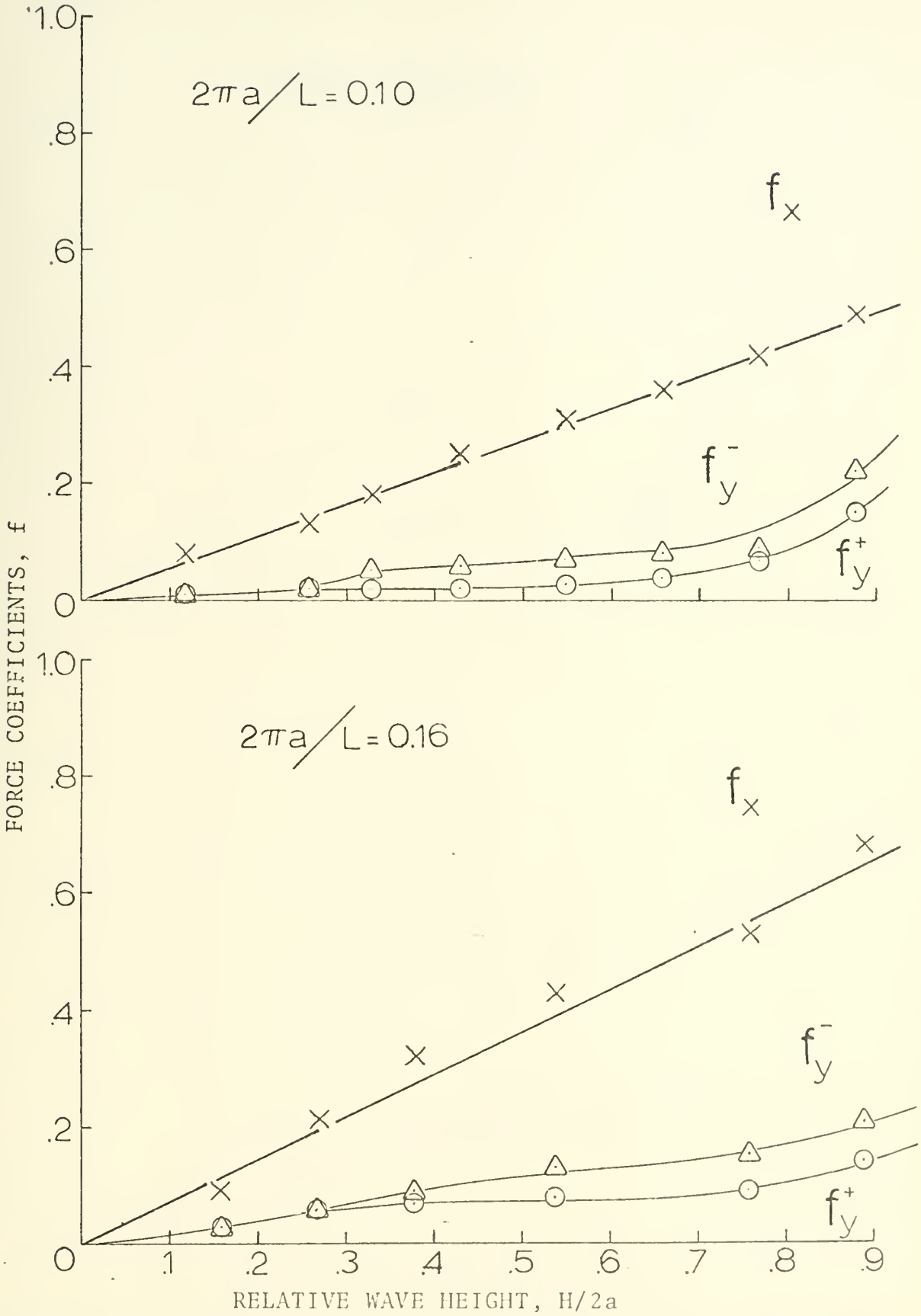

Figure 41. Wave Force Coefficients for h/a= 6.0, d/a= 4.0.

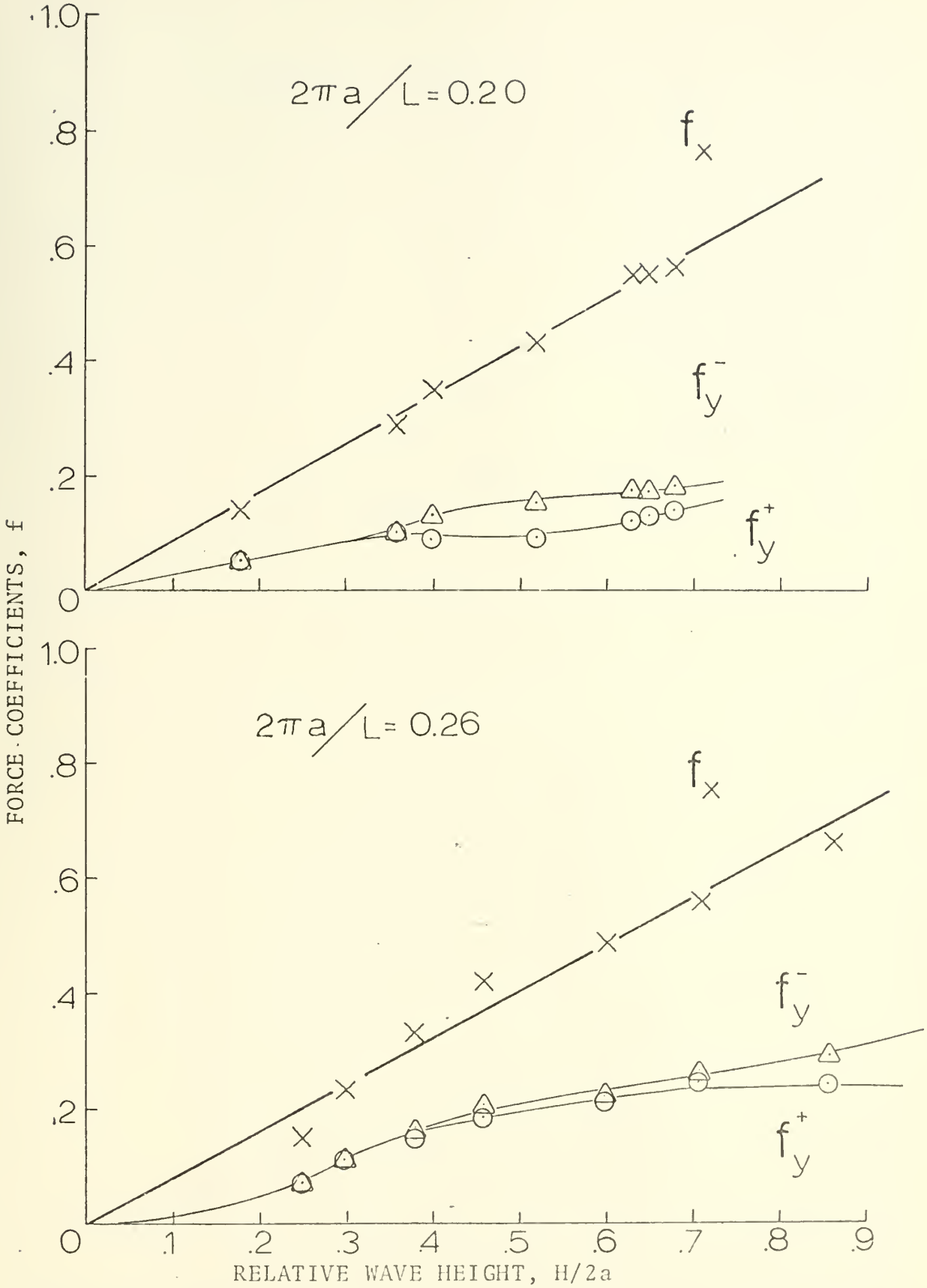

Figure 42. Wave Force Coefficients for h/a= 6.0, d/a= 4.0.

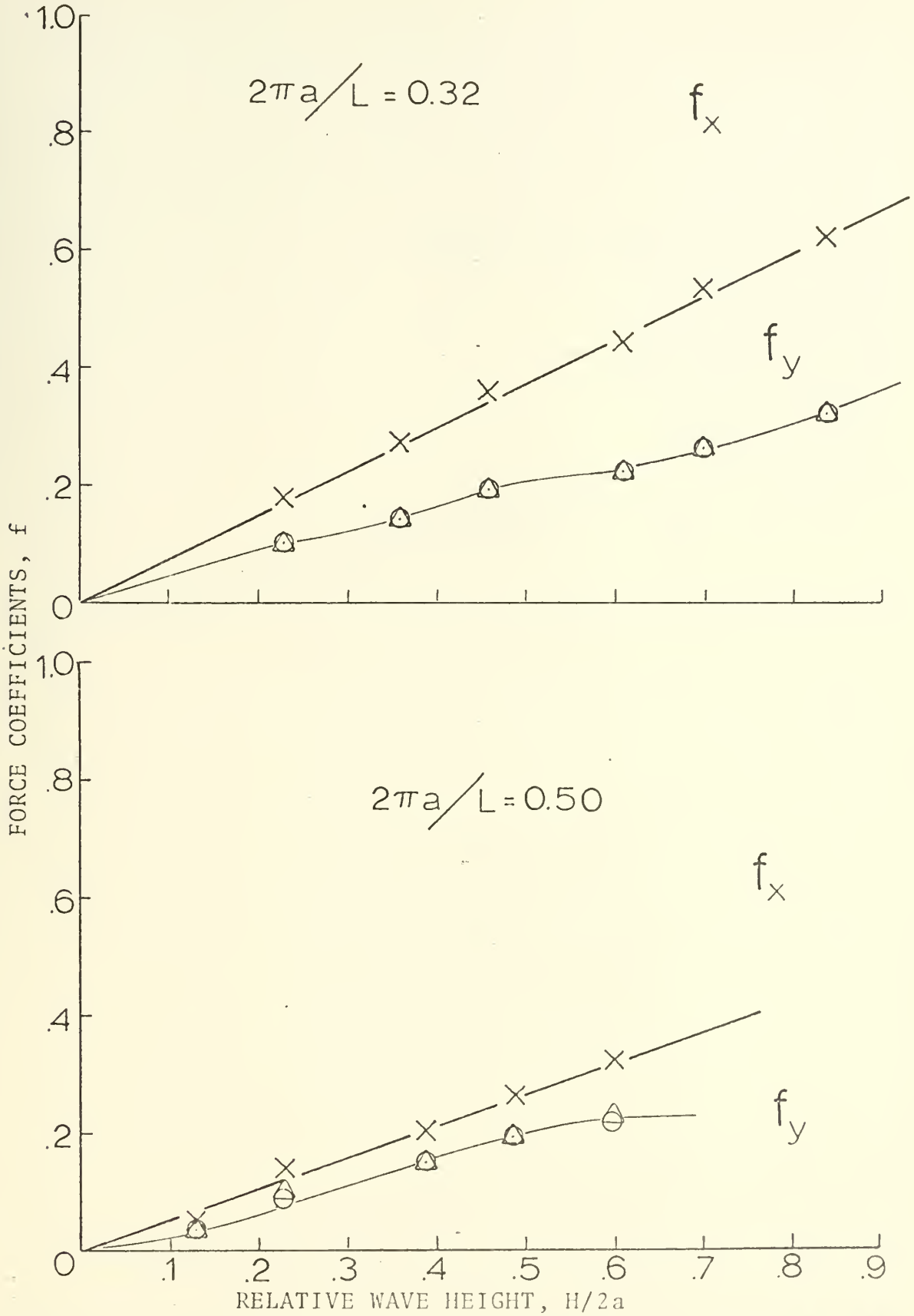

Figure 43. Wave Force Coefficients for h/a= 6.0, d/a= 4.0.

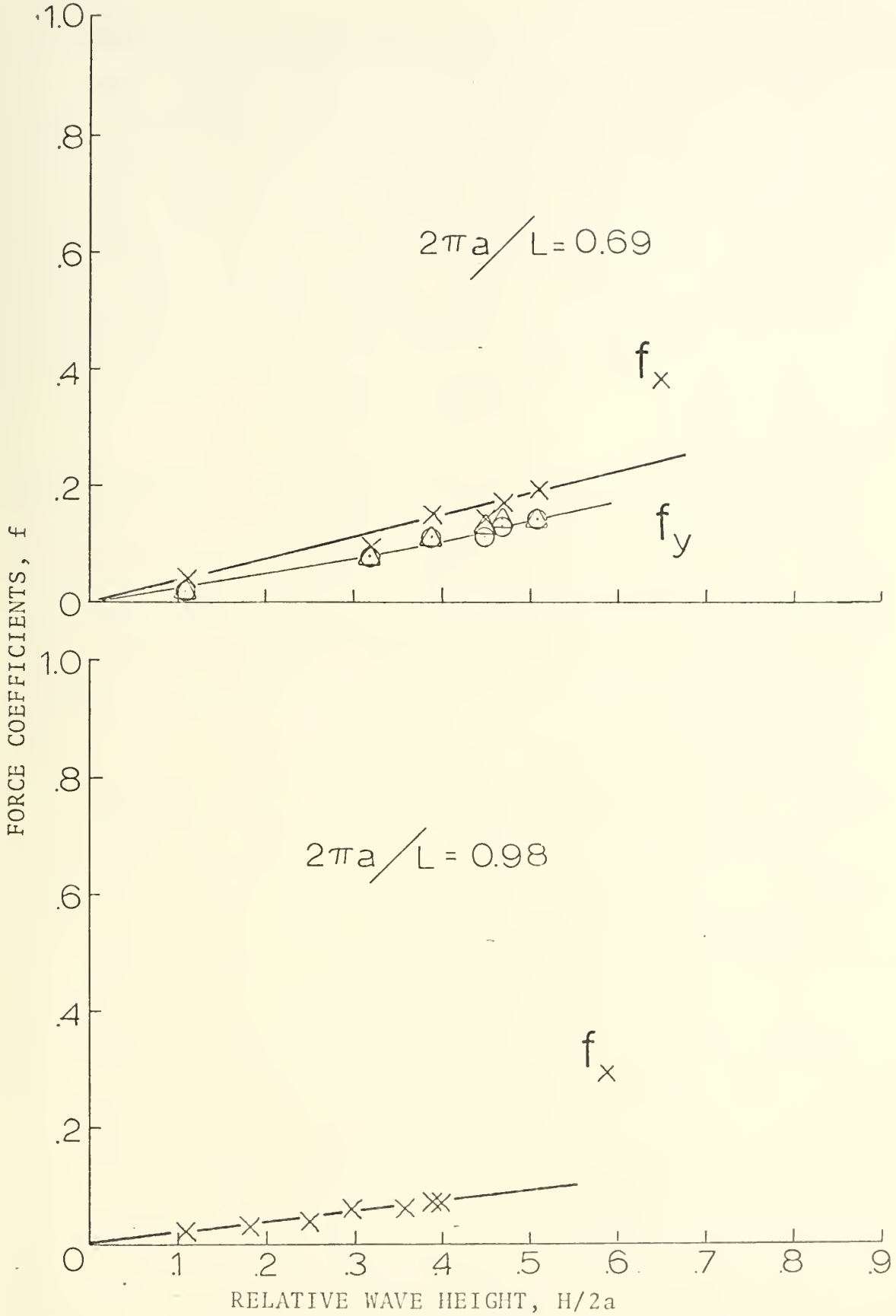

Figure 44. Wave Force Coefficients for h/a= 6.0, d/a= 4.0.

C. HORIZONTAL FORCE COEFFICIENT

The maximum values of the horizontal force coefficient f_x, as shown in Figures(29-40), are seen to vary linearly with the relative wave height, H/2a. In view of this linear behavior, it is possible to represent these forces in a much more condensed form. That is, since the force coefficients are linear with H/2a, the parameter,

$$F_x/[\rho g a^2 (H/2a)],$$

which actually represents the slopes of these curves can be presented in a single figure as a function of the relative wave length, $2\pi a/L$. Such a plot is presented in Figure (45) wherein this force coefficient is represented as a function of $2\pi a/L$ for the four series of tests carried out at different water depths and depths of submergence.

The upper three curves shown in Figure (45) represent three different water depths wherein the cylinder was located on the bottom. The effect of water depth is clearly indicated, as the curves corresponding to decreasing depths lie above the one at a maximum water depth of $h/a = 6.0$. The general trends of these three curves are all similar, maximum values of force coefficients occurring near $2\pi a/L = 0.3$ with decreasing force at shorter wave lengths. At longer wave lengths than those corresponding to the maximum value for the force coefficient, the curves tend to become flat while the linear theory would indicate a decrease similar to that associated with the curve corresponding to

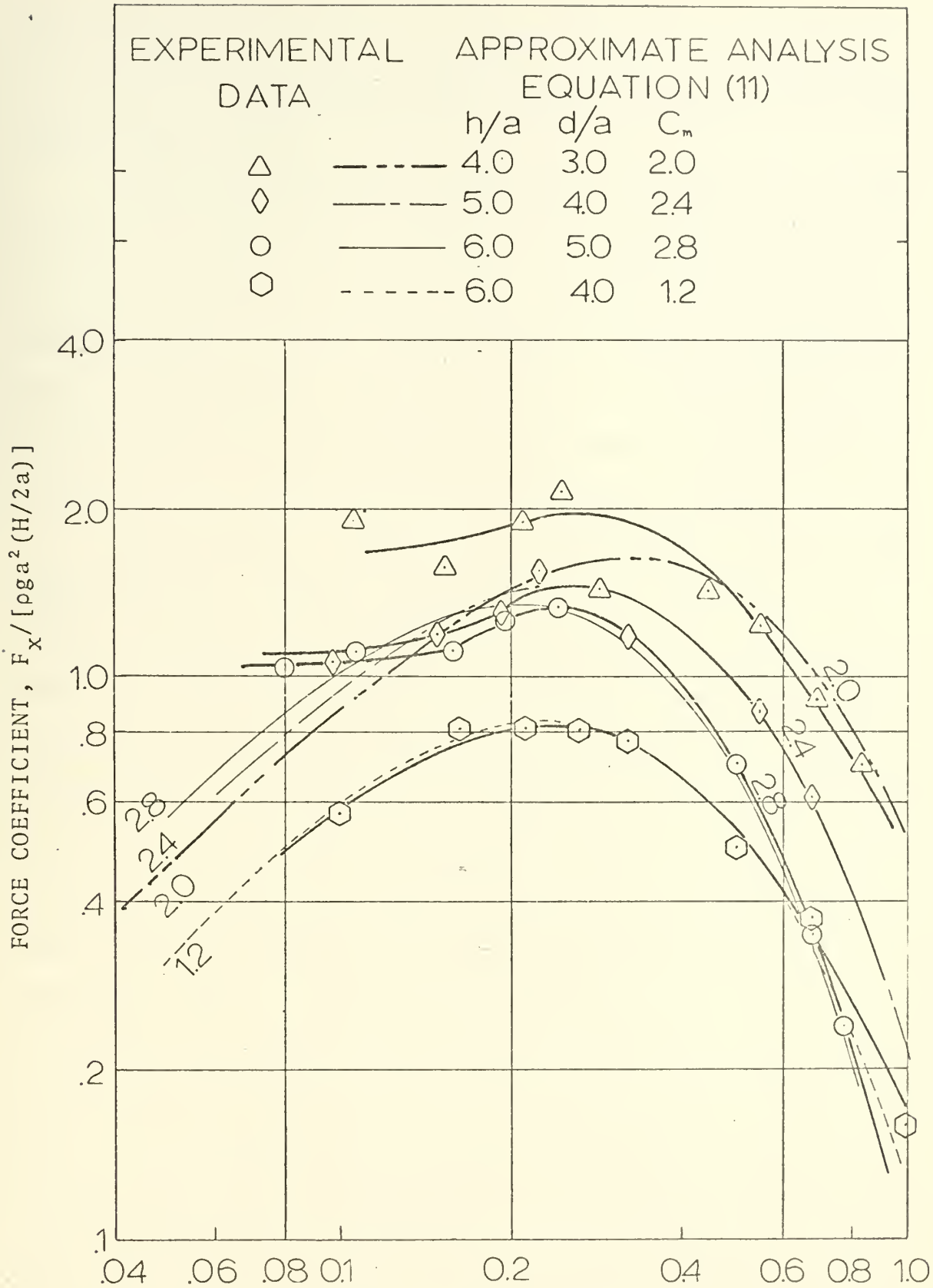

Figure 45. Horizontal Force Coefficients.

h/a= 6.0 and d/a= 4.0. It is possible that this behavior is caused by the fact that the wave is becoming a nonlinear shallow water wave.

The horizontal force coefficients corresponding to the fourth series of tests carried out at a water depth ratio of h/a= 6.0 and with the cylinder suspended at one radii off the bottom is also shown in Figure (45) as the lowest curve. The general trends are seen to be somewhat similar to the cases where the cylinder was located on the bottom except that the curve tends to be somewhat flatter.

In an attempt to compare the experimental results with the approximate theory, Equation (11) was programmed on a digital computer, and values for the horizontal force coefficients were generated as a function of $2\pi a/L$ assuming various values for the added mass coefficient, C_m. These results were then plotted and compared with the experimental results in order to determine which value of C_m gave the best fit. These curves representing the "best fit" were then plotted on Figure (45) and were compared with the experimental plots. As might be expected, it was possible to obtain good agreement between the approximate theory and the experimental data for the largest depth ratios. In these cases, the proximity of the free surface, which was disregarded in the approximate analysis, was probably not particularly important. However, for the shallowest depth where the free surface was more influential, it appeared to be impossible to find a value for C_m which gave reasonable agreement with the plotted experimental results.

One point of interest in Figure (45) was to compare the two curves associated with a maximum depth of h/a= 6.0, the one case corresponding to the cylinder located on the bottom, d/a= 5.0, and the other with the cylinder elevated one radii off the bottom, d/a= 4.0. As can be seen from the figure, the latter curve is considerably below the former and corresponds to an added mass coefficient of approximately C_m= 1.2. The data corresponding to a similar situation with the cylinder located on the bottom appears to agree relatively well with the curve based on C_m = 2.8. This marked increase in C_m corresponding to the case where the cylinder was located on the bottom apparently results from the proximity of the bottom.

A second interesting feature in Figure (45) was the apparent discontinuity in the two curves associated with the two shallowest steps near $2\pi a/L$= 0.3. The cause of this discontinuity is not certain, and it might be dismissed as scatter in the experimental data. There is, however, a second explanation which is equally probable. It is possible to have a small amount of reflection at this value of $2\pi a/L$, and it is possible that this reflected waves affected the wave height measurement. Depending on the phase of the reflected wave, it may either add or subtract and cause an apparent increase or decrease in the value of the wave force coefficient. The absence of this discontinuity in the curves corresponding to the greater depths is in agreement with this hypothesis since reflection decreases with relative depth.

V. CONCLUSIONS

An experimental study of gravity wave interaction with a submerged horizontal cylinder has been conducted. From the results of this study, the following conclusions are drawn.

1. For the range of wave heights tested in the experiment, the horizontal forces resulting from gravity wave interaction with the cylinder increased linearly with wave height.

2. The vertical force was always much smaller than the horizontal force when the cylinder was located on the bottom. The downward part of this force fluctuation was nearly zero while the upward part showed a nonlinear increase with wave amplitude. At very small amplitudes where the velocity squared contribution to the pressure was small, a sinusoidal variation of the vertical force resulted.

3. For the case corresponding to the cylinder suspended one radii off the bottom, the horizontal force was reduced and the downward force was greater than the upward force.

4. For cases where the depth of submergence was large, the approximate analysis appeared to give valid results provided the proper value of the added mass coefficient was known.

5. When the value of $2\pi a/L$ becomes small, corresponding to long waves, the wave force trace shows features dissimilar to those associated with the more sinusoidal waves. In particular, a null period in the horizontal wave trace occurs during the passage of the trough.

TABLE I. Experimental Wave and Force Data, h/a= 6.0, d/a= 5.0.

RUN	T (sec.)	H (in.)	F_x (lb.)	F_y^+ (lb.)	F_y^- (lb.)	L (ft.)	$\frac{2\pi a}{L}$	$\frac{H}{2a}$	f_x	f_y^+	f_y^-
82	2.66	5.17	4.67	2.04	0.08	17.80	0.09	0.86	0.96	0.42	0.02
81	2.70	3.91	4.03	1.56	0.10	18.10	0.09	0.65	0.83	0.32	0.02
80	2.69	3.42	3.11	1.10	0.08	18.03	0.09	0.57	0.64	0.23	0.02
79	2.69	2.77	2.29	0.61	0.06	18.03	0.09	0.46	0.47	0.13	0.01
78	2.67	2.13	1.76	0.31	0.04	17.88	0.09	0.35	0.36	0.06	0.01
77	2.69	1.37	1.21	0.10	0.02	18.03	0.09	0.23	0.25	0.02	0.00
76	2.27	4.77	4.67	2.25	0.10	14.91	0.11	0.79	0.96	0.46	0.02
75	2.25	4.56	4.24	2.10	0.25	14.75	0.11	0.76	0.87	0.43	0.05
74	2.26	4.22	3.72	1.86	0.10	14.83	0.11	0.70	0.76	0.38	0.02
73	2.25	4.09	3.62	1.68	0.14	14.79	0.11	0.68	0.74	0.34	0.03
72	2.25	3.66	3.23	1.40	0.10	14.75	0.11	0.61	0.66	0.29	0.02
71	2.25	3.37	3.07	1.16	0.07	14.75	0.11	0.56	0.63	0.24	0.01
70	2.25	3.00	2.52	1.05	0.06	14.75	0.11	0.50	0.52	0.22	0.01
69	2.26	2.60	2.36	0.80	0.06	14.83	0.11	0.43	0.48	0.16	0.01
68	2.25	2.22	2.14	0.70	0.05	14.75	0.11	0.37	0.44	0.14	0.01
67	2.25	2.06	1.82	0.61	0.05	14.75	0.11	0.34	0.37	0.13	0.01
66	2.25	1.78	1.55	0.38	0.04	14.75	0.11	0.30	0.32	0.08	0.01
65	2.25	1.32	1.39	0.30	0.03	14.75	0.11	0.22	0.29	0.06	0.01
64	2.25	0.92	0.95	0.18	0.03	14.75	0.11	0.15	0.19	0.04	0.01
30	1.63	3.92	3.47	0.88	0.02	9.99	0.16	0.65	0.71	0.18	0.00
31	1.63	3.26	3.09	0.73	0.01	9.99	0.16	0.54	0.63	0.15	0.00
32	1.61	2.91	2.81	0.68	0.03	9.86	0.16	0.48	0.58	0.14	0.01
33	1.62	2.47	2.24	0.48	0.03	9.96	0.16	0.41	0.46	0.10	0.01
34	1.61	2.10	1.83	0.41	0.07	9.89	0.16	0.35	0.38	0.08	0.01
35	1.61	1.66	1.47	0.28	0.12	9.86	0.16	0.28	0.30	0.06	0.02
36	1.62	1.21	1.07	0.17	0.06	9.96	0.16	0.20	0.22	0.03	0.01
37	1.61	0.68	0.67	0.09	0.05	9.92	0.16	0.11	0.14	0.02	0.01
38	1.61	0.31	0.28	0.04	0.03	9.92	0.16	0.05	0.06	0.01	0.01
39	1.38	4.22	3.97	1.28	0.02	8.10	0.19	0.70	0.81	0.26	0.00
40	1.38	3.63	3.62	1.14	0.14	8.09	0.19	0.60	0.74	0.23	0.03
41	1.39	3.12	3.02	0.76	0.16	8.13	0.19	0.52	0.62	0.16	0.03
42	1.38	2.52	2.58	0.59	0.10	8.10	0.19	0.42	0.53	0.12	0.02
43	1.39	1.96	1.99	0.44	0.09	8.10	0.19	0.33	0.41	0.09	0.02
44	1.38	1.38	1.38	0.26	0.08	8.07	0.19	0.23	0.28	0.05	0.02
45	1.38	0.68	0.71	0.14	0.05	8.02	0.20	0.11	0.15	0.03	0.01
46	1.38	0.27	0.31	0.07	0.01	8.08	0.19	0.04	0.06	0.01	0.00

TABLE I - continued

RUN	T (sec.)	H (in.)	F_x (lb.)	F_y^+ (lb.)	F_y^- (lb.)	L (ft.)	$\frac{2\pi a}{L}$	$\frac{H}{2a}$	f_x	f_y^+	f_y^-
47	1.19	3.86	4.08	1.23	0.22	6.55	0.24	0.64	0.84	0.25	0.05
48	1.20	3.41	3.62	1.04	0.22	6.56	0.24	0.57	0.74	0.21	0.05
49	1.19	3.04	3.17	0.86	0.27	6.53	0.24	0.51	0.65	0.18	0.06
50	1.20	2.42	2.55	0.66	0.25	6.56	0.24	0.40	0.52	0.14	0.05
51	1.19	1.75	2.03	0.43	0.21	6.52	0.24	0.29	0.42	0.09	0.04
52	1.20	1.28	1.44	0.32	0.16	6.56	0.24	0.21	0.30	0.07	0.03
53	1.20	0.92	0.96	0.20	0.13	6.56	0.24	0.15	0.20	0.04	0.03
54	1.19	0.50	0.47	0.09	0.07	6.48	0.24	0.08	0.10	0.02	0.01
55	0.79	3.00	1.54	0.72	0.51	3.18	0.49	0.50	0.32	0.15	0.10
56	0.79	2.33	1.05	0.46	0.45	3.20	0.49	0.39	0.22	0.09	0.09
57	0.79	1.17	0.73	0.28	0.28	3.20	0.49	0.20	0.15	0.06	0.06
58	0.79	0.90	0.51	0.19	0.18	3.20	0.49	0.15	0.11	0.04	0.04
59	0.79	0.44	0.28	0.08	0.08	3.20	0.49	0.07	0.06	0.02	0.02
232	0.67	2.78	1.01	0.40	0.40	2.32	0.68	0.46	0.21	0.08	0.08
202	0.68	2.68	0.92	0.38	0.36	2.35	0.67	0.45	0.19	0.08	0.07
203	0.68	2.62	0.79	0.37	0.33	2.36	0.67	0.44	0.16	0.08	0.07
204	0.68	2.59	0.74	0.36	0.32	2.36	0.67	0.43	0.15	0.07	0.07
205	0.68	2.47	0.72	0.33	0.30	2.36	0.67	0.41	0.15	0.07	0.06
206	0.67	2.04	0.59	0.30	0.27	2.32	0.68	0.34	0.12	0.06	0.06
207	0.67	1.46	0.39	0.19	0.17	2.34	0.67	0.24	0.08	0.04	0.03
60	0.63	2.62	0.46	0.27	0.26	2.04	0.77	0.44	0.10	0.06	0.05
61	0.63	2.25	0.38	0.22	0.22	2.06	0.76	0.38	0.08	0.05	0.05
62	0.63	1.56	0.27	0.15	0.15	2.05	0.76	0.26	0.06	0.03	0.03
63	0.63	0.70	0.14	0.08	0.08	2.04	0.77	0.12	0.03	0.02	0.02

TABLE II - Experimental Wave and Force Data, h/a= 5.0, d/a= 4.0.

RUN	T (sec.)	H (in.)	F_x (lb.)	F_y^+ (lb.)	F_y^- (lb.)	L (ft.)	$\frac{2\pi a}{L}$	$\frac{H}{2a}$	f_x	f_y^+	f_y^-
143	2.66	4.02	3.79	1.68	0.0	16.36	0.10	0.67	0.78	0.34	0.0
144	2.65	3.41	3.01	0.95	0.0	16.30	0.10	0.57	0.62	0.19	0.0
145	2.65	2.74	2.39	0.65	0.0	16.30	0.10	0.46	0.49	0.13	0.0
146	2.64	2.46	2.30	0.56	0.0	16.26	0.10	0.41	0.47	0.11	0.0
147	2.66	1.95	1.50	0.26	0.26	16.34	0.10	0.32	0.31	0.05	0.05
148	2.66	1.55	1.12	0.16	0.01	16.34	0.10	0.26	0.23	0.03	0.00
149	2.63	0.77	0.79	0.08	0.01	16.19	0.10	0.13	0.16	0.02	0.00
150	2.64	0.52	0.42	0.05	0.04	16.22	0.10	0.09	0.09	0.01	0.01
151	1.81	4.90	4.44	1.51	0.01	10.58	0.15	0.82	0.91	0.31	0.00
152	1.80	4.62	4.27	1.28	0.0	10.54	0.15	0.77	0.88	0.26	0.0
153	1.79	4.30	3.79	1.13	0.01	10.47	0.15	0.72	0.78	0.23	0.00
154	1.79	3.70	3.43	1.00	0.02	10.47	0.15	0.62	0.70	0.21	0.00
155	1.80	3.35	3.02	0.84	0.03	10.51	0.15	0.56	0.62	0.17	0.01
156	1.78	2.38	2.25	0.49	0.06	10.40	0.15	0.40	0.46	0.10	0.01
157	1.79	1.52	1.52	0.30	0.08	10.46	0.15	0.25	0.31	0.06	0.02
158	1.79	0.63	0.79	0.10	0.04	10.49	0.15	0.10	0.16	0.02	0.01
159	1.47	3.95	4.30	1.66	0.28	8.20	0.19	0.66	0.88	0.34	0.06
160	1.45	3.68	4.05	1.32	0.25	8.12	0.19	0.61	0.83	0.27	0.05
161	1.46	2.86	3.13	1.04	0.24	8.18	0.19	0.48	0.64	0.21	0.05
162	1.46	2.74	2.83	0.87	0.24	8.15	0.19	0.46	0.58	0.18	0.05
163	1.45	2.50	2.49	0.61	0.16	8.09	0.19	0.42	0.51	0.13	0.03
164	1.46	1.78	1.93	0.45	0.12	8.18	0.19	0.30	0.40	0.09	0.02
165	1.46	0.90	1.05	0.18	0.09	8.18	0.19	0.15	0.22	0.04	0.02
166	1.29	4.30	5.19	2.00	0.15	6.93	0.23	0.72	1.06	0.41	0.03
167	1.30	3.97	4.69	1.80	0.20	6.99	0.22	0.66	0.96	0.37	0.04
168	1.28	3.10	3.93	1.37	0.38	6.90	0.23	0.52	0.81	0.28	0.08
169	1.29	2.73	3.61	1.04	0.33	6.97	0.23	0.45	0.74	0.21	0.07
170	1.29	2.10	2.75	0.84	0.24	6.93	0.23	0.35	0.56	0.17	0.05
171	1.29	1.76	2.28	0.60	0.24	6.93	0.23	0.29	0.47	0.12	0.05
172	1.29	1.35	1.63	0.37	0.20	6.93	0.23	0.22	0.33	0.08	0.04
173	1.29	0.75	1.08	0.22	0.13	6.93	0.23	0.13	0.22	0.05	0.03
174	1.01	5.20	4.88	1.90	0.80	4.88	0.32	0.87	1.00	0.39	0.16
175	1.02	4.72	4.46	1.65	0.84	4.96	0.32	0.79	0.92	0.34	0.17
176	1.02	4.30	4.15	1.59	0.79	4.90	0.32	0.72	0.85	0.29	0.16
175	1.02	3.72	3.44	1.17	0.64	4.89	0.32	0.62	0.71	0.24	0.13
178	1.02	2.76	2.70	0.79	0.56	4.90	0.32	0.46	0.55	0.16	0.11

TABLE II - continued

RUN	T (sec.)	H (in.)	F_x (lb.)	F_y^+ (lb.)	F_y^- (lb.)	L (ft.)	$\frac{2\pi a}{L}$	$\frac{H}{2a}$	f_x	f_y^+	f_y^-
179	1.02	1.95	2.02	0.61	0.64	4.92	0.32	0.32	0.41	0.13	0.13
180	1.02	1.35	1.37	0.36	0.33	4.89	0.32	0.22	0.28	0.07	0.07
181	0.75	4.10	2.95	1.34	1.24	2.86	0.55	0.68	0.61	0.27	0.25
182	0.75	4.20	3.05	1.43	1.25	2.87	0.55	0.70	0.63	0.29	0.26
183	0.75	4.00	2.96	1.34	1.18	2.89	0.54	0.67	0.61	0.27	0.24
184	0.75	3.34	2.34	1.24	1.08	2.86	0.55	0.56	0.48	0.25	0.22
185	0.75	2.52	1.82	0.81	0.81	2.87	0.55	0.42	0.37	0.17	0.17
186	0.75	1.79	1.07	0.57	0.57	2.86	0.55	0.30	0.22	0.12	0.12
187	0.75	0.87	0.49	0.20	0.20	2.88	0.55	0.14	0.10	0.04	0.04
188	0.68	3.04	1.46	0.77	0.67	2.37	0.66	0.51	0.30	0.16	0.14
189	0.68	3.00	1.56	0.76	0.60	2.35	0.67	0.50	0.32	0.14	0.12
190	0.68	3.20	1.66	0.80	0.70	2.37	0.66	0.53	0.34	0.16	0.14
191	0.68	3.20	1.63	0.77	0.68	2.34	0.67	0.53	0.34	0.16	0.14
192	0.67	3.00	1.40	0.73	0.66	2.30	0.68	0.50	0.29	0.15	0.14
193	0.67	2.40	1.22	0.57	0.48	2.33	0.67	0.40	0.25	0.12	0.10
194	0.67	1.55	0.75	0.37	0.37	2.32	0.68	0.26	0.15	0.08	0.08

TABLE III. Experimental Wave and Force Data, h/a= 4.0, d/a= 3.0.

RUN	T (sec.)	H (in.)	F_x (lb.)	F_y^+ (lb.)	F_y^- (lb.)	L (ft.)	$\frac{2\pi a}{L}$	$\frac{H}{2a}$	f_x	f_y^+	f_y^-
83	2.65	3.75	5.34	1.99	0.20	14.67	0.11	0.63	1.10	0.41	0.04
84	2.66	3.41	4.54	1.82	0.17	14.73	0.11	0.57	0.93	0.37	0.03
85	2.67	2.58	3.79	1.46	0.20	14.79	0.11	0.43	0.78	0.30	0.04
86	2.68	2.18	3.10	1.35	0.15	14.85	0.11	0.36	0.64	0.28	0.03
87	2.68	1.59	2.55	0.77	0.12	14.85	0.11	0.26	0.52	0.16	0.02
88	2.68	1.18	2.01	0.53	0.09	14.85	0.11	0.20	0.41	0.11	0.02
89	2.67	0.85	1.38	0.32	0.06	14.79	0.11	0.14	0.28	0.07	0.01
90	2.68	0.66	0.90	0.26	0.05	14.85	0.11	0.11	0.18	0.05	0.01
98	1.91	3.91	4.42	1.48	0.20	10.29	0.15	0.65	0.91	0.30	0.04
91	1.90	3.62	3.90	1.35	0.15	10.23	0.15	0.60	0.80	0.28	0.03
92	1.91	2.72	3.61	1.20	0.11	10.26	0.15	0.45	0.74	0.25	0.02
93	1.91	2.47	3.26	1.02	0.16	10.25	0.15	0.41	0.67	0.21	0.03
94	1.91	2.31	2.86	0.98	0.12	10.26	0.15	0.38	0.59	0.20	0.02
95	1.91	1.96	2.35	0.72	0.16	10.29	0.15	0.33	0.48	0.15	0.03
96	1.91	1.40	1.78	0.35	0.10	10.24	0.15	0.23	0.37	0.07	0.02
97	1.90	0.71	0.92	0.15	0.04	10.23	0.15	0.12	0.19	0.03	0.01
99	1.47	3.63	4.59	1.68	0.25	7.59	0.21	0.50	0.94	0.34	0.05
100	1.45	2.85	4.31	1.50	0.32	7.46	0.21	0.47	0.89	0.31	0.07
101	1.46	2.53	3.74	1.21	0.32	7.53	0.21	0.42	0.77	0.25	0.07
102	1.46	2.09	3.10	0.86	0.26	7.50	0.21	0.35	0.64	0.18	0.05
103	1.46	1.67	2.60	0.72	0.25	7.53	0.21	0.28	0.53	0.15	0.05
104	1.46	1.25	1.97	0.50	0.22	7.53	0.21	0.21	0.41	0.10	0.05
105	1.46	0.85	1.34	0.32	0.18	7.53	0.21	0.14	0.27	0.07	0.04
106	1.47	0.59	0.91	0.21	0.12	7.56	0.21	0.10	0.19	0.04	0.02
107	1.29	2.47	4.40	1.72	0.73	6.45	0.24	0.41	0.90	0.35	0.15
108	1.28	2.33	3.89	1.54	0.69	6.37	0.25	0.39	0.80	0.32	0.14
109	1.29	1.86	3.04	0.90	0.53	6.43	0.24	0.31	0.62	0.18	0.11
110	1.29	1.44	2.59	0.73	0.45	6.46	0.24	0.24	0.53	0.15	0.09
111	1.28	1.30	2.16	0.51	0.36	6.40	0.25	0.22	0.44	0.11	0.07
112	1.28	0.85	1.56	0.37	0.29	6.36	0.25	0.14	0.32	0.08	0.06
113	1.28	0.56	0.95	0.20	0.20	6.40	0.25	0.09	0.20	0.04	0.04
114	1.28	0.21	0.44	0.09	0.09	6.40	0.25	0.03	0.09	0.02	0.02
115	1.14	4.18	4.56	1.45	0.72	5.49	0.29	0.70	0.94	0.30	0.15
116	1.14	3.82	4.20	1.33	0.70	5.45	0.29	0.64	0.86	0.27	0.14
117	1.14	3.23	3.34	1.13	0.62	5.47	0.29	0.54	0.69	0.23	0.13
118	1.14	2.56	2.85	0.89	0.56	5.46	0.29	0.43	0.59	0.18	0.11

TABLE III - continued

RUN	T (sec.)	H (in.)	F_x (lb.)	F_y^+ (lb.)	F_y^- (lb.)	L (ft.)	$\frac{2\pi a}{L}$	$\frac{H}{2a}$	f_x	f_y^+	f_y^-
119	1.14	1.87	2.27	0.63	0.50	5.44	0.29	0.31	0.47	0.13	0.10
120	1.14	1.26	1.46	0.38	0.28	5.45	0.29	0.21	0.30	0.08	0.06
121	1.14	0.61	0.80	0.20	0.16	5.47	0.29	0.10	0.17	0.04	0.03
122	0.85	3.20	3.59	1.70	1.31	3.51	0.45	0.53	0.74	0.35	0.27
123	0.85	2.90	3.32	1.54	1.25	3.51	0.45	0.48	0.68	0.32	0.26
124	0.85	2.54	2.61	1.21	1.02	3.51	0.45	0.42	0.54	0.25	0.21
125	0.85	2.28	2.42	1.09	0.93	3.51	0.45	0.38	0.50	0.22	0.19
126	0.85	1.29	1.61	0.66	0.59	3.51	0.45	0.21	0.33	0.14	0.12
127	0.85	0.61	0.62	0.27	0.23	3.51	0.45	0.10	0.13	0.06	0.05
128	0.75	3.95	4.02	1.73	1.20	2.85	0.55	0.66	0.83	0.35	0.25
129	0.76	3.75	3.85	1.68	1.11	2.87	0.55	0.63	0.79	0.34	0.23
130	0.75	3.53	3.59	1.60	1.08	2.82	0.56	0.59	0.74	0.33	0.22
131	0.75	3.15	3.32	1.51	1.03	2.84	0.55	0.52	0.68	0.31	0.21
132	0.76	2.79	2.94	1.35	1.00	2.86	0.55	0.46	0.60	0.28	0.21
133	0.75	2.49	2.36	1.17	1.10	2.85	0.55	0.41	0.48	0.24	0.23
134	0.75	1.67	1.67	0.88	0.88	2.80	0.56	0.28	0.34	0.18	0.18
135	0.75	0.97	0.80	0.47	0.37	2.84	0.55	0.16	0.16	0.10	0.08
195	0.67	3.16	2.31	1.31	1.07	2.26	0.69	0.53	0.47	0.27	0.22
196	0.68	3.09	2.23	1.25	1.20	2.33	0.67	0.51	0.46	0.26	0.25
197	0.67	3.01	2.19	1.19	1.03	2.28	0.69	0.50	0.45	0.24	0.21
198	0.67	2.91	2.16	1.14	1.05	2.30	0.68	0.48	0.44	0.23	0.22
199	0.67	2.83	2.09	1.12	1.00	2.30	0.68	0.47	0.43	0.23	0.21
200	0.67	2.41	1.90	1.00	0.88	2.29	0.69	0.40	0.39	0.21	0.18
201	0.67	1.60	1.12	0.60	0.61	2.28	0.69	0.27	0.23	0.12	0.13
136	0.62	2.61	1.58	0.88	0.75	1.97	0.80	0.43	0.32	0.18	0.15
137	0.62	2.45	1.53	0.89	0.85	1.95	0.80	0.41	0.31	0.18	0.17
138	0.61	2.40	1.41	0.87	0.60	1.92	0.82	0.40	0.29	0.18	0.12
139	0.62	2.32	1.31	0.81	0.59	1.95	0.81	0.39	0.27	0.17	0.12
140	0.61	1.95	1.07	0.65	0.64	1.90	0.82	0.32	0.22	0.13	0.13
141	0.61	1.61	0.92	0.58	0.59	1.91	0.82	0.27	0.19	0.12	0.12
142	0.61	0.79	0.41	0.29	0.21	1.89	0.83	0.13	0.08	0.06	0.04

TABLE IV. Experimental Wave and Force Data, h/a= 6.0, d/a= 4.0.

RUN	T (sec.)	H (in.)	F_x (lb.)	F_y^+ (lb.)	F_y^- (lb.)	L (ft.)	$\frac{2\pi a}{L}$	$\frac{H}{2a}$	f_x	f_y^+	f_y^-
277	2.40	0.70	0.38	0.05	0.06	15.81	0.10	0.12	0.08	0.01	0.01
278	2.40	1.55	0.65	0.08	0.10	15.81	0.10	0.26	0.13	0.02	0.02
279	2.40	1.96	0.89	0.10	0.23	15.81	0.10	0.33	0.18	0.02	0.05
280	2.36	2.59	1.21	0.12	0.31	15.54	0.10	0.43	0.25	0.02	0.06
281	2.36	3.31	1.52	0.14	0.34	15.54	0.10	0.55	0.31	0.03	0.07
282	2.38	3.97	1.74	0.19	0.40	15.73	0.10	0.66	0.36	0.04	0.08
283	2.38	4.63	2.04	0.33	0.45	15.73	0.10	0.77	0.42	0.07	0.09
284	2.38	5.28	2.38	0.75	1.05	15.71	0.10	0.88	0.49	0.15	0.22
233	1.59	0.96	0.45	0.13	0.16	9.76	0.16	0.16	0.09	0.03	0.03
234	1.59	1.61	1.04	0.30	0.33	9.76	0.16	0.27	0.21	0.06	0.07
235	1.60	2.28	1.54	0.36	0.43	9.78	0.16	0.38	0.32	0.07	0.09
236	1.60	3.23	2.12	0.37	0.64	9.78	0.16	0.54	0.43	0.08	0.13
237	1.60	4.58	2.57	0.43	0.72	9.84	0.16	0.76	0.53	0.09	0.15
238	1.57	5.32	3.32	0.68	1.04	9.60	0.16	0.89	0.68	0.14	0.21
239	1.35	1.10	0.68	0.25	0.24	7.81	0.20	0.18	0.14	0.05	0.05
240	1.35	2.14	1.40	0.47	0.48	7.81	0.20	0.36	0.29	0.10	0.10
241	1.35	2.41	1.70	0.43	0.62	7.81	0.20	0.40	0.35	0.09	0.13
242	1.34	3.15	2.10	0.45	0.75	7.76	0.20	0.52	0.43	0.09	0.15
243	1.34	3.77	2.66	0.59	0.83	7.76	0.20	0.63	0.55	0.12	0.17
244	1.30	4.10	2.75	0.67	0.87	7.39	0.21	0.68	0.56	0.14	0.18
245	1.30	3.90	2.67	0.62	0.83	7.39	0.21	0.65	0.55	0.13	0.17
246	1.13	1.49	0.75	0.34	0.35	6.03	0.26	0.25	0.15	0.07	0.07
247	1.13	1.82	1.11	0.55	0.55	6.03	0.26	0.30	0.23	0.11	0.11
248	1.13	2.27	1.60	0.75	0.76	6.03	0.26	0.38	0.33	0.15	0.16
249	1.11	2.78	2.06	0.87	0.98	5.88	0.27	0.46	0.42	0.18	0.20
250	1.11	3.59	2.41	1.00	1.08	5.88	0.27	0.60	0.49	0.21	0.22
251	1.14	4.25	2.75	1.18	1.28	6.10	0.26	0.71	0.56	0.24	0.26
252	1.12	5.18	3.22	1.19	1.40	5.93	0.26	0.86	0.66	0.24	0.29
253	1.00	1.40	0.88	0.50	0.50	4.89	0.32	0.23	0.18	0.10	0.10
254	1.00	2.16	1.30	0.69	0.70	4.89	0.32	0.36	0.27	0.14	0.14
255	0.99	2.78	1.75	0.91	0.91	4.83	0.33	0.46	0.36	0.19	0.19
256	0.99	3.64	2.16	1.07	1.09	4.87	0.32	0.61	0.44	0.22	0.22
257	0.99	4.20	2.60	1.27	1.27	4.87	0.32	0.70	0.53	0.26	0.26
258	1.00	5.04	3.00	1.54	1.54	4.91	0.32	0.84	0.62	0.32	0.32
259	0.79	0.77	0.26	0.20	0.19	3.17	0.50	0.13	0.05	0.04	0.04
260	0.79	1.36	0.70	0.48	0.45	3.17	0.50	0.23	0.14	0.10	0.09

TABLE IV - continued

RUN	T (sec.)	H (in.)	F_x (lb.)	F_y^+ (lb.)	F_y^- (lb.)	L (ft.)	$\frac{2\pi a}{L}$	$\frac{H}{2a}$	f_x	f_y^+	f_y^-
261	0.78	2.36	0.97	0.71	0.71	3.15	0.50	0.39	0.20	0.15	0.15
262	0.79	2.95	1.29	0.94	0.94	3.21	0.49	0.49	0.26	0.19	0.19
263	0.79	3.59	1.57	1.06	1.10	3.19	0.49	0.60	0.32	0.22	0.23
264	0.67	0.65	0.21	0.08	0.08	2.27	0.69	0.11	0.04	0.02	0.02
265	0.67	1.90	0.44	0.40	0.39	2.27	0.69	0.32	0.09	0.08	0.08
266	0.67	2.32	0.71	0.52	0.52	2.27	0.69	0.39	0.15	0.11	0.11
267	0.67	2.68	0.68	0.62	0.56	2.27	0.69	0.45	0.14	0.13	0.11
268	0.67	2.81	0.85	0.63	0.66	2.33	0.67	0.47	0.17	0.13	0.14
269	0.67	3.06	0.93	0.70	0.70	2.33	0.67	0.51	0.19	0.14	0.14
270	0.56	0.69	0.08	0.07	0.08	1.61	0.97	0.11	0.02	0.01	0.02
271	0.56	1.10	0.17	0.12	0.11	1.61	0.97	0.18	0.03	0.02	0.02
272	0.56	1.51	0.21	0.15	0.16	1.61	0.97	0.25	0.04	0.03	0.03
273	0.56	1.81	0.28	0.17	0.19	1.59	0.99	0.30	0.06	0.03	0.04
274	0.56	2.14	0.28	0.22	0.24	1.59	0.99	0.36	0.06	0.05	0.05
275	0.56	2.37	0.33	0.22	0.26	1.60	0.98	0.39	0.07	0.05	0.05
276	0.56	2.43	0.34	0.27	0.28	1.60	0.98	0.40	0.07	0.06	0.06

TABLE V. Wave Forces With and Without Barrier, h/a= 6.0, d/a= 5.0.

RUN	T (sec.)	H (in.)	F_x (lb.)	F_y^+ (lb.)	F_y^- (lb.)	L (ft.)	$\frac{2\pi a}{L}$	$\frac{H}{2a}$	f_x	f_y^+	f_y^-
208	1.11	5.44	4.65	1.66	0.48	5.85	0.27	0.91	0.95	0.34	0.10
209	1.11	4.95	4.35	1.50	0.40	5.82	0.27	0.82	0.89	0.31	0.08
210	1.11	4.10	3.75	1.20	0.36	5.85	0.27	0.68	0.77	0.25	0.07
211	1.11	3.49	3.05	1.03	0.32	5.83	0.27	0.58	0.63	0.21	0.07
212	1.10	2.59	2.16	0.65	0.32	5.79	0.27	0.43	0.44	0.13	0.07
213	1.10	1.98	1.65	0.47	0.27	5.80	0.27	0.33	0.34	0.10	0.06
214	1.11	1.35	1.07	0.29	0.20	5.81	0.27	0.22	0.22	0.06	0.04
215	1.11	0.57	0.41	0.12	0.10	5.81	0.27	0.09	0.08	0.02	0.02
216	1.10	5.24	4.06	0.90	1.71	5.80	0.27	0.87	0.83	0.18	0.35
217	1.11	4.70	3.71	0.80	1.62	5.81	0.27	0.78	0.76	0.16	0.33
218	1.11	4.03	2.91	0.59	1.32	5.82	0.27	0.67	0.60	0.12	0.27
219	1.10	3.36	2.51	0.45	1.05	5.77	0.27	0.56	0.51	0.09	0.22
220	1.10	2.61	1.95	0.31	0.65	5.80	0.27	0.43	0.40	0.06	0.13
221	1.11	1.95	1.41	0.20	0.56	5.81	0.27	0.32	0.29	0.04	0.11
222	1.11	1.41	0.95	0.17	0.31	5.87	0.27	0.23	0.19	0.03	0.06
223	1.11	0.47	0.40	0.10	0.14	5.82	0.27	0.08	0.08	0.02	0.03
224	1.10	5.32	4.15	1.00	1.42	5.78	0.27	0.89	0.85	0.21	0.29
225	1.10	4.57	3.42	0.95	1.21	5.80	0.27	0.76	0.70	0.19	0.25
226	1.11	4.05	2.93	0.78	0.98	5.85	0.27	0.67	0.60	0.16	0.20
227	1.11	3.38	2.40	0.58	0.88	5.82	0.27	0.56	0.49	0.12	0.18
228	1.09	2.80	1.92	0.43	0.60	5.67	0.28	0.47	0.39	0.09	0.12
229	1.11	2.12	1.45	0.23	0.46	5.81	0.27	0.35	0.30	0.05	0.09
230	1.10	1.28	0.91	0.17	0.33	5.79	0.27	0.21	0.19	0.03	0.07
231	1.11	0.48	0.39	0.08	0.12	5.85	0.27	0.08	0.08	0.02	0.02

"WAVE FORCES ON A SUBMERGED HORIZONTAL CYLINDER"

THESIS TOPIC SCHILLER,F.

JUNE 1971

PROGRAM FOR REDUCTION OF DATA RUNS 030 - 284

```
      NRUN IS THE RUN NUMBER
      DEPTH IS RECORDED IN FEET
      PERIOD OF THE WAVE IS RECORDED IN SECONDS
      WHGT IS THE WAVE HEIGHT AND IS RECORDED IN INCHES
      FXMAX IS THE HORIZONTAL FORCE ON THE CYLINDER DUE TO
THE INCIDENT WAVE
      FYUMAX IS THE VERTICAL UPWARD FORCE ON THE CYLINDER
      FYDMAX IS THE VERTICAL DOWNWARD FORCE ON THE CYLINDER
      SABAR IS THE RADIUS OF THE CYLINDER RECORDED IN FEET
      NCARD IS THE TOTAL NUMBER OF CARDS BEING REDUCED
      SL IS THE LENGTH OF THE CYLINDER RECORDED IN FEET
      RELWH IS THE WAVE HEIGHT  TO CYLINDER RADIUS RATIO
      ANU IS AN EXPRESSION USED TO DETERMINE WAVE LENGTH
      H IS THE DEPTH TO CYLINDER RADIUS RATIO
      HDRAT IS THE DEPTH TO CYLINDER DIAMETER RATIO
      FXONE IS THE DIMENSIONLESS HORIZONTAL FORCE COEFFICIENT
      FYUTWO IS THE DIMENSIONLESS VERTICAL UPWARD FORCE COEFFICIENT
      FYDTWO IS THE DIMENSIONLESS VERTICAL DOWNWARD FORCE COEFFICIENT
      WL IS THE WAVE LENGTH RECORDED IN FEET

      NCARD=0284                                                        0050
      SABAR =0.25                                                       0060
      SL = 1.25                                                         0070
      WRITE(6,1939)                                                     0080
1939  FORMAT('1',////////////////////)                                  0080
      DO 1938 I=1,NCARD                                                 0090
      READ(5,1937) NRUN,DEPTH,PERIOD,WHGT,FXMAX,FYUMAX,FYDMAX           0130
1937  FORMAT(I10,6E10.4)                                                0140
      RELWH = (WHGT/12.)/(2.*SABAR)                                     0150
      ANU =(6.28/PERIOD)**2*SABAR/32.2                                  0160
      H=DEPTH/SABAR                                                     0170
      HDRAT=H/2.0                                                       0180
      A = ANU                                                           0190
      DO 1936 J=1,100                                                   0200
      ANUP = A*TANH(A*H)                                                0210
      A=A+0.5*(ANU-ANUP)                                                0220
      IF(ABS(ANU-ANUP).LT..001)GO TO 1935                               0230
1936  CONTINUE                                                          0240
```

```
      WRITE(6,1934)                                                     0250
1934  FORMAT (16HDID NOT CONVERGE)                                      0260
1935  CONTINUE                                                          0270
      SAVTME=(62.4*SABAR**2*WHGT/(24.*SABAR))                           0280
      CXONE=(FXMAX/SL)/SAVTME                                           0290
      FXONE=CXONE*WHGT/(24.*SABAR)                                      0300
      CYUTWO = (FYUMAX/SL)/SAVTME                                       0310
      FYUTWO= CYUTWO*WHGT/(24.*SABAR)                                   0320
      CYDTWO=(FYDMAX/SL)/SAVTME                                         0330
      FYDTWO=CYDTWO*WHGT/(24.*SABAR)                                    0340
      WL=(3.14/A)*6.28*SABAR                                            0350
      WRITE(6,1933)NRUN,PERIOD,WHGT,FXMAX,FYUMAX,FYDMAX,WL,A,RELWH,FXONE 0360
     C,FYUTWO,FYDTWO                                                    0370
1933  FORMAT(' ',36X,I8,11F7.2)                                         0380
1938  CONTINUE                                                          0390
      STOP                                                              0400
      END                                                               0410
```

LIST OF REFERENCES

1. Stokes, G. G., "On the Effect of the Internal Friction of Fluids on the Motion of Pendulums," Proceedings of the Cambridge Philosophical Society, v. 1, part 7, p. 104-106, 9 December 1850.

2. Morison, J. R., O'Brien, M. P., Johnson, J. W., and Schaaf, S. A., "The Force Exerted by Surface Waves on Piles," Journal of Petroleum Technology, American Institute of Mining and Metallurgical Engineers, v. 189, p. 149-154, May 1950.

3. Keulegan, G. H., and Carpenter, L. H., "Forces on Cylinders and Plates in an Oscillating Fluid," Journal of Research of the National Bureau of Standards, v. 60, no. 5, p. 423-440, May 1958.

4. Sarpkaya, T., and Garrison, C. J., "Vortex Formation and Resistance in Unsteady Flow," Journal of Applied Mechanics Transactions of the ASME, v. 30, series E, no. 1, p. 16-24, March 1963.

5. Johnson, R. E., "Regression Model of Wave Forces on Ocean Outfalls," Journal of the Waterways and Harbors Division Proceedings of the ASCE, v. 96, no. WW2, p. 289-305, May 1970.

6. Herbich, J. B., and Shank, G. E., "Forces Due to Waves on Submerged Structures," Journal of the Waterways, Harbors, and Coastal Engineering Division Proceedings of the ASCE, v. 97, no. WW1, p. 57-71, February 1971.

7. Garrison, C. J., Rao, V. S., and Snider, R. H., Wave Interaction with Large Submerged Objects, paper presented at American Society of Civil Engineers National Structural Meeting, Portland, Oregon, 6 April 1970.

INITIAL DISTRIBUTION LIST

		No. Copies
1.	Defense Documentation Center Cameron Station Alexandria, Virginia 22314	2
2.	Library, Code 0212 Naval Postgraduate School Monterey, California 93940	2
3.	Asst Professor C. J. Garrison, Code 59 Gm Department of Mechanical Engineering Naval Postgraduate School Monterey, California 93940	3
4.	Asst Professor E. B. Thornton, Code 58 Tm Department of Oceanography Naval Postgraduate School Monterey, California 93940	1
5.	LT Peter K. Bowden, USN Box 1403 Naval Postgraduate School Monterey, California 93940	1
6.	Mr. Fred M. Schiller 3802 Main Street Stratford, Connecticut 06497	1
7	LCDR Frederick C. Schiller, USN U. S. Naval Shipyard Portsmouth, New Hampshire 03801	2

DOCUMENT CONTROL DATA - R & D

(Security classification of title, body of abstract and indexing annotation must be entered when the overall report is classified)

1 ORIGINATING ACTIVITY (Corporate author)

Naval Postgraduate School
Monterey, California 93940

2a. REPORT SECURITY CLASSIFICATION

UNCLASSIFIED

2b. GROUP

3 REPORT TITLE

WAVE FORCES ON A SUBMERGED HORIZONTAL CYLINDER

4 DESCRIPTIVE NOTES (Type of report and inclusive dates)

Master's Thesis; June 1971

5 AUTHOR(S) (First name, middle initial, last name)

Frederick C. Schiller

6 REPORT DATE	7a. TOTAL NO. OF PAGES	7b. NO. OF REFS
June 1971	102	7

8a. CONTRACT OR GRANT NO.	9a. ORIGINATOR'S REPORT NUMBER(S)
b. PROJECT NO.	
c.	9b. OTHER REPORT NO(S) (Any other numbers that may be assigned this report)
d.	

10 DISTRIBUTION STATEMENT

Approved for public release; distribution unlimited.

11. SUPPLEMENTARY NOTES	12. SPONSORING MILITARY ACTIVITY
	Naval Postgraduate School Monterey, California 93940

13. ABSTRACT

The oscillatory forces generated by the interaction of a train of gravity waves with a rigid horizontal circular cylinder located near a simulated ocean floor were determined experimentally. A circular cylinder of six inch diameter was subjected to gravity waves of wave lengths varying from 2 to 18 feet in a two-dimensional wave channel. Both the horizontal and vertical components of the hydrodynamic force were measured.

Experimental results are plotted in dimensionless form. The horizontal and vertical dimensionless force coefficients are plotted as a function of the relative water depth, the relative wave length, and the relative wave height. It was found that the horizontal force coefficient varied quite linearly with the wave height, and the maximum value was approximately equal in either direction. The vertical force component, however, showed a much more complex variation. The upward and downward magnitudes were approximately equal for small amplitude waves, but as the wave height increased, the variations became quite nonlinear and the magnitudes in the two directions differed considerably.

DD FORM 1 NOV 65 1473 (PAGE 1)

S/N 0101-807-6811

KEY WORDS	LINK A		LINK B		LINK C	
	ROLE	WT	ROLE	WT	ROLE	WT
Wave Interaction with Cylindrical Bodies						
Gravity Wave Forces						
Wave Channel						
Gravity Wave Simulations						